



SNTs have shown high sensitivity and high selectivity for the detection of multianalytes in the multiplexed immunoassays.

Magnetic field separation is one promising technique to replace tedious filtration or centrifugation separation for rapid, gentle, and reliable isolation of target analytes. Barcoded SNTs have been coupled with magnetic bead (MB) separation for protein detection and analysis. The species and number of final collected SNTs represent the types and amount of analyte proteins, respectively. By using barcoded SNTs instead of fluorescence as signals, these suspension arrays overcome the problems existing in current MB suspension arrays, such as fluorescence quenching and interference of MBs' autofluorescence.

Barcoded magnetic nanotubes (BMNTs) have also been successfully fabricated as dual-functional microcarriers for multiplexed immunoassays and cancer biomarker detection with magnetic separation. BMNTs combine the shape variety of barcoded SNTs and superparamagnetic properties of magnetic nanotubes. BMNTs overcome the problems in the existing dual-functional particles. The iron oxide nanocrystals are evenly dispersed in the inner void of the tubular structures without interference with the optical barcoded patterns. BMNTs have shown high selectivity when applied in multiplexed assays and cancer biomarker detection. The identification of BMNTs with software shows promising results for rapid data analysis. The dual-functional BMNTs provide a promising way for ultrafast, gentle, efficient, and automated detection of target chemical/biochemical molecules for diagnosis and drug screening.

BARCODED SILICA NANOTUBES FOR  
BIOANALYSIS

By

Bo He

Dissertation submitted to the Faculty of the Graduate School of the  
University of Maryland, College Park, in partial fulfillment  
of the requirements for the degree of  
Doctor of Philosophy  
2007

Advisory Committee:  
Professor Sang Bok Lee, Chair  
Professor Janice Reutt-Robey  
Professor Kyu Yong Choi  
Professor Bryan Eichhorn  
Professor Neil Blough

© Copyright by  
Bo He  
2007

*This dissertation is dedicated to my dear parents  
He, Gengfu and Dong, Shuqin  
Who always love me and support me*

## Table of Contents

<b>LIST OF ABBREVIATIONS</b>	v
<b>LIST OF TABLES</b>	vi
<b>LIST OF FIGURES</b>	vii
<b>1</b>	<b>1</b>
<b>Chapter 1 Scientific Background of Barcoded Nano/microparticles for Bioanalysis</b>	<b>1</b>
1.1 Introduction: Nanotechnology and Life Science	3
1.2 Nanoparticles for Bioanalysis: Detection and Quantification of Biomolecules	4
1.2.1 Nanoparticles as Quantitation Tags	6
1.2.2 Semiconductor Nanowires Sensors for Bioanalysis	7
1.2.3 Barcoded Nano/microparticles as Substrates	7
1.3 Barcoded Nano/microparticles for Bioanalysis	10
1.3.1 Graphical Encoding	15
1.3.2 Spectrometric Encoding	17
1.4 Project Description: Barcoded Silica Nanotubes for Bioanalysis	<b>22</b>
<b>Chapter 2 Barcoded Silica Nanotubes for Biosensing</b>	<b>22</b>
2.1 Introduction	23
2.2 Experimental Section	25
2.3 Results and Discussion	38
2.4 Conclusion	38
2.5 Acknowledgement	
	<b>39</b>
<b>Chapter 3: Suspension Array with Barcoded Silica Nanotubes for Multiplexed Immunoassays</b>	<b>39</b>
3.1 Introduction	41
3.2 Experimental Section	48
3.3 Results and Discussion	61
3.4 Conclusion	62
3.5 Acknowledgement	
	<b>63</b>
<b>Chapter 4: Barcoded Silica Nanotubes Coupled with Magnetic Bead Separation for Bioassays</b>	<b>63</b>
4.1 Introduction	65
4.2 Experimental Section	70
4.3 Results and Discussion	81
4.4 Conclusion	81
4.5 Acknowledgement	
	<b>82</b>
<b>Chapter 5: Barcoded Magnetic Nanotubes: Dual-Functional Microcarriers for Multiplexed Immunoassays and Cancer Marker Detection</b>	<b>82</b>
5.1 Introduction	84
5.2 Experimental Section	89

5.3 Results and Discussion	101
5.4 Conclusion	102
5.5 Acknowledgement	<b>103</b>
<b>Chapter 6: Conclusions</b>	<b>106</b>
<b>REFERENCE</b>	

## List of Abbreviations

NTs	Nanotubes
SNTs	Silica nanotubes
MB	Magnetic Bead
MNTs	Magnetic nanotubes
BMNTs	Barcoded magnetic nanotubes
IgG	Immunoglobulin G
QDs	Quantum dots
FETs	Field-effect transistors
MRI	Magnetic resonance imaging
PBS	Phosphate buffered saline
DI water	Deionized water

## List of Tables

Table 2-1 Coding patterns for the barcoded silica nanotubes (SNTs) with.....	31
Table 4-1 The effect of different surface modifications on selectivity values.....	74
Table 4-2 The effect of the types of antibodies on selectivity values.....	75
Table 4-3 The effect of the volume of magnetic beads on selectivity values.....	76

## List of Figures

Figure 1-1 Nanomaterials applied in life science.....	3
Figure 1-2 The barcodes patterns of striped metallic nanowires.....	12
Figure 2-1 Scheme for fabrication of a template with two segments.....	26
Figure 2-2 FESEM images of alumina templates with two segments.....	26
Figure 2-3 TEM and optical microscope images of silica nanotubes (SNTs): SNT1, SNT2, SNT3, and SNT4 .....	28
Figure 2-4 TEM, optical microscope, and FESEM images of SNTs with three segments.....	29
Figure 2-5 Typical patterns of SNTs.....	30
Figure 2-6 TEM image of a 200 nm long SNT with two segments.....	34
Figure 2-7 Sandwich assay with the mixture of SNT2 and SNT3 for protein detection.....	36
Figure 2-8 Sandwich assay with the mixture of SNT2 and SNT3 for cancer marker detection.....	37
Figure 3-1 Scheme of the fabrication process of templates with four segments.....	43
Figure 3-2 TEM, optical microscope, and FESEM images of SNTs with four segments.....	50
Figure 3-3 The reflectance value of barcoded SNTs.....	52
Figure 3-4 Stability of SNTs in DI water.....	54
Figure 3-5 Stability of SNTs in PBS buffer.....	54
Figure 3-6 The sedimentation rate of SNTs in DI water.....	56
Figure 3-7 Sensitivity of SNTs arrays at different concentrations of SNTs.....	57
Figure 3-8 Multiplexed sandwich assay with the mixture of barcoded SNTs.....	59
Figure 3-9 Quantitative data of multiplexed sandwich assay with barcoded SNTs....	60
Figure 3-10 The specificity experiment with two different fluorescent labels .....	61
Figure 4-1 Scheme of barcoded SNTs coupled with magnetic beads (MBs) separation for detection.....	69
Figure 4-2 Optical microscope images of SNTs interacting with MBs.....	71
Figure 4-3 Fluorescent images of barcoded SNTs interacting with MBs.....	72

Figure 4-4 TEM images of SNTs interacting with MBs.....	72
Figure 4-5 SNTs coupled with MBs for quantitative analysis of proteins .....	78
Figure 4-6 Optical images of final SNTs after elution .....	79
Figure 4-7 Images of the mixture of SNTs in the bubbles of PBS.....	80
Figure 5-1 Scheme for fabrication of the barcoded magnetic nanotubes (BMNTs)...	86
Figure 5-2 TEM images of bare SNT2 and BMNT2 nanotubes.....	90
Figure 5-3 The optical microscope images of SNT2 and BMNT2.....	91
Figure 5-4 Photos of magnetic field separation of BMNTs.....	92
Figure 5-5 Protein detection assay with BMNT2 and BMNT3 nanotubes.....	93
Figure 5-6 Multiplexed assay with BMNT2 and BMNT3 nanotubes.....	94
Figure 5-7 Quantitative data of the multiplexed assay with BMNTs mixture.....	95
Figure 5-8 Sandwich assay with BMNTs mixture for cancer marker detection.....	97
Figure 5-9 Automated identification of BMNTs by software.....	98

# **Chapter 1: Scientific Background of Barcoded Nano/microparticles for Bioanalysis**

## **1.1 Introduction: Nanotechnology and Life Science**

Nanotechnology is affecting and revolutionizing many practical industries, including health care, energy, manufacturing, defense, electronics, information and communications. The combination of nanotechnology with life science is attracting more and more attention in recent years. It brings together physics, chemistry, biology, medicine and engineering, and promises a technology revolution in health care. For example, it provides novel and powerful tools to enable direct, rapid and sensitive multiplexed analysis of dozens, hundreds, or even thousands of biomolecules, such as DNA and proteins, at one time. These tools or devices will greatly improve diagnosis of diseases and screening of new drugs.

At present, the interface between nanotechnology and life science is one of the most promising areas in science and technology. The most direct way to understand the relationship between them is the size and organization of typical structures. Nanotechnology studies the synthesis and application of materials with at least one dimension less than 100 nm. Natural materials, such as double strand DNA and proteins, and synthetic nanostructures, such as quantum dots (QDs, one form of semiconductor nanocrystals) and nanotubes (or nanospheres and nanowires), have similar dimensions with average diameters at the nanometer scale. DNA and proteins are constituents of cells, and basic nanomaterials are assembled into electronic circuits, whose dimensions are at micrometer scale. Finally, cells are organized into

tissues and circuits are integrated into sensor chips, respectively, with millimeter dimensions. Because nanomaterials have the similar sizes with DNA and proteins, they can be used as probes or substrates to detect and quantify these basic biological components.

Analysis of the biological and chemical species involved in healthcare is the crucial step to diseases diagnosis and the screening of new drugs. Nanomaterials provide new and important progress in this area.<sup>1</sup> Nanoparticles,<sup>2-9</sup> semiconductor nanowires<sup>10-14</sup> and inorganic nanotubes<sup>15, 16</sup> offer unique optical, electronic, and magnetic properties, which can be applied to the sensing and imaging of biomolecules. For example, colloidal Au/Ag particles and QDs have been applied to detect and quantify antibodies and other disease markers because of their unique optical properties.<sup>17</sup> Semiconductor nanowires, which work as field-effect transistors (FETs), are assembled into electronic circuits for real-time detection of cancer markers because they produce conductance changes responding to the surface binding of target biomolecules. In addition, magnetic nanoparticles are developed as contrast agents in magnetic resonance imaging (MRI) for *in vivo* tumor detection.<sup>18</sup> One commercialized example of using nanoparticles in health care is colloid Au in some pregnancy test kits. The colloidal Au nanoparticles are combined with latex microbeads to amplify signals in commercial lateral flow assays. Both the Au nanoparticles and microbeads are modified with antibodies for human chorionic gonadotropin (HCG), a hormone found in the urine of pregnant women. When these particles are mixed with a sample containing HCG, they will aggregate together and a pink color will appear on the test strip because of Au nanoparticles surface plasmon.

## 1.2 Nanoparticles for Bioanalysis: Detection and Quantification of Biomolecules

Nanomaterials can be used in life science in various formats (As shown in Figure 1-1), such as labels for detection, cosmetics powders, textile coatings and drug carriers. This chapter centers on the nanoparticles that are used in detection and quantification of chemical and biological species concerned with health care. Here, these nanoparticles are discussed in three classes. The first class nanoparticles have been used as quantitation tags, including colloid Au/Ag plasmon resonant nanoparticles, QDs and magnetic nanoparticles for MRI. The second class nanoparticles are semiconductor nanowire sensors, which are used as FETs in nanoelectronic devices for direct and real-time bioanalysis. The third class nanoparticles have barcoded information, such as dyes/QDs embedded nanoparticles and inorganic barcoded nanowires/nanotubes, and have been used as substrates for biosensing.

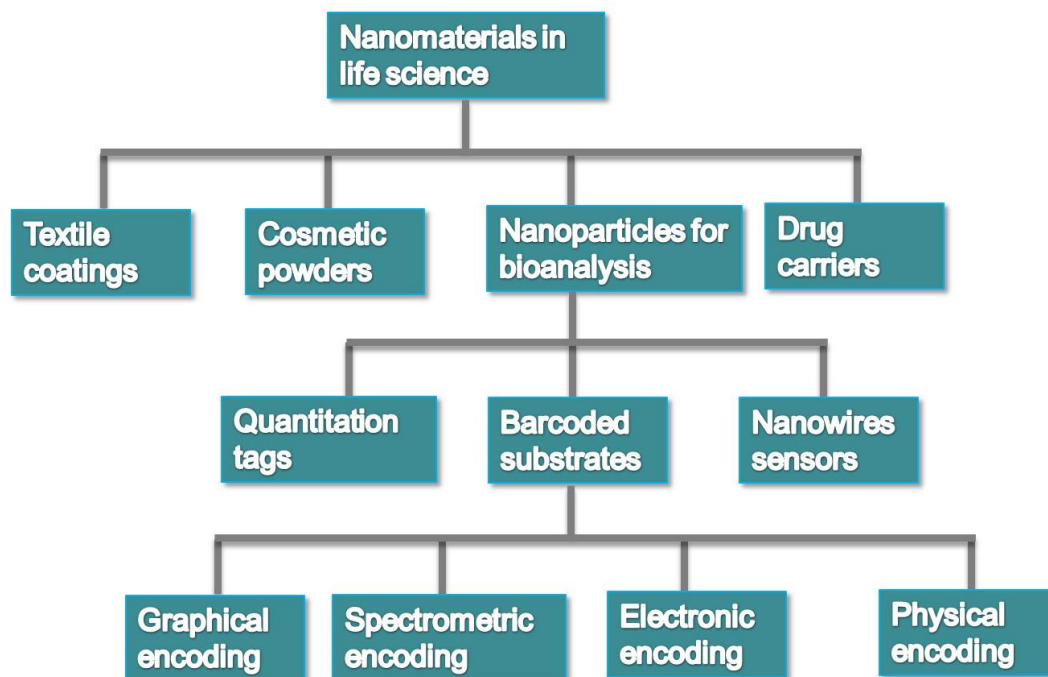


**Figure1-1.** Nanomaterials applied in life science.

### 1.2.1 Nanoparticles as Quantitation Tags

The driving force of using nanoparticles as a new class of quantitation tags in bioassays is the need to overcome the drawbacks of organic dyes and radioactive labeling. For organic dyes, their fluorescence signatures cannot be changed, their emission spectra are broad and may cause spectral overlap problems, and their photostability is poor. For radioactive labeling, the safety problem is always the most concern. Newly developed nanoparticles, including semiconductor quantum dots (QDs) and colloidal metallic nanoparticles, eliminate these problems and show great performance in various assays.

Semiconductor QDs are photoluminescent nanocrystals that take advantage of the quantum confinement effect, and thus have unique optical and electrical properties. The emission spectra of QDs are narrow (20-30 nm full width at half maximum) and tunable. It is possible to excite all colors at the same wavelength. In comparison with organic dyes, QDs are much brighter and more resistant to photobleaching. These advantages of QDs make them an ideal alternative for organic dyes. After many years of research into the basic properties of QDs, scientists can fabricate specific QDs with specific optical properties and surface modification. Many groups are doing research into application of QDs in a diverse range of assays with promising results. For example, QDs have been applied in a Her2 assay for breast cancer,<sup>9</sup> in a mouse lung *in vivo* targeting detection,<sup>19</sup> and for investigation of a *Xenopus* embryo development.<sup>20</sup> In addition, several groups and companies load different combinations of QDs into microspheres that are employed as barcoded substrates for biomolecules analysis. This topic will be described in details in 1.3.2.

Colloidal metallic nanoparticles are another kind of quantitation tags. There are many detection methods for Au/Ag nanoparticles, including optical microscopy,<sup>21</sup> Raman spectrometry,<sup>22, 23</sup> electrochemistry,<sup>24, 25</sup> and mass spectrometry.<sup>26</sup> The colloidal Au/Ag nanoparticles with diameters of 30-120 nm efficiently scatter light in the visible spectrum and can be detected by optical microscopy. The color is determined by the particles' size, shape, and material properties. The light scattering of these nanoparticles is dominated by the collective oscillation of the conduction electrons induced by the light. This phenomenon is called surface plasmon resonance. Plasmon resonant colloidal Au or Ag nanoparticles have several advantages: they are not photobleachable; they can be designed to scatter a chosen color; they are ultra-bright and no special light source is needed; and their conjugation with biomolecules can be stable in a buffer solution. The combination of these attractive properties with the automation of the colloid metallic nanoparticles identification and quantification enables the development of ultrasensitive multiplexed assays with multicolors.<sup>27</sup> For example, different sized gold nanoparticles have been used as probes in “two color labeling” detection in microarrays,<sup>3</sup> and resonance light scattering nanoparticles have been applied in high sensitive DNA hybridization detection on microarrays.<sup>28</sup>

Superparamagnetic nanoparticles, such as iron oxide nanocrystals, are being developed as contrast agents in MRI. They have been applied in a wide range of detection, both in basic research and clinical areas, and shown great performance. For example, superparamagnetic nanoparticles have been used for *in vivo* detection of murine arthritis,<sup>29</sup> clinically occult lymph-node metastases in prostate cancer,<sup>18</sup> brain inflammation in human ischaemic stroke,<sup>30</sup> and human atherosclerotic plaques.<sup>31</sup> Our

group is also researching the use of magnetic nanotubes as contrast agents in MRI. In addition, we have used these nanotubes with superparamagnetic properties in magnetic-field-assisted bioseparation, drug delivery,<sup>32, 33</sup> and multiplexed detection of cancer markers (please see Chapter 5 for detailed information).

### **1.2.2 Semiconductor Nanowires Sensors for Bioanalysis**

Semiconductor nanowires sensors provide a unique and powerful detection approach for health care with their direct and real-time electrical readout.<sup>1</sup> There is no labeling step in the detection process. These sensors employ well-controlled semiconductor nanowires as building blocks and assemble them together into functional devices by standard microfabrication techniques. Semiconductor nanowires, such as silicon nanowires, have been used as FETs, which exhibit conductance changes responding to variations in the electric field on the surface of these nanowires.<sup>10-14</sup> For detection of biomolecules, such as proteins with a net negative/positive charge, the surfaces of the nanowires have been modified with the biomolecules' receptors in advance. When the nanowires are exposed to the sample solution, the specific binding of the biomolecules and their receptors will cause a change in the surface charge and conductance of the nanowire device.

The conducting properties of semiconductor nanowires are reproducible and tunable, and mature silane chemistry provide various and reliable modifications on silicon oxide surfaces. Therefore, semiconductor nanowire devices have been applied to detect a wide range of chemical and biochemical species, and shown great performance.<sup>1, 34</sup> For example, silicon nanowire sensors have been used for

ultrasensitive detection of DNA with the detection limitation down to femtomolar concentrations.<sup>35</sup> They have also been applied in multiplexed detection of multiple cancer markers<sup>36</sup> and viruses<sup>37</sup>, achieving very high selectivity and sensitivity.

### **1.2.3 Barcoded Nano/microparticles as Substrates**

Nano/microparticles with barcoded information can be used as substrates to attach the compounds to be screened for multiplexed analysis of their corresponding biological or chemical species in the solution.<sup>38, 39,40</sup> For example, the Luminex xMAP system (commercial product by Luminex Corporation) uses 100 types of microspheres with 100 different colors, which can be identified by two laser beams, in genetic human lymphocyte antigen (HLA) typing and allergy testing.<sup>41-45</sup> Barcoded nano/microparticles provide a new and promising opportunity for disease diagnosis, combinatorial library, drug screening and drug discovery. The next section will introduce recent developments in barcoded nano/microparticles, also called microcarriers, and their various applications.

### **1.3 Barcoded Nano/microparticles for Bioanalysis**

Barcodes are a typical symbol of the “information age”. You can see them on products in supermarkets. Barcodes provide the information of one product in the widths and spacings of printed parallel lines. Each product has a unique barcode which can be scanned by an optical scanner/reader and managed in computer systems. The barcode’s data collection method is simple, fast, accurate and highly efficient. It

has been the most popular data entry method to track information in the macroscopic world for the last 15 years. On the basis of the same principle, barcoded nano/microparticles are attracting more and more interest for tracking and identifying multiple chemical/biological species and chemical reactions in the microscopic world. The barcode information on the particles can be read out by microscopy or spectroscopy, and the data collected and analyzed by computers.

After the first draft of the Human Genome project was completed in 2001, the quest of gaining more and more biomolecular information from a small amount of samples has increased greatly in both basic research and clinical application areas. The most promising approach is in microarray technology which attempts to analyze thousands of entities at the same time.

There are two types of microarrays: one is planar arrays, and the other is suspension arrays. Planar arrays use hundreds, or thousands of microspots on a plate to anchor receptors. The position of each microspot represents the specie of target molecules that specifically interact with the receptors on the spot. Suspension arrays use barcoded nano/microparticles (with diameters of 10 nm to 10  $\mu\text{m}$ ) dispersed in solution as substrates to anchor receptors. In comparison to planar arrays, suspension arrays have several advantages, such as higher reproducibility, higher flexibility for detecting new analytes by simply adding corresponding particles, as well as showing faster reaction kinetics in solution due to the radial diffusion of analytes or probes. In addition, suspension arrays consume less of the samples and enable higher surface coverage of analytes bound to capture proteins on reduced total available surface area of the arrays, leading to higher sensitivity.<sup>46</sup>

Suspension arrays with barcoded nanoparticles provide a new opportunity for disease diagnosis, drug screening, and drug discovery. Researchers in these areas prefer screening for thousands of compounds of interest in the test samples at the same time, such as antigens, antibodies, DNA, RNA and cancer markers. As microcarriers of compounds of interest, barcoded nano/microparticles can be mixed together and assayed at the same time. This process allows analysis of multiplexed discrete assays simultaneously in a microvolume sample.

For a barcoded nano/microparticles based suspension array, first, the compounds(or receptors) that can specifically interact with an analyte are anchored on the surface of a certain type of barcoded particles. Then, different types of particles are mixed together in a vial to interact with the analyte solution. Each analyte with spectrometric/chemical labels will specifically bind with its receptors on the surface of the particles. Finally, detectors will identify the analytes with the barcode information from the particles and quantify the analytes using the intensity of the labels on the particles.

This section focuses on barcoded nano/microparticles for diseases diagnosis, combinatorial libraries and drug screening. There are four types of barcoded nano/microparticles categorized by encoding methods: graphical encoding, spectrometric (mainly optical) encoding, electronic encoding, and physical encoding.<sup>38, 39,40</sup>

The first two encoding concepts are widely researched. Graphical encoding is the most promising approach in terms of a large number of codes, whereas optical encoding is excellent at rapid and automatic decoding of particles. With the

development of identification software and automation of the detection process, graphically barcoded particles will improve their performance and may have broader applications than optical encoding particles, which have limited numbers of codes. On the other hand, it is very difficult for optical encoding systems to increase the number of codes because of spectral overlap problems. Several well known graphical and optical barcoded particles systems, both commercially available and highlighted by literature, will be discussed here. For electronic encoding that uses radio frequency memory tags, and physical encoding that uses different detectable physical properties, please read the well-written reviews.<sup>38, 39,40</sup>

### **1.3.1 Graphical Encoding**

The barcodes on the products in supermarkets and the printed words are examples of graphical encoding technologies, which employ and recognize two dimensional patterns. In the microscopic world, graphical encoding means that two dimensional patterns, like a series of light and dark lines, or a group of dots, are encoded in the nano/microparticles by various technologies and can be decoded by optical microscopy.

One distinguished example of graphical encoding particles is striped metallic nanowires, which show a series of light and dark lines barcoded patterns under a certain wavelength of light because of different reflectivity values of metals.<sup>47-49</sup> For example, gold reflects only half the light that silver does at 430 nm. These barcoded nanowires are composed with adjacent stripes of alternating metals, and show great performance in miniaturization and multiplexed analysis. Striped metallic nanowires, also called metallic nanobarcodes, are fabricated by sequentially electrochemical

deposition of different metal layers into the regular cylindrical pores in alumina membranes. Metallic nanobarcodes are released from the membranes by selectively dissolving alumina in base or acid solution. The length of each metal layer can be controlled by the amount of current passed in each electroplating step. The minimum length for a distinguishable metal layer is 500 nm, determined by the resolution of the optical microscope. The total length of a typical nanowire is just a few micrometers and its diameter is about 300 nm determined by the pore size of the alumina membranes. The codes of these striped metallic nanowires can be “read-out” with a conventional microscope, and the detection signals, can be captured with a fluorescence microscope. No complex and special detection instruments are necessary. This encoding method has the potential to produce a library that is composed of a massive number of unique barcodes. For example, six layers of two different metals, Ag/Au/Ag/Au/Ag/Au, are electrochemically deposited into the pores of the membranes. In optical microscope images, the brighter parts correspond to Ag, coded as “1”, and the darker parts correspond to Au, coded as “0”. These particles’ codes (As shown in Figure1-2) can be: 0000000, 010101, 010100, 010000, 111000, 111110, and etc. The total number of the codes is  $2^6$  in this case. In theory, the number of barcodes can reach thousands, and even millions by varying the species and the length of each metal layer. All the above features make metallic nanobarcodes very promising in miniaturization and multiplexed analysis of DNA, RNA and proteins. However, there are still some problems in metallic nanobarcode systems, for example, material instability in aqueous buffer solutions, a rapid settling rate of the metal nanowires, and quenching of fluorescence signals near a metal surface.<sup>50, 51</sup>

Barcoded nanoparticles developed by our group also use reflectance patterns as barcodes to identify analytes. More detailed information will be discussed in Section 1.4.



**Figure 1-2.** The barcodes patterns of striped metallic nanowires.

Another graphical encoding example is “Smart Beads”, which use barcoded aluminum rods with a pattern of holes fabricated by photolithography and an etching technique.<sup>52</sup> The microfabrication techniques produce two million rods per 3-inch wafer, which are enough to carry out 1000 assays. The dimensions of the barcoded

rods are  $100 \times 10 \times 1 \mu\text{m}$ . The relative density of aluminum is 2.7, which is lower than that of noble metals, e.g. gold (19.3) and silver (10.5), and therefore less vigorous mixing is needed during bioassays than the other metallic nanowires. In theory, the number of codes can reach millions by varying the widths of the bars and those of the empty spaces. Probe molecules are anchored on each aluminum strip by surface chemistry and bound target molecules are reported by fluorescence signals. “Smart Beads” have been used in multiplexed assays in 96-well filter plates, which are operated and imaged automatically. The “Smart Beads” Ultroplex platform is commercially available in the autoimmune diagnostics market. This system is very attractive in reproducibility and automation, however, there is a practical difficulty that probe molecules, e.g. proteins, bind weakly on the untreated aluminum surface.

Polymer wafers encoded with a graphical pattern of holes have been developed by 3D Molecular Sciences Ltd (Cambridge, UK).<sup>53</sup> The patterns of holes in these barcoded polymer particles, named as ImageCodes, are fabricated by photolithography with UV light. In every ImageCodes particle, an L-shaped pattern of holes along the perimeter is used for orientation and the inner pattern of holes is used for identification. The company claimed that several thousand particles could be decoded at the same time with pattern-reading software. These barcoded polymer particles ( $500 \times 300 \times 25 \mu\text{m}$ ) are much larger than traditional microparticles, which may limit their application in low concentration multiplexed biomolecules analysis.

Recently, a new species of graphical encoding polymer particles, named as dot-coded particles, have been developed for high-throughput biomolecules analysis.<sup>54</sup> The unique advantage of the fabrication process is that it combines particle

synthesis, pattern encoding, and probe incorporation in just one step with continuous-flow lithography.<sup>55</sup> These barcoded particles have two regions, one is for encoding patterns and the other is for capturing targets. In a typical synthesis experiment, two monomer streams are flowed adjacently down a microfluidic channel. The continuous-flow lithography is used to polymerize particles across the streams. The pattern of a particle is determined by its mask, which is inserted into the field-stop position of the microscope. The number of the codes can reach  $2^{20}$  (over 1 million). These barcoded particles are scanned rapidly (1200  $\mu\text{m/s}$ ) in a flow-through microfluid channel and “read-out” with a fluorescent microscope. A multiplexed analysis of a DNA oligomers with the dot-coded particles has been carried out with a single fluorescence signal, achieving high selectivity. The sensitivity of this system is 500 attomoles for DNA oligomers, which is as sensitive as present commercially available detection technologies. Overall, these dot-coded particles are very attractive for particle-to-particle reproducibility, integration of pattern encoding and probes incorporation, and automation of fabrication and detection. However, the dimensions of these particles are  $200 \times 90 \times 30 \mu\text{m}$ , which is very large as molecules substrates. The large size of the particles may limit the throughput of this system and increase the volumes of analytes samples.

Other graphical encoding particles include microspheres with UPC-like patterns fabricated by spatial selective photobleaching of fluorescence<sup>56</sup> and shape-modulated gold wires made by pulsed current controlling anodization of silicon molds.<sup>57</sup>

### 1.3.2 Spectrometric Encoding

Spectrometric encoding technologies encode nano/microparticles with chemical tags, like dyes or special functional groups, which can be decoded by spectrometry, including optical microscopy,<sup>38, 39,40</sup> mass spectroscopy,<sup>58</sup> nuclear magnetic resonance (NMR),<sup>59</sup> energy-dispersive X-ray spectroscopy,<sup>60</sup> and infra-red (IR) spectroscopy.<sup>61</sup> Those technologies are mainly used for combinatorial chemistry libraries, especially in the “split-and-mix” method, in which hundreds of or thousands of compounds are synthesized simultaneously on polymer beads inside the same vessels by combining sets of basic materials or building blocks in a few reaction steps.<sup>62</sup> The technologies above involving complex instruments have been reviewed in other papers.<sup>63</sup>

Optical encoding technology has become the most important spectrometric encoding method in the past few years. It identifies the analytes bound on one nano/microparticle by the emission or absorption spectrum of the particle. These particles are encoded with different combinations of multiple organic dye molecules or QDs, which are binding inside of or on the surface of the particles.<sup>64</sup> At the same time, reporter molecules with another color are applied for quantifying analytes. The most important advantage of this approach is that the decoding process is easy, fast, and automatic by a flow cytometer with two laser beams. However, the number of codes is limited (less than 100) because there are spectral overlap problems of fluorescence signals from identifying particles and quantifying analytes, especially in multiplexed analysis.

One famous example is xMAP technology (Luminex Corporation), which use 5.6  $\mu\text{m}$  polystyrene beads loaded with precise ratios of two dyes (red and orange). A third fluorescence (green) is modified on reporter molecules for quantifying analytes. The Luminex color encoded beads are composed of 100 distinct sets, that is, 100 combinations of these two dyes. Each bead set is coated with a type of specific receptors for detection of their corresponding analytes from a sample. There are two laser beams in the Luminex analyzer: one for exciting the internal dyes that identify each bead, and the other for quantifying the reporter dye. Thus, xMAP technology allows the analysis of 100 different multiplexed assays simultaneously within a single sample. Luminex color coded beads system has shown great performance in many applications, throughout the drug-discovery and diagnostics fields, as well as in basic research.<sup>41-45</sup>

As stated in section 1.2.1, QDs are an ideal alternative for organic dyes because of controllable fluorescence signatures, narrow emission spectra, good photostability, and high emission intensity. Polymer microspheres embedded/absorbed with different ratios of two colors of QDs have been used as barcoded substrates for biomolecules detection.<sup>64-66</sup> Reporter molecules with another color are still need for detection and quantification of analytes. A flow cytometer is the main tool for decoding and detection. Nie and his collaborators have used microspheres with 11 different QD codes in multiplexed DNA assays.<sup>64-66</sup> The Quantum Dot Corporation has developed QD encoded microspheres with nine different spectral codes (two colors at three intensities) to identify ten different single nucleotide polymorphisms (SNPs).<sup>67</sup> Although hundreds of codes are possible by

changing the color and intensity of QDs, in practice, the spectral overlap between the different intensities limits the number of codes less than 100.

#### **1.4 Project Description: Barcoded Silica Nanotubes for Bioanalysis**

Among various barcoded nano/microparticles, the optical encoding particles and graphical encoding metallic nanobarcodes have shown great potential for miniaturization and multiplexing analysis by providing a large number of codes and reliable elements. Miniaturization is a driving force in recent assay development for the purpose of obtaining more and more information from decreasing volumes of samples. However, optical encoding particles need to overcome spectral overlap of fluorescent signals between identifying particles and quantifying analytes, especially in multiplexed analysis;<sup>68</sup> and metallic nanobarcodes need to be improved in terms of material stability in aqueous buffer solutions and fluorescence quenching near a metal surface.<sup>50, 51</sup>

In this point of view, we have invented and developed a new species of graphical encoding particles, barcoded silica nanotubes (SNTs) (in Chapter 2 and Chapter 3), which could give us an opportunity to solve the problems mentioned above in barcoded particles.<sup>69</sup> Barcoded SNTs provide thousands of encoded information by reflectance patterns on the nanotubes, avoiding the spectral overlap problems of optically encoded particles. The principle of encoding patterns in barcoded SNTs is similar to that of the metallic nanobarcodes. However, instead of degradable metals, very stable silica material is used in aqueous solution, and silica does not exhibit fluorescence signals quenching problems. Furthermore, we use

hollow tubular structures, which endow barcoded SNTs with attractive properties, replacing filled nanowire structures.

Barcoded SNTs are composed of several segments showing different optical reflectance values with respect to the segments' diameters. The difference in reflectance values of the segments in the individual SNT under a conventional microscope produces an authentic reflectance pattern for each SNT, which can be used to identify the codes of the SNTs and enable these barcoded SNTs to work as coding materials for biosensing.

Barcoded SNTs are fabricated by a multistep anodization template synthesis and a "surface sol-gel" method. The diameter, length, and wall thickness of each segment in one SNT can be controlled down to one nanometer scale. The numbers of barcodes can reach several thousand by increasing the number of SNT segments up to four.

Template synthesis enables barcoded SNTs to be multifunctional. The differential functionalization between the inside and outside of nanotubes prepared from template synthesis makes it possible to introduce various functional groups into the inside without significant perturbation to the outer surface of the nanotubes, where probing and sensing molecules are immobilized for the immunoassay.<sup>32, 33, 70-74</sup> For example, the inside of SNTs can be modified by magnetic nanoparticles that provide superparamagnetic properties to these barcoded nanotubes, while the outside surfaces of the SNTs are the still clear substrates to anchor receptors for detecting target biomolecules.

Barcoded SNTs also display high stability and dispersibility in aqueous buffer media.<sup>32, 69</sup> SNTs have remained stable in aqueous solution without any visible degradation for 7 months. In comparison to a dense metallic rod structure, the hollow tubular structure renders SNTs easier to suspend in solution without sinking by apparently reducing the density of the SNTs. The tubular structures and hydrophilic silanol groups on the surface allow SNTs to disperse evenly in a buffer solution. In addition, mature silane chemistry provides variable and reliable modification to the surface of SNTs.

Barcoded SNTs have been used to detect single and multiple proteins, with a detection limit down to a concentration of 6 picomolar. We have proved that higher sensitivity can be reached by decreasing the number of SNTs, in other words, the total available analytes' binding areas. We have also demonstrated high selectivity by barcoded SNT suspension arrays for detecting multiple analytes, including IgGs and cancer markers, in the multiplexed assays.

Combining barcode SNTs with microchip technology for rapid, integrated, automatic detection and screening of biomolecules will make barcoded SNT technology not only a novel concept in the labs, but also a powerful tool for basic research and clinical practice.

Magnetic field separation is one promising technique for realizing this goal. It provides rapid, gentle, reliable and reproducible isolation of target analytes, and is easily adapted to automated platforms, such as microchips or microplates. There are two strategies for employing magnetic field separation in barcoded SNT suspension arrays. One way is to combine barcoded particles with commercially available

magnetic beads (MBs), the other is to endow these barcoded SNTs themselves with superparamagnetic properties.

In Chapter 4, we couple barcoded SNTs with commercially available MBs for detection of proteins. Barcoded SNTs replace fluorescence as the target signals. The species and numbers of barcoded SNTs represent the species and concentrations of corresponding target biomolecules. This strategy overcomes a major problem existing in fluorescence signal arrays, where the beads' autofluorescence strongly interferes with the analytes detection fluorescence signal. It also allows mild, fast, and effective magnetic separation of target barcoded SNTs from the mixture solution.

In Chapter 5, a novel type of barcoded SNTs, called barcoded magnetic nanotubes (BMNTTs), have been successfully fabricated as dual-functional microcarriers for multiplexed immunoassays and cancer biomarker detection with magnetic separation. BMNTTs combine the shape variety of barcoded SNTs and superparamagnetic properties of magnetic nanocrystals. The iron oxide nanocrystals are evenly dispersed in the inner voids of the tubular structures without interfering with the optical barcoded patterns. BMNTTs have been applied in multiplexed assays and cancer biomarker detection and demonstrated high selectivity. By using dual-functional BMNTTs with magnetic field separation, the assay time will be shortened and procedures will be simplified. Magnetic field separation of BMNTTs has several excellent advantages over tedious filtration or centrifugation separation. It provides rapid, gentle, reliable and reproducible isolation of target analytes. The identification of BMNTTs with software shows promising results for analyzing large amount of data. BMNTTs provide a promising way to integrate barcoded nanoparticles inside a

microchip/plate for ultrafast, efficient, and automatic detection of target chemical/biochemical molecules for diseases diagnosis and drug screening.

## Chapter 2: Barcoded Silica Nanotubes for Biosensing

This chapter has been reproduced in part with permission from the paper<sup>69</sup>:  
He, B.; Son, S. J.; Lee, S. B., “Shape-Coded Silica Nanotubes for Biosensing”  
*Langmuir* **2006**, 22, (20), 8263-8265.

### 2.1 INTRODUCTION

Microarrays technology has been the most promising method in the research of biomolecular information because it realizes to detect and quantify thousands of target molecules simultaneously. In recent years, the suspension microarrays, such as color encoded nano / microparticles<sup>64, 66, 75</sup> and striped metal nanorods,<sup>47, 50</sup> have attracted significant interest in multiplexing and miniaturization in the field of bioanalytical technology. Compared with the conventional microarrays on a plate, the suspension system may offer greater flexibility in the preparation of new additional assays, higher diffusional flux of analytes due to the radial diffusion, less consumption of sample and reagents, and higher sensitivity.<sup>46, 76</sup> However, these suspension systems are still in the development stages. For example, the bead based assay requires fluorescence measurements to both identify the particles and quantify an analyte, which may cause spectral overlap of signals,<sup>64, 66</sup> and striped metal nanorods have to improve their properties in stability and fluorescence signal quenching.<sup>47, 50</sup>

The tubular structure of nanoparticles has become highly attractive in the aspect of multifunctionality as a result of their structural attributes, such as the distinctive inner and outer surfaces that can be differentially functionalized.<sup>70-72</sup> Recently, the template-synthesized silica nanotubes (SNTs) have proven to be an

ideal multifunctional nanostructures candidate for the biomedical applications such as drug delivery and bioseparation.<sup>32, 74</sup> In addition, the silane chemistry offers the reliable and robust surface functionalization of SNTs. In this chapter, we describe the synthesis of well controlled barcoded SNTs and their applications in detection of proteins, including IgGs and cancer markers, in suspension arrays. The barcoded SNTs can be easily identified by their different shapes (codes) using a conventional optical microscope. Because of the low density and high surface area of hollow tubular structure compared to those of spheres and nanorod structure, SNTs can be well suspended and are stable in solution. These properties may give us an opportunity to solve the problems mentioned above in the suspension microarray field.

## 2.2 EXPERIMENTAL SECTION

**Materials:** Silicon tetrachloride (SiCl<sub>4</sub>, Aldrich), oxalic acid (Fisher), and perchloric acid (70%, Fisher) were used as supplied without further purification. The alumina templates were home-made. Phosphate buffered saline (pH 7.4, PBS), bovine serum albumin (BSA), and all IgGs were purchased from Sigma-Aldrich. Monoclonal antibody (MAb) to Alpha Fetoprotein (MAb AFP) with catalog number of H45301M and H45610M, MAb to Carcinoembryonic Antigen (MAb CEA) with catalog number of MAM02-008 and MAM02-009, Carcinoembryonic Antigen (CEA) were bought from Meridian Life Science. Alpha Fetoprotein (AFP) was purchased from United States Biological.

**Alumina Template Synthesis:** Alumina template was prepared according to the reference S1. Pre-annealed aluminum sheets (0.5mm thick) were first degreased in acetone, then electropolished in the mixture of perchloric acid and ethanol (volume ratio 1: 5) at 5°C and 15 V. After that, the pre-anodization was proceeded in a 0.3 M oxalic acid solution for 15 to 20 h at 10 °C and 40 V, then the resulting irregular aluminum oxide layer was etched away using a solution of phosphoric acid (6 wt%) and chromic acid (1.5 wt%) at 60 °C. With the regular concave structure on the bottom, the resultant aluminum sheet was then conducted with first and second anodization steps for desired time, followed with pore-widening steps in an aqueous 0.1 M phosphoric acid solution at 38 °C.

**Surface Sol-Gel Method:** Barcoded SNTs were synthesized by a surface sol-gel (SSG) method.<sup>32, 77</sup> First, an alumina template was soaked in SiCl<sub>4</sub> (99.8%) solution for 2 min; then it was quickly washed with hexane for several times and immersed in fresh hexane for 5 min to remove the unabsorbed SiCl<sub>4</sub>. After that, the template was placed in methanol/hexane (1:1) and ethanol for 5 min respectively to replace the hexane and dried in nitrogen flow. Finally, the template was placed into the deionized water (5min), followed by washed with methanol and dried in nitrogen stream. This is one cycle of SSG process. The number of cycles determines the wall thickness of the SNTs.

**Measurement:** Alumina templates were characterized by field emission scanning electron microscopy (FESEM, Hitachi S-4700), SNTs were characterized by transmission electron microscopy (TEM, Zeiss EM10CA) and fluorescence microscopy (Zeiss, Axioskop 2 MAT).

## 2.3 RESULTS AND DISCUSSION

**Multisegment Templates Synthesized by Multistep anodizations.** The template synthesis of barcoded SNTs begins with the fabrication of a porous alumina film that has well-defined cylindrical pores with two or more different diameter segments along the pores through a multistep anodization of aluminum.<sup>78, 79</sup> Figure 2-1 shows a schematic of the preparation of the template, which has two different pore diameters segmented in the pores. First, the aluminum foil (A) was pre-anodized in 0.3 M oxalic acid solution, and the resulting irregular alumina layer was etched away to get a well-ordered concave structure on the aluminum substrate (B). After the first anodization at 40 V for the desired time, the alumina film with well-ordered pores (first layer) was formed (C). Pore-widening was performed in a 0.1 M phosphoric acid solution to make a larger pore diameter (D), and then the second anodization step was used to produce the smaller pores (second layer) consecutively below the larger pores (E).<sup>7</sup> In this process, the duration of the first and second anodizations determine the length of each segment in the pores. The duration time of the pore-widening step after each anodization determines the diameter of each segment in the pores. We fabricated three kinds of templates, named T1, T2, and T3, with the first and second anodization time combinations of 10 and 50 min, 30 and 30 min, and 50 and 10 min, respectively, while the total anodization time was kept constant at 60 min, corresponding to 4.6  $\mu\text{m}$  in total length. The scanning electron microscope (SEM) image in Figure 2-2 shows the cross sections of well-ordered shape-differentiated pores in the alumina template: T1, T2, and T3.

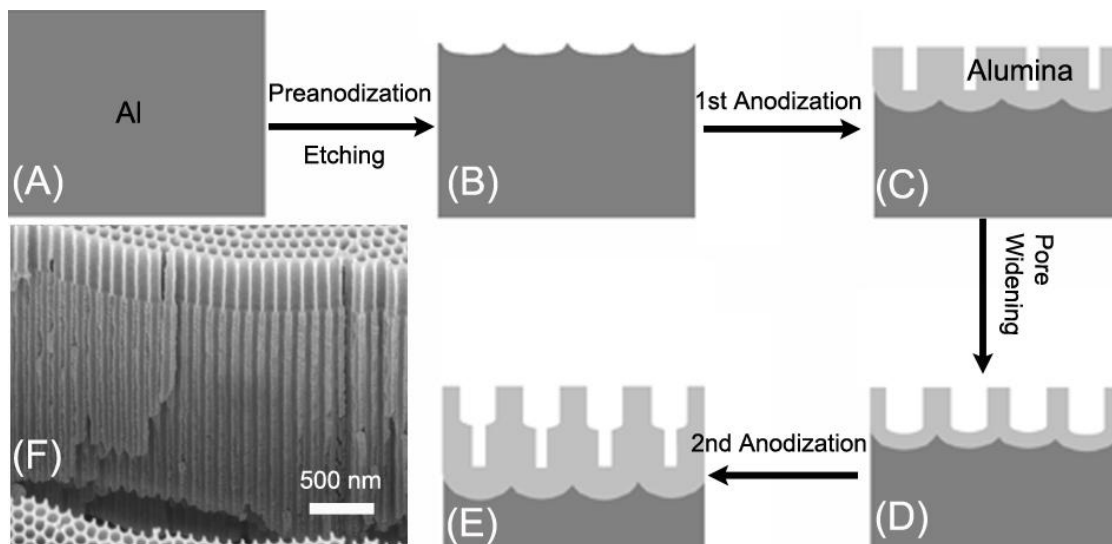


**Figure 2-1.** Schematic diagram for the fabrication of the template which has two different pore diameters segmented along the cylindrical pores (A – E). (F) SEM image of the cross-sectional view of T1 alumina template.

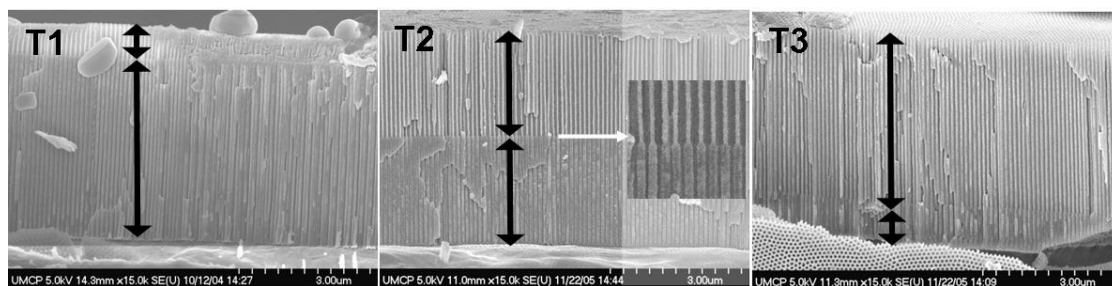


**Figure 2-2.** (A), (B) and (C) FESEM images of alumina template of T1, T2 and T3 after multi-step aluminum anodization respectively.

**Barcoded SNTs Characterization.** SNTs were synthesized within the pores of the alumina template by the previously reported “surface sol-gel” method after minor modification.<sup>32, 77</sup> Figure 2-3 shows the TEM and dark field optical microscope images of SNTs, named with SNT1, SNT2, and SNT3, produced from template T1,

T2, and T3, respectively. The outer diameters of the two segments of SNTs are  $80 \pm 5$  and  $45 \pm 5$  nm. The lengths are  $0.8 \mu\text{m}$  and  $3.8 \mu\text{m}$ ,  $2.3 \mu\text{m}$  and  $2.3 \mu\text{m}$ , and  $3.8 \mu\text{m}$  &  $0.8 \mu\text{m}$  for SNT1, SNT2, and SNT3, respectively. Furthermore, SNTs with three (As shown in Figure 2-4) and four segments (Figure 2-3D and H) were successfully synthesized by three- and four-step anodizations. Upon comparison with TEM images, it is obvious that conventional optical microscope images reflect each different SNT shape as a result of the large difference in reflectance between two segments of the individual SNT. The reflectance of each segment depends on its own diameter, wall thickness, and microscope parameters. Generally, a larger difference in diameter between the two segments gives better contrast in reflectance to distinguish the shape of the SNT.

Overall, this optical reflectance property of segmented SNTs makes it very convenient to identify each nanotube and enables these barcoded SNTs to work as coding materials in a new suspension microarray sensor. In other words, the different shape of SNTs offers the identification information that works similarly to the position in conventional plate microarray analysis. In addition, because of the hollow tubular structure with the thin wall, SNTs are well suspended in the “solution arrays”, which leads to rapid interactions between SNTs and chemical/biochemical reagents. When it comes to coding materials, another important issue is the number of codes determined by detection methods. According to Rayleigh criterion, the resolution of an optical microscope is about  $0.2 \mu\text{m}$ ,<sup>47,50</sup> then in theory the number of codes for  $6\text{-}\mu\text{m}$  SNT with four segments can be increased up to 4960. (As shown in Figure 2-5) Figure 2-3D and 2H show TEM and optical microscope images of the four segmented

SNTs (named as SNT4) synthesized from the four-step anodized alumina template. Through this four (larger number and longer) segmented SNTs, the larger number of codes can be created. The reflectance differences between the segments are under the optimization process.

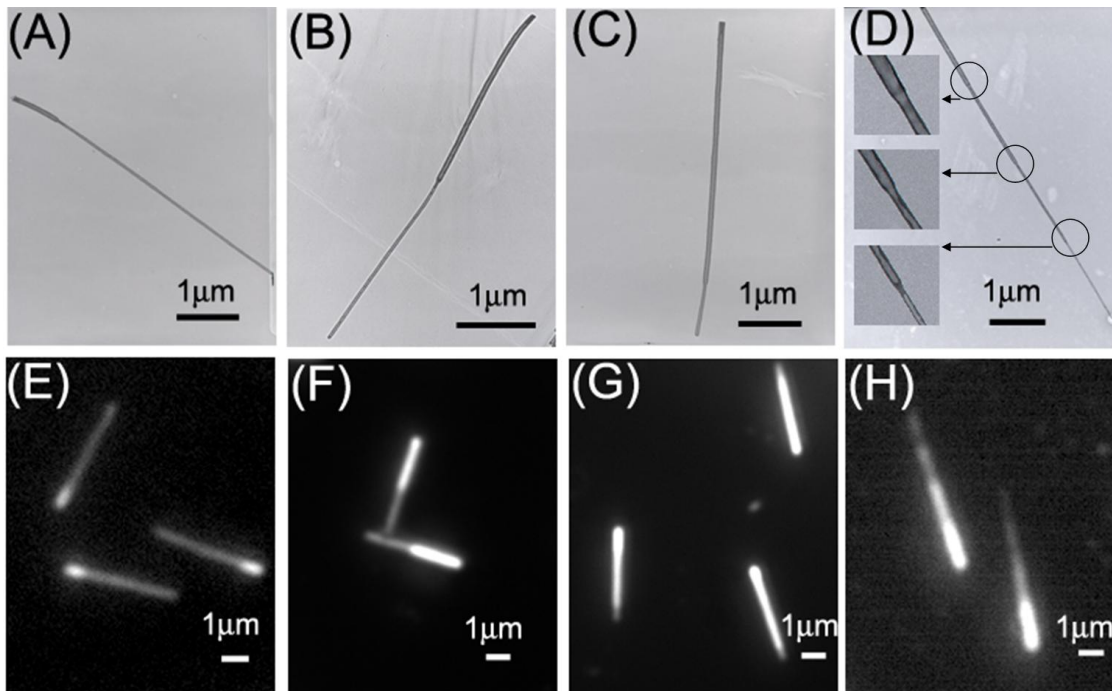


**Figure 2-3.** (A), (B), (C), and (D): TEM images of SNT1, SNT2, SNT3, and SNT4 respectively; (E), (F), (G), and (H): the optical microscope images in dark field of SNT1, SNT2, SNT3, and SNT4 respectively.

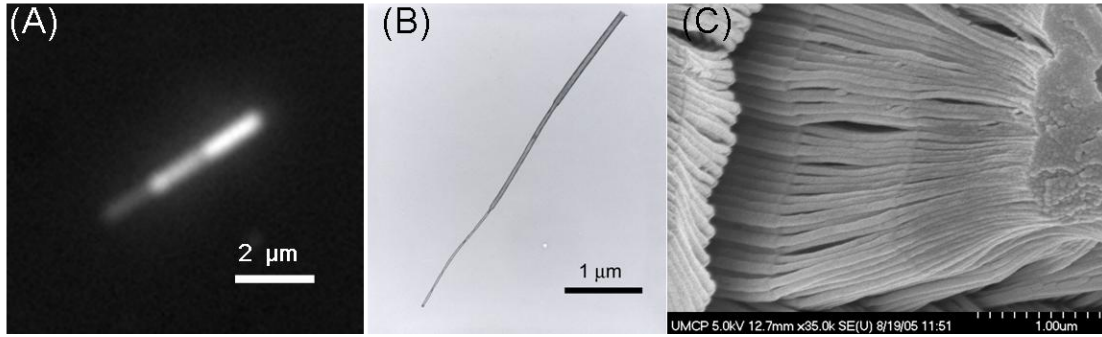


**Figure 2-4.** (A) Optical microscope image in dark field; (B) TEM image; and (C) FESEM image of SNTs nanotubes with three segments.

**Calculation of the number of coding:** According to Rayleigh criterion, the resolution of an optical microscope is  $0.5\lambda/NA$ , where NA is the numerical aperture of the objective.<sup>47, 50</sup> For the Zeiss Axioskop 2 MAT microscope with mercury lamp (with 400 nm band pass filters) and oil-immersion lens (NA=1.3), the resolution is 154 nm. In theory, for SNT with four segments, the possibility (P) of its shape,

$$P = \sum_{n=1}^n \frac{n(n+1)}{2}$$

where  $n = (\text{length} / \text{resolution})$ . Thus, for a 6- $\mu\text{m}$  four-segment SNT with the resolution of 0.2- $\mu\text{m}$ , the number of coding (possibility) is 4960. The detailed calculation process is shown below.

***Definition of each diameter on a nanotube and the rule of sequence***

For barcoded SNTs fabricated by our procedure, diameter of each segment **declines** from left to right. Let's define the diameter of each segment from left to right as **4, 3, 2, 1** (Diameter **4>3>2>1**) with the actual value of 85 nm, 68 nm, 52 nm and 40 nm, obtained from TEM images. The sequence can be 4431, 4421, etc, but

never 3412, 3341. In the Figure 2-5, the segment with diameter of **4, 3, 2, 1** is colored with red, blue, green and purple respectively.

***The idea of the possibility of the codes***

The resolution of optical microscope is 0.2  $\mu\text{m}$ . So the minimum length of each segment that can be resolvable is 0.2  $\mu\text{m}$ . So for the SNTs with length of 0.8  $\mu\text{m}$ , 1.0  $\mu\text{m}$  and 1.2  $\mu\text{m}$ , the sequence can be 4321, 44321, 444321, respectively. The Figure 2-5 shows some examples from random patterns of SNTs with length of 0.8, 1.0  $\mu\text{m}$ , and 1.2  $\mu\text{m}$ , respectively. Table 2.1 presents all the possibility of coding for the SNTs with length of 0.8  $\mu\text{m}$ , 1.0  $\mu\text{m}$  and 1.2  $\mu\text{m}$ . In this table,  $a_1$  represents the possibility under the situation of no variable, which means all diameters are **4** (the biggest diameter);  $a_2$  represents the possibility under the situation of one variable, which means all other diameters are **4** except one 0.2- $\mu\text{m}$  length has other kind of diameter;  $a_3$  represents the possibility under the situation of two variables, which means all other diameters are **4** except two 0.2- $\mu\text{m}$  lengths have other kind of diameter; and etc.

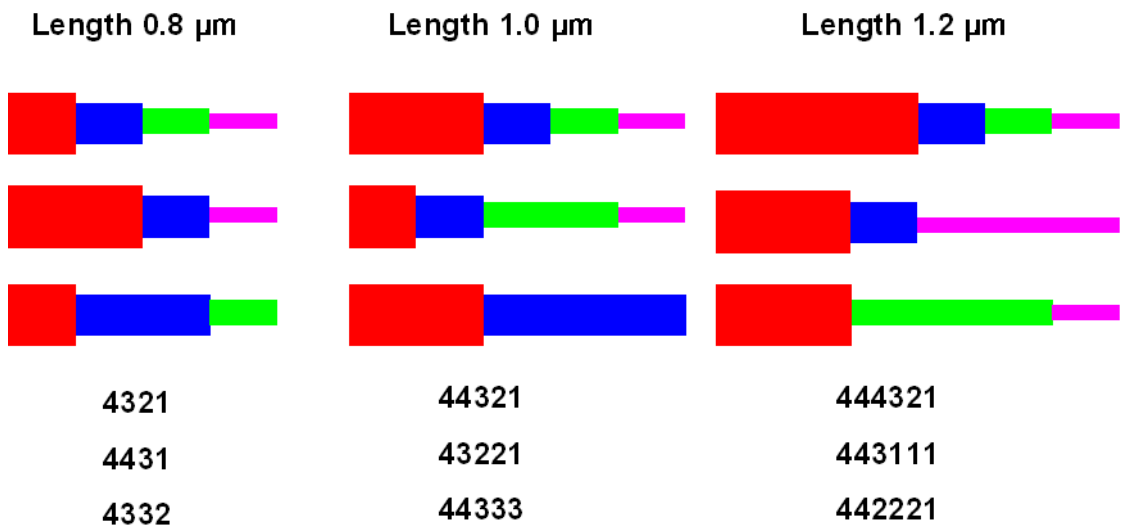


**Figure 2-5.** Typical patterns of SNTs with the length of 0.8, 1.0 and 1.2  $\mu\text{m}$ , respectively.

**Table 2-1** All coding patterns for the SNTs with length of 0.8, 1.0 and 1.2  $\mu\text{m}$ .

	Total length 0.8 $\mu\text{m}$	Total length 1.0 $\mu\text{m}$	Total length 1.2 $\mu\text{m}$
<b>No variable</b> ( all 4) $a_1 = 1$	4444	44444	444444
<b>One variable</b> $a_2 = 3$	4443,4442,4441	44443,44442,44441,	444443,444442,444441,
<b>Two variables</b> $a_3 = 6$	4433,4432,4431, 4422,4421,4411,	44433,44432,44431, 44422,44421,44411,	444433,444432,444431, 444422,444421,444411,
<b>Three variables</b> $a_4 = 10$	4333,4332,4331, 4322,4321,4311, 4222,4221,4211, 4111,	44333,44332,44331, 44322,44321,44311, 44222,44221,44211, 44111,	444333,444332,444331, 444322,444321,444311, 444222,444221,444211, 444111,
<b>Four variables</b> $a_5 = 15$		43333,43332,43331, 43322,43321,43311, 43222,43221,43211, 43111,42222,42221, 42211,42111,41111,	443333,443332,443331, 443322,443321,443311, 443222,443221,443211, 443111,442222,442221, 442211,442111,441111,
<b>Five variables</b> $a_6 = 21$			433333,433332,433331, 433322,433321,433311, 433222,433221,433211, 433111,432222,432221, 432211,432111,431111,

			422222,422221,422211, 422111,421111,411111,
<b>Total Possibility</b> $(a_1 + a_2 + \dots + a_n)$	<b>20</b>	<b>35</b>	<b>56</b>

\*To make segments' diameter difference more obvious, we always keep at least one segment with biggest diameter (85 nm), named **4**, in the SNTs.

**Equation**

From above,

$$a_1 = 1; a_2 - a_1 = 2; a_3 - a_2 = 3; a_4 - a_3 = 4; \dots$$

$$a_n - a_{n-1} = n$$

$$a_n = 1 + 2 + 3 + \dots + n = \sum_{n=1}^n n = \frac{n(n+1)}{2}$$

The total possibility (P) of its shape is

$$P = \sum a_n = \sum_{n=1}^n \frac{n(n+1)}{2} = \frac{1}{2} (\sum n^2 + \sum n) = \frac{1}{6} n(n+1)(n+2)$$

where the value of **n** is **total length / 0.2 (optical resolution)**. For example, n is 4, 5, and 6 respectively for the SNT's length of 0.8 μm, 1.0 μm and 1.2 μm.

**For the 6 micron wire with four segments,**

$$n = \frac{6.0}{0.2} = 30$$

So, the possibility of coding is  $P = \frac{1}{6} * 30 * (30 + 1)(30 + 2) = 4960$

**Note**

In the above situations, for making diameter difference more obvious between the segments, we always keep at least one segment with biggest diameter (85 nm), named **4**, in the SNTs. In other words, we didn't count 44444 or 33333 because we expect there will not be much difference between 44444 and 33333 in optical microscope image. However, if we count the possibility without any **4** in the SNTs, for a 0.8  $\mu\text{m}$  SNTs, for example 3333, 3332, then the total number of possibility will be 35. For a 6.0  $\mu\text{m}$  SNTs, the total number of possibility can reach 5456.

**Length control over individual segments:** First, the length control in terms of variation between particles is very good. It is less than 3 % variation based on the analysis of TEM images. Second, the length control over individual segments (of different diameter): The smallest size that we ever made is 200-nm nanotube in total length with two segments. As shown in the Figure 2-6, the length of individual segment can be controlled in 100 nm. The total length of the SNT is 200 nm. For fabrication of the template for this SNT, 2<sup>nd</sup> and 3<sup>rd</sup> anodization times were 1.5 min and 1.5 min, and 1<sup>st</sup> and 2<sup>nd</sup> pore widening times were 20 min and 10 min. So, the resolution of the length control over individual segments is better than that of optical microscope.

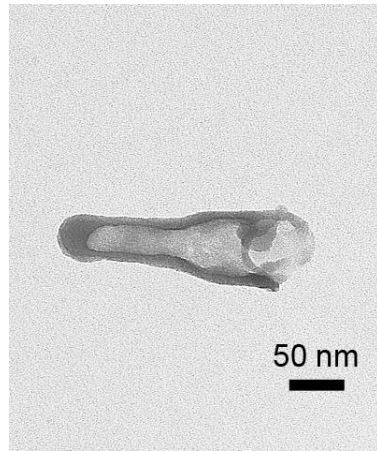


**Figure 2-6.** TEM image of a 200 nm long SNT with two segments.

**Suspension Microarrays with Barcoded SNTs for IgGs detection in Sandwich Assays.** For the proof-of-concept experiment for the use of barcoded SNTs in a suspension microarray biosensing system, a sandwich immunoassay (Figure 2-7A) was performed for the target analyte, rabbit IgG (Immunoglobulin G), with two different shapes of SNTs: SNT2 and SNT3. Anti-human IgG-modified SNT2 and anti-rabbit IgG-modified SNT3 were prepared using 3-glycidyloxypropyltrimethoxysilane (GPTMS) as a linker.<sup>80</sup> The unreacted epoxide group of GPTMS on the SNT surface was treated with a 1% bovine serum albumin (BSA) phosphate-buffered saline (PBS) buffer solution.

Then, a 1:1 mixture solution of SNT2 and SNT3 ( $3.3 \times 10^9$  nanotubes each in 200  $\mu$ L) was prepared and incubated with rabbit IgG (3  $\mu$ M). After being washed with PBS, the mixture of SNTs was incubated with Cy3-labeled anti-rabbit IgG for 30 min and washed with 1% BSA PBS buffer (0.05% Tween 20) and deionized water. Figure 2-7 shows the optical microscope images of the resulting mixture of SNT2 and SNT3. The shape of each nanotube can be clearly distinguished in the optical dark

field image (Figure 2-7B). This means that we know that SNT3 has anti-rabbit IgG on its surface and is supposed to recognize rabbit IgG, followed by the binding interaction with Cy3-labeled anti-rabbit IgG resulting in a red fluorescent signal whereas anti-human IgG modified SNT2 does not. The fluorescence microscope image (Figure 2-7C) proves the above expectation that the analyte (rabbit IgG) binds selectively to the corresponding nanotube (SNT3) by giving the strong red fluorescence signal only on SNT3. There is no detectable nonspecific interaction between SNT2 and rabbit IgG. The quantitative analysis is also performed with the various concentrations of rabbit IgG. Figure 2-7D shows the plot of fluorescence intensity from SNT3 with various concentrations of rabbit IgG. The result shows that the detection limit of the analyte, rabbit IgG, is practically about 30 nM. The detection limit and deviations in the experimental data in the sub-micro molar concentration range still need to be improved and the improvement is underway by decreasing the number of nanotubes or the overall surface area available for the binding of analytes.

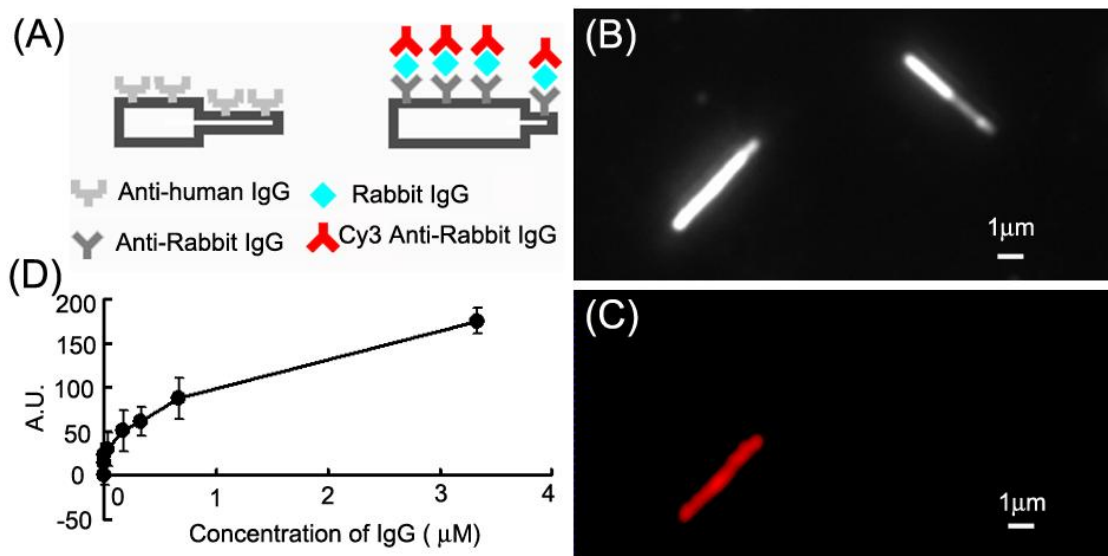


**Figure 2-7.** (A) Scheme of the sandwich assay with the mixture of SNT2 and SNT3. (B) Optical (in dark field) and (C) fluorescence microscope images of the mixed SNTs after incubation with rabbit IgG and Cy3-labeled anti-rabbit IgG. (D) Plot of fluorescence intensity from SNT3 vs. concentration of rabbit IgG.

### Suspension Microarrays with Barcoded SNTs for Cancer Marker

**Detection.** Biomarker detection is very important for diseases diagnosis. Suspension arrays with barcoded SNTs provide a new opportunity to rapidly and accurately detect single or multiple cancer markers in a microvolume sample. We have applied barcoded SNTs in cancer marker detection. A sandwich immunoassay (Figure 2-8A) was designed and performed to detect target cancer marker: AFP, with the mixture of SNT2 and SNT3.

First, SNT2 and SNT3 were modified with monoclonal antibody of AFP (MAb AFP) and monoclonal antibody of CEA (MAb CEA), respectively. Then, a 1:1 mixture solution of SNT2 and SNT3 (100 μL of  $3.0 \times 10^8$  NTs/mL nanotubes for

each) was prepared and incubated with AFP (0.6  $\mu$ M). After being washed with PBS, the mixture of SNTs was incubated with Alexa488 MAb AFP (Green) and Alexa488 MAb CEA (Green) for 1 h and washed with 1% BSA PBS buffer and deionized water. Figure 2-8 shows the optical microscope images of the resulting mixture of SNT2 and SNT3. The shape of each nanotube can be clearly distinguished in the optical dark field image (Figure 2-8B). SNT2 has MAb AFP on its surface and is supposed to recognize AFP, followed by binding with Alexa488 MAb AFP resulting in a green fluorescent signal, whereas MAb CEA modified SNT3 does not. The fluorescence microscope image (Figure 2-8C) demonstrates the above expectation that the analyte (AFP) binds selectively to the corresponding nanotube (SNT2) by giving the strong green fluorescence signal only on SNT2. There is no detectable nonspecific interaction between SNT3 and AFP.

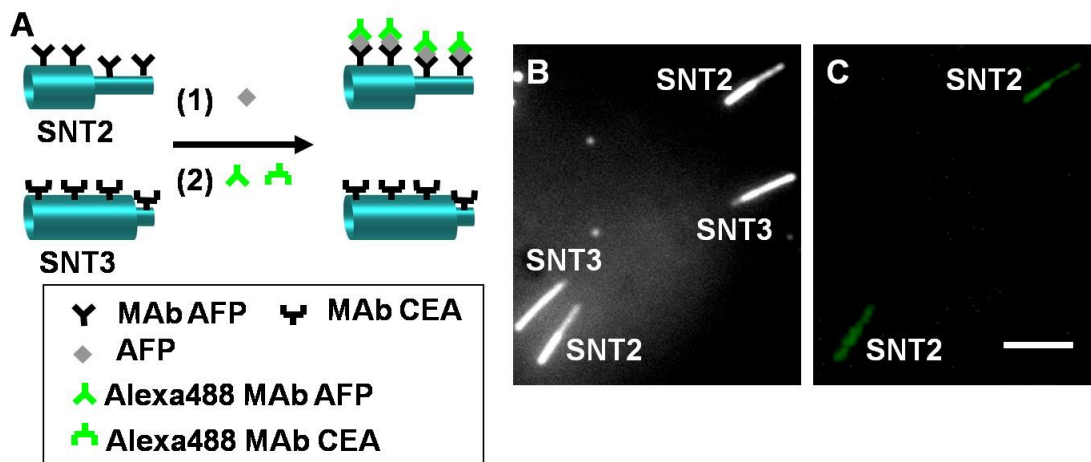


**Figure 2-8.** (A) Scheme of the sandwich assay with the mixture of SNT2 and SNT3 for cancer marker detection. (B) Optical (in dark field), and (C) fluorescence microscope images of SNTs after incubation with AFP, and the mixture of Alexa488 MAb AFP (Green) and Alexa488 MAb CEA (Green).

## **2.4 CONCLUSION**

In conclusion, barcoded SNTs have been successfully synthesized through the multistep anodized alumina template and used for the proof-of-concept experiment of a new suspension microarray biosensor with high specificity, selectivity, and sensitivity. The barcoded SNTs can avoid the fluorescence signal quenching, spectral overlap, and material degradation problems reported as concerns in suspension microarray systems. However, much work has to be done to improve this barcoded SNT system. For example, SNTs with four or more segments that can offer a much larger number of codes ( $> 1000$ ) are being developed and optimized to set up the library. Multiplex assays of SNTs are being studied for the higher selectivity and sensitivity by optimizing the number of nanotubes. Finally, the inner void of the SNT is being further functionalized with magnetic nanoparticles for magnetic-field-assisted assays and separation.<sup>81</sup> Please see Chapter 5 for fabrication and application of magnetic barcoded SNTs.

## **2.5 ACKNOWLEDGMENT**

This work was supported by the National Institutes of Health, University of Maryland, College Park, and the Laboratory for Physics Science.

## Chapter 3: Suspension Array with Barcoded Silica

### Nanotubes for Multiplexed Immunoassays

This chapter has been reproduced in part with permission from the paper<sup>82</sup>:  
He, B.; Son, S. J.; Lee, S. B., “Suspension Array with Shape-Coded Silica Nanotubes for Multiplexed Immunoassays” *Analytical Chemistry* **2007**, 79, (14), 5257-5263.

#### 3.1 INTRODUCTION

Suspension arrays,<sup>46, 68</sup> which use barcoded nano/micro particles (10 nm to 10  $\mu\text{m}$ ) in solution as elements, are attracting increasing interest for detection and multiplexed analysis of DNA, proteins, and cells.<sup>8, 47, 83-86</sup> In comparison to conventional chip-based microarrays, suspension arrays have several advantages, such as higher flexibility for detecting new analytes by simply adding corresponding particles as well as showing faster reaction kinetics in solution due to the radial diffusion of analytes or probes. In addition, suspension arrays consume less samples and enable higher surface coverage of analytes bound to capture proteins on reduced total available surface area of the arrays, leading to higher sensitivity.<sup>46, 68</sup>

Among various suspension arrays, those arrays with color-encoded nanoparticles (embedded with organic dyes or QDs)<sup>49, 64, 66, 87, 88</sup> and metallic nanobarcodes<sup>49</sup> have shown great potential in miniaturization and multiplexing analysis by providing a large number of codes and reliable elements. However, color-encoded nanoparticle arrays need to circumvent spectral overlap of fluorescent signals from the identifying particles and the quantifying analytes, especially in multiplexed analysis;<sup>68</sup> and metallic nanobarcodes need to be improved in terms of

material stability in aqueous buffer solutions and fluorescence-quenching near a metal surface.<sup>50, 51</sup>

In this point of view, we have reported that barcoded silica nanotubes (SNTs) could give us an opportunity to solve the problems mentioned above in the suspension array field.<sup>69</sup> In this array, the barcoded nanoparticles are SNTs composed of several segments showing different optical reflectance values with respect to the segments' diameters. The difference in reflectance values between the segments in the individual SNT under a conventional microscope produces authentic reflectance pattern for each SNT, which can be used to identify the codes of the SNTs and enable these barcoded SNTs to work as coding materials for biosensing.

The use of SNTs in a suspension array is advantageous, both in terms of dispersibility and multifunctionality. In comparison to a dense rod structure, the hollow tubular structure allows SNTs to be more readily suspend in solution by apparently reducing the density of SNTs. The differential functionalization between the inside and outside of nanotubes prepared from template synthesis makes it possible to introduce various functional groups into the inside without significant perturbation of the outer surface of the nanotubes, where probing and sensing molecules are immobilized for the immunoassay.<sup>32, 33, 70-74</sup>

The SNT suspension array also displays high stability and dispersibility in aqueous buffer media.<sup>32, 69</sup> We found that the SNTs remained stable in aqueous solution without any visible degradation for 7 months. The tubular structures and hydrophilic silanol groups on the surface allow SNTs to disperse evenly in buffer

solution. In addition, mature silane chemistry provides variable and reliable modification on the surface of SNTs.

In our previous work, we have fabricated the barcoded SNTs using two-step anodization template synthesis and demonstrated a proof-of-concept experiment for the detection of an antigen.<sup>69</sup> However, much work has to be done to improve this barcoded SNT array technology in terms of high sensitivity and multiplexed sensing. In this study, we describe the suspension array using SNTs for multiple antigen detection and expand the code library by increasing the number of SNT segments up to four. In addition, the reflectance values of SNTs and the number of nanotubes involved in the assay are optimized to increase sensitivity in quantitative analysis.

### 3.2 EXPERIMENTAL SECTION

**Materials.** Silicon tetrachloride ( $\text{SiCl}_4$ , 99.8%, Acros Organics), oxalic acid (dehydrate, Acros), o-phosphoric acid (85%, Fisher), chromic acid (10%, W/C, LabChem, Inc), ethanol (Pharmco-AAPER), 3-glycidyloxypropyltrimethoxysilane (95%, TCI America), hexane (Fisher), methanol (Fisher), and perchloric acid (70%, Fisher) were used as supplied without further purification. Aluminum foils (99.99%) were purchased from Alfa Aesar. Deionized (DI) water was obtained by a Milli-Q A10 system. Alexa Fluor 350 goat antimouse IgG (H + L) (heavy chains and light chains), Alexa Fluor 555 goat antimouse IgG (H + L), and Alexa Fluor 555 goat antirabbit IgG (H+L) were purchased from Invitrogen. Phosphate-buffered saline (pH 7.4, PBS), bovine serum albumin (BSA), mouse IgG, rabbit IgG, human IgG, goat

antihuman IgG, goat antimouse IgG, goat antirabbit IgG, and Cy3 goat antihuman IgG were obtained from Sigma-Aldrich.

**Instrumentation.** Alumina templates were characterized by field emission scanning electron microscope (FESEM, Hitachi S-4700). SNTs were characterized by a transmission electron microscope (TEM, Zeiss EM10CA) and fluorescence microscope (Zeiss, Axioskop 2 MAT).

**Fabrication of Multisegment Nanopores in Alumina Templates.** The two-step anodization technique was used to fabricate two-segment cylindrical pores on aluminum template films.<sup>69</sup> On the basis of the same principle, the four-segment nanopores were fabricated by four-step anodization. First, aluminum foils were electropolished twice (6 and 8 min respectively) by a fresh mixture of perchloric acid and ethanol (v/v 1:5) with 15 V at 5 °C. (Caution: Perchloric acid is a strong oxidizer. Please check the MSDS before handling with it.) After electropolishing, the surface of the aluminum foils had a mirror-like reflectance. Then, pre-anodization of the foil was preformed in 0.3 M oxalic acid solution at 40 V, 10°C for 5 to10 h, and the resulting irregular alumina layer was etched away by the mixture of chromic acid (1.5 wt%) and phosphoric acid (6 wt%) at 60 °C to obtain a well-ordered concave structure on the aluminum substrate. After that, the first anodization was performed at 40 V for the desired time, followed by the first pore widening step with 0.1 M phosphoric acid solution at 38 °C for 15 min to expand the pore diameter. The first layer of cylindrical regular pores was formed on the surface of aluminum foil. Under the same conditions, the second and third anodization, followed by a corresponding pore widening step (for 15 min each), produced the second (Figure 3-1A) and third

layer (Figure 3-1B) of smaller pores consecutively below the bigger pores of the first layer. Finally, the fourth anodization fabricated the smallest pores at the bottom of the alumina layer (Figure 3-1C). Anodization time determines the length of each segment within the pore. Three templates, named as T4A, T4B and T4C (Figure 3-1D, E, and F), were fabricated with anodization times of 10/30/20/20 min, 20/20/20/20 min, and 30/10/20/20 min, respectively. On the basis of our results, the growth rate of the alumina layer was calculated to be  $78 \pm 2$  nm / min.

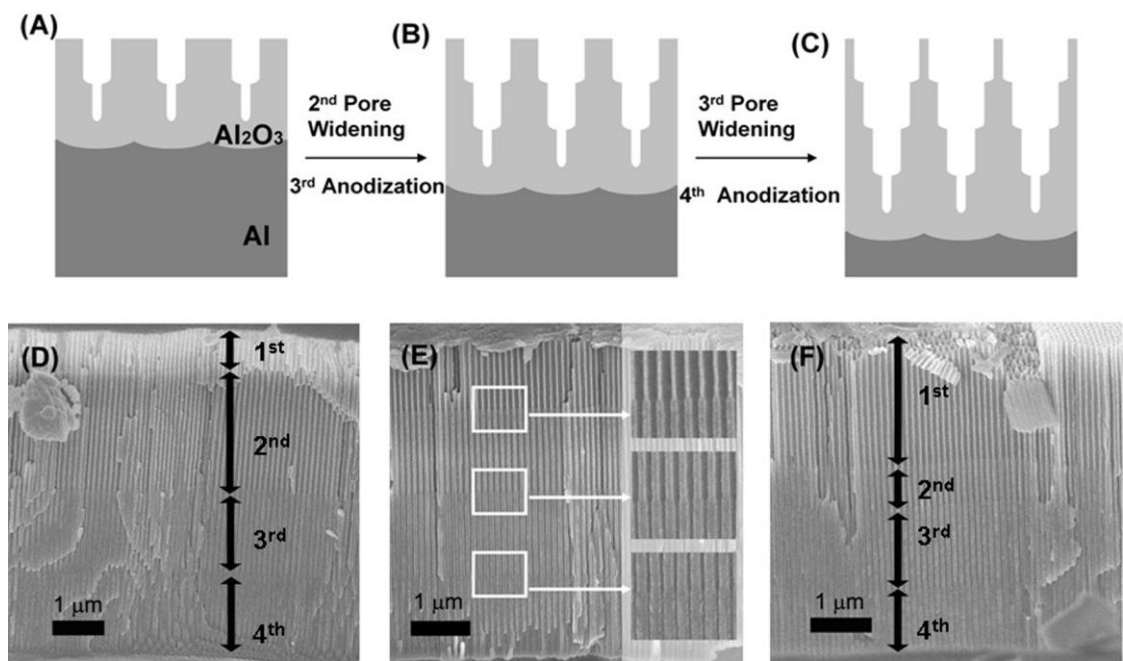


**Figure 3-1.** (A-C) Scheme of the fabrication process of the alumina templates: cross section view of the templates (A) after the second anodization step, (B) after the third anodization step, and (C) after the fourth anodization step. (D-E) FESEM images of the templates T4A, T4B, and T4C, respectively.

**Fabrication of Barcoded SNTs.** Barcoded SNTs were synthesized via a modified surface sol-gel (SSG) method.<sup>77</sup> First, the alumina templates were immersed

in  $\text{SiCl}_4$  (99.8%) solution for 2 min, gently shaken by a rocking platform; second, they were quickly washed by fresh hexane twice and then soaked in another hexane solution for 5 min to remove the unreacted  $\text{SiCl}_4$  molecules. The templates were then placed in a mixture of methanol and hexane (v/v, 2:1) for 5 min and then to ethanol for another 5 min consecutively to replace the hexane on the templates. The templates were then dried with a continuous flow of nitrogen. Finally, the templates were immersed in DI water for 5 min and washed with methanol, and dried completely in a nitrogen stream. The above procedure represents one complete cycle of the SSG process. The number of the performed SSG cycles performed determines the wall thickness of the SNTs. Although the relationship between wall thickness and SSG cycles was not linear from the first cycle, the average growth rate of wall thickness was kept constant at  $0.8 \pm 0.3$  nm per cycle from the 3rd cycle to the 13th cycle. The SNTs were released by dissolving the templates in 25% phosphoric acid overnight.

The number of nanotubes produced at a time is  $3.2 \times 10^{11}$  SNTs from  $16 \text{ cm}^2$  of the template (the pore density =  $10^{10}/\text{cm}^2$ ). For each single immunoassay experiment, only  $1.5 \times 10^5$  to  $3.8 \times 10^6$  SNTs were needed for each shape of nanotube. The number of nanotubes for each shape obtained from a given preparation is enough for 100000 immunoassay experiments.

**Barcoded SNTs Functionalized with Probe IgGs.** First, the  $150 \mu\text{l}$  of SNTs solution ( $3 \times 10^8$  NTs/mL) was treated with  $500 \mu\text{l}$  10% (v/v) glycidyloxypropyltrimethoxysilane (GPTMS) ethanol/water (v/v, 95%/5%) solution for 30 min. The epoxide groups of GPTMS formed covalent bonds with the amine groups of proteins.<sup>80</sup> After washing in a centrifuge at 9000 rpm for three sessions with

500  $\mu$ l of ethanol/water (95%/5%) solution and one time with 500  $\mu$ l of PBS buffer solution (pH 7.4), SNTs were then mixed with 100  $\mu$ l of antirabbit IgG (1mg/mL) at 4  $^{\circ}$ C overnight. The unreacted epoxide groups of GPTMS on the SNTs' surfaces were then passivated by 1% bovine serum albumin (BSA) PBS buffer solution for 2 h. These antirabbit IgG-modified SNTs were then used for quantitative analysis, involved with sandwich immunoassays for detecting rabbit IgG. For multiplexed immunoassays, three shapes of SNTs, SNT1, SNT2 and SNT3 were modified with antirabbit IgG, antimouse IgG, and antihuman IgG, respectively, using the same GPTMS as a linker.

**Reflectance Measurement.** The optical images were taken by a fluorescent microscope (Zeiss, Axioskop2 MAT) with a CCD camera (AxioCam MRm) under dark field. A volume of 5  $\mu$ L of SNT dispersed in water was dropped onto a glass slide (Fisher brand, treated with the piranha solution before use) and dried out in the air before microscope measurement. A volume of 5 $\mu$ l of ethanol was added for better dispersion of the SNTs on the microscope slide. The light source was a mercury vapor short-arc lamp (HBO 100), and exposure time was 300 ms. For samples in reflectance measurement, all optical parameters, including brightness, contrast, were kept consistent. In addition, all images were recorded after the mercury lamp had stabilized (20 min after being tuned on). The reflectance of one silica nanotube or one segment on the SNT was represented by the mean brightness value (named as grayscale value) in gray mode by Adobe Photoshop. The average reflectance value and the standard deviation were calculated based on the reflectance of 15 SNTs under the same experimental conditions.

**Fluorescence Intensity Measurement.** The fluorescence intensity measurement c. The fluorescence images were taken by the same fluorescence microscope above with several Zeiss filter sets in a dark room. For example, filter set 20 (BP546/12, FT560, BP 575-640) was suitable for Alexa Fluor 555 (a superior alternative of Cy3 dye from Invitrogen). After immunoassay experiments, a volume of 5  $\mu$ l of SNTs dispersed in PBS buffer solution (or DI water to show the clear shape of each nanotube for multiplexed immunoassays) was dropped onto a glass slide and dried out in the air before microscope measurement. The light source was a mercury vapor short-arc lamp, and exposure time was 200 ms. The fluorescence intensity on one silica nanotube was represented by the mean brightness value in Adobe Photoshop. The average fluorescence intensity and standard deviation were calculated on the basis of the fluorescence intensities of 10 different SNTs.

**Quantitative Sandwich Assays.** For quantitative analysis, sandwich immunoassays that detect rabbit IgG were performed with respect to three different concentrations of the antirabbit-IgG-modified SNTs solutions ( $1.5 \times 10^6$ ,  $7.5 \times 10^6$ , and  $3.8 \times 10^7$  NTs/mL). First, rabbit IgGs (from 6 pM to 600 nM) were incubated with SNTs at room temperature for 2 h, and unbound rabbit IgGs were then washed with 1% BSA PBS buffer. To a 100  $\mu$ l solution of each sample, 5  $\mu$ l of Alexa Fluor 555 goat antirabbit IgG (H + L) (1mg/mL) was added and incubated for 30 min. Fluorescent images were taken after thoroughly washing with 1% BSA PBS buffer (0.05% Tween 20).

**Multiplexed Sandwich Assays.** Three shapes of SNTs, SNT1, SNT2 and SNT3 modified with antirabbit IgG, antimouse IgG and antihuman IgG, respectively,

were mixed together and the final volume was adjusted to 100  $\mu$ l. The mixed solution was then incubated with 5  $\mu$ l of rabbit IgG (1mg/mL) and 5  $\mu$ l of mouse IgG (1mg/mL) in PBS buffer for 2 h. All buffer solutions contained 1% BSA to reduce nonspecific interactions. Finally, after washing, the mixture of SNTs was incubated with 5  $\mu$ l of Alexa Fluor 555 goat antirabbit IgG (H + L) (1mg/mL), 5  $\mu$ l of Alexa Fluor 555 goat antimouse IgG (H + L) (1mg/mL), and 5  $\mu$ l of Cy3 goat antihuman IgG (1mg/mL), for 30 min. The fluorescent images and optical microscopy images in dark field (for identifying SNTs) were taken after washing with buffer solution and DI water.

Usually, all modifications and incubation procedures were carried out within two days. Immunoassay experiments proved that the antibody-modified SNTs could be kept in PBS buffer solution at 4  $^{\circ}$ C for at least 1 week without loss of affinity to the antigen. The stability of the chemical bonding between the epoxysilane linker and the proteins was reported to be strong enough to survive a series of 100 treatments with 60 s pulses of 50 mM HCl within 12 h continuous running.<sup>89</sup>

**Safety Considerations.** *Perchloric Acid in Electropolishing.* Caution: Perchloric acid is a strong oxidizer. Please check MSDS before handling with it and electropolishing steps must be operated at/below 5  $^{\circ}$ C. Piranha solutions (3:1 mixture of sulfuric acid and 30% hydrogen peroxide) are extremely energetic and may cause explosion or skin burns if not handled with extreme caution. Please check the MSDS and be very careful while handling it.

### 3.3 RESULTS AND DISCUSSION

**Barcoded SNTs Characterization.** Highly uniform SNTs were fabricated by combining the multistep anodization technique and the SSG method. The multistep anodization technique that involves repeated sequential anodization and pore-widening steps can precisely produce well-defined cylindrical pores in the alumina template. The SSG method allows one nanometer or subnanometer control over the wall thickness of the SNT and it is very reliable and reproducible. The SNTs were characterized by TEM, SEM and an optical microscope. Figure 3-2(A-C) represent the TEM images of SNTs, named with S4A, S4B and S4C, fabricated from template T4A, T4B and T4C. The total length of S4A, S4B and S4C is  $6.30 \pm 0.08 \mu\text{m}$  and the outer diameters of the four segments of SNTs are  $96 \pm 4 \text{ nm}$  and  $72 \pm 4 \text{ nm}$ ,  $48 \pm 4 \text{ nm}$  and  $28 \pm 4 \text{ nm}$ , respectively. The four segments' lengths of S4A, S4B and S4C are  $0.8/2.4/1.6/1.6 \mu\text{m}$ ,  $1.6/1.6/1.6/1.6 \mu\text{m}$  and  $2.4/0.8/1.6/1.6 \mu\text{m}$ , respectively. The TEM images show the shapes and tubular structures of SNTs clearly. The FESEM image of S4B also shows the four segments of SNTs (Figure 3-2D). Attractively, not only high-resolution electron microscopy images, but also conventional optical microscope images (Figure 3-2E) show each SNT's shape because of the significant difference in the reflectance values between the four segments on the individual SNT. For suspension arrays, it is very important to make hundreds or perhaps thousands of individually coded particles. The theoretical number of codes for a  $6 \mu\text{m}$  SNT with four segments is 4960 when the optical resolution of the different segments is  $0.2 \mu\text{m}$ .<sup>69</sup> The practical number of codes may be limited by the practical resolution of the microscope and the identification ability of the software which can distinguish the

shape of SNTs. However, the number of codes can be increased by using the longer SNTs or employing new anodization technology to fabricate complex pores structures of alumina templates, such as combination of hard anodization and mild anodization.<sup>90</sup>

In comparison with the SNTs with four segments, the SNTs with two segments (Figure 3-2F) are easier to identify. In the study of SNTs' physical and chemical properties, and their applications in immunoassays, we mainly used the SNTs with two segments, named as SNT1, SNT2, and SNT3, with the segments' length as 0.8  $\mu\text{m}$  and 3.8  $\mu\text{m}$ , 2.3  $\mu\text{m}$  and 2.3  $\mu\text{m}$ , and 3.8  $\mu\text{m}$  and 0.8  $\mu\text{m}$ , respectively. From TEM images analysis, the SNTs' length variation is less than 5% and the wall thickness variation is less than 7% within one batch or from batch to batch with the same protocol.

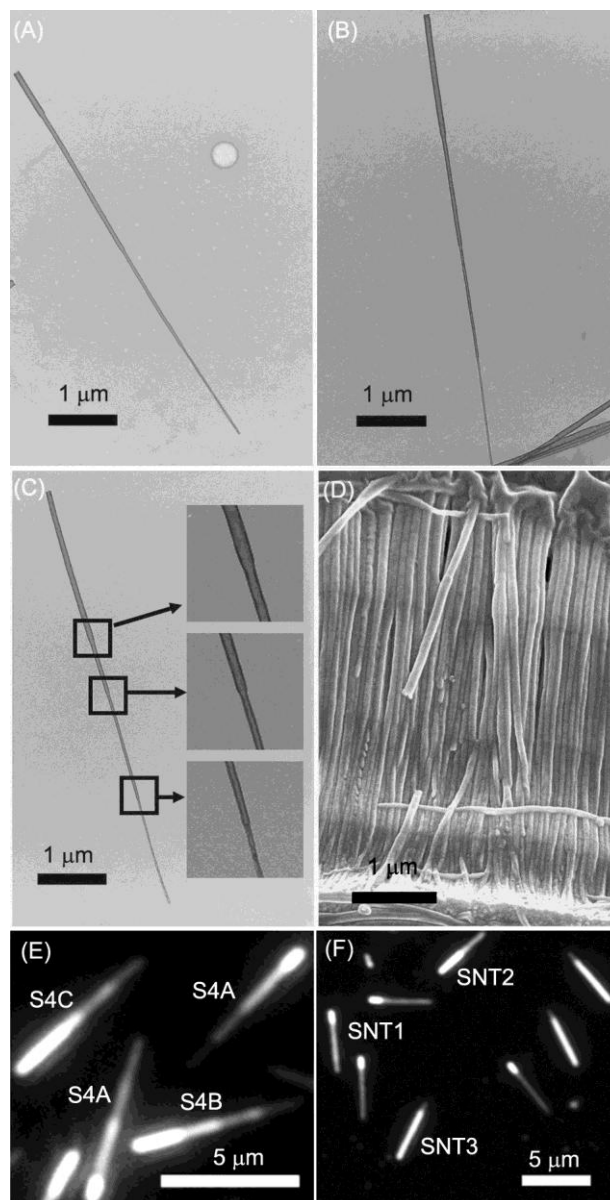


**Figure 3-2.** (A-C) TEM images of S4A, S4B and S4C with the four segments' lengths 0.8/2.4/1.6/1.6  $\mu\text{m}$ , 1.6/1.6/1.6/1.6  $\mu\text{m}$  and 2.4/0.8/1.6/1.6  $\mu\text{m}$ , respectively. (D) FESEM images of S4B. (E) Optical microscopy images of the mixture of S4A, S4B and S4C in dark field, (F) Optical microscopy images of the mixture of SNT1, SNT2 and SNT3 in dark field.

**The Reflectance Value of Barcoded SNTs.** The distinctive optical property of a SNT enables barcoded SNTs to work as coding materials. Basically, the reflectance of each segment depends on its own diameter, wall thickness, and parameters of the microscope. In practice, all parameters of the optical microscope, such as brightness and contrast, were kept constant in one set of experiments. This section focuses primarily on the dependence of reflectance on the diameter of each segment and the wall thickness of the SNTs. Three SNT2 samples with the ratios of the bigger diameter (the segment named as segment  $D_b$ ) to the smaller diameter (the segment named as segment  $D_s$ ) as 1.5, 1.8, and 2.1, respectively (based on TEM images measurement), were detected to get the relationship of the reflectance ratio and the diameter ratio of segment  $D_b$  to segment  $D_s$  (Figure 3-3A). The only difference between the three samples was the combination of the first and second pore widening times, 20 min/20 min, 30 min/10 min, and 40 min/0 min, respectively. The data represented here were based on measurement of 10 SNTs of each sample. As shown in Figure 3-3, the larger difference in diameters between the two segments gives the higher ratio of reflectance, thus better contrast to distinguish the shapes of the SNTs. On the other hand, as shown in the inset images of Figure 3-3, when the second pore widening time was less than 10 min, Segment  $D_s$  on one SNT became less distinguishable from the background. Therefore, we can conclude that the optimized ratio of  $D_b/D_s$  is between 1.5 and 1.8, which corresponds to the ratio of the first pore-widening time to the second one of 1:1 - 1:3.

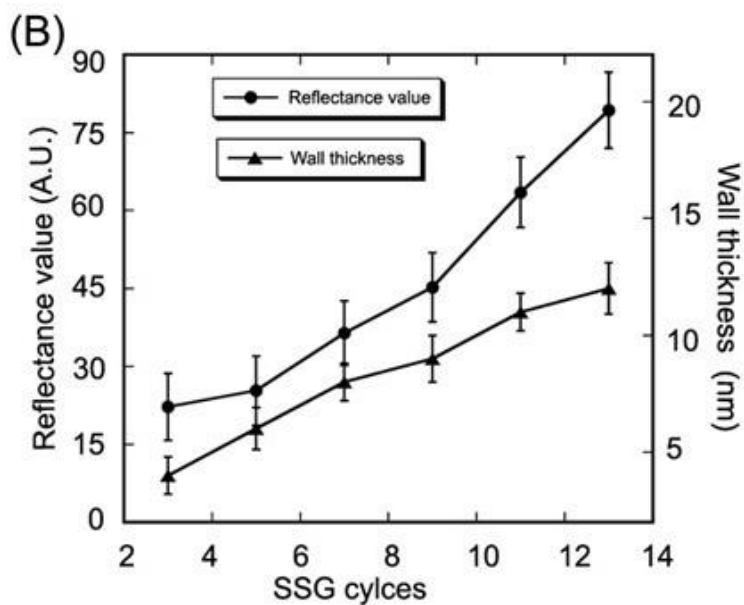
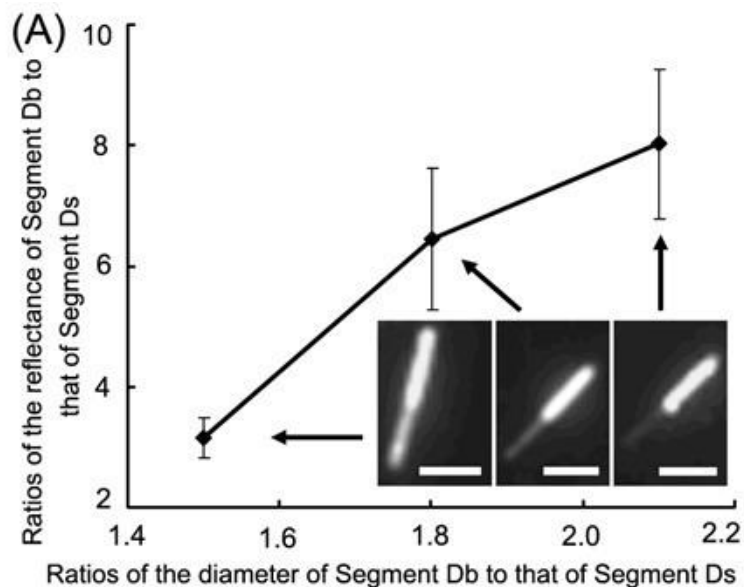


**Figure 3-3.** (A) The relationship of the reflectance difference between the two segments on one silica nanotube (ratios of the reflectance of Segment  $D_b$  to that of Segment  $D_s$ ) vs. their diameters' difference (ratios of the diameter of Segment  $D_b$  to that of the Segment  $D_s$ ). Inserted images: optical microscopy images of SNTs in dark field with the first and second pore widening time as 20 min/20min (left), 30 min/10 min (middle), and 40 min/0 min (right), respectively. Scale bars are 2  $\mu\text{m}$ . (B) the relationship

between the reflectance values/wall thickness of the SNTs and SSG cycles involved to fabricate the SNTs.

TEM and optical microscope analysis were performed on a series of SNTs prepared from 3, 5, 7, 9, 11, and 13 cycles of surface sol-gel (SSG) to exploit the influence of the number of SSG cycles on the reflectance and the wall thickness. The data (Figure 3-3B) based on measurement of 15 nanotubes of each sample demonstrated that the reflectance of SNTs increases with the SNTs' wall thickness. However, after 13 SSG cycles, the connection part between the bigger diameter segment and the smaller diameter segment became clogged sometimes, influencing the homogeneity of the SNTs' shape. Therefore, by considering both their reflectance and shape homogeneity, we used the SNTs with 11 SSG cycles in our research.

**Dispersibility and Stability.** SNTs show great performance in dispersibility in water and PBS buffer solution because the density of silica is low ( $2.17 \text{ g cm}^{-3}$ )<sup>77</sup> and their inner space is hollow. In addition, silica is very stable in aqueous solutions and biocompatible, which makes SNTs good candidates as biomolecules carriers in biomedical research. TEM images of four segmented SNTs show that there is no visible degradation of SNTs in DI water after 7 months. Antibody-modified SNTs also show great stability over 2 months in PBS buffer solution (as shown in Figure 3-4 and Figure 3-5). SNTs are very stable in both DI water and PBS buffer.

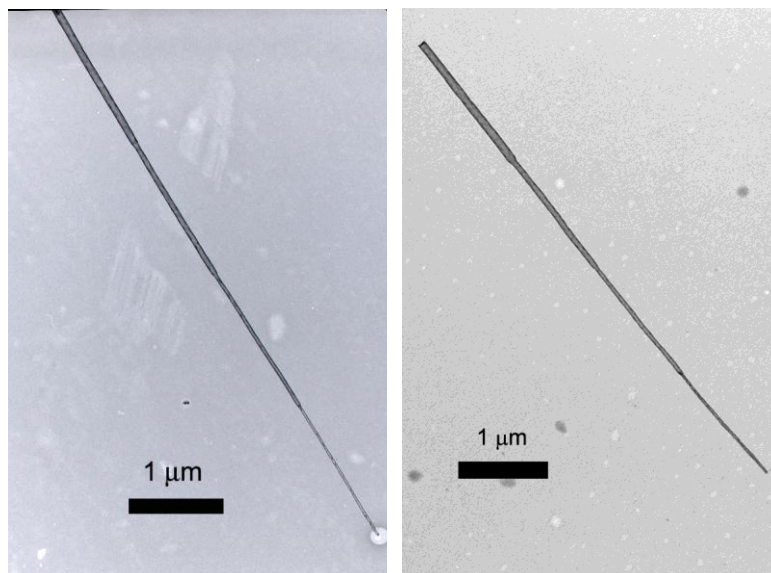


**Figure 3-4.** (left) TEM image of SNTs with four segments (right) SNTs from the same sample in DI water after seven months.

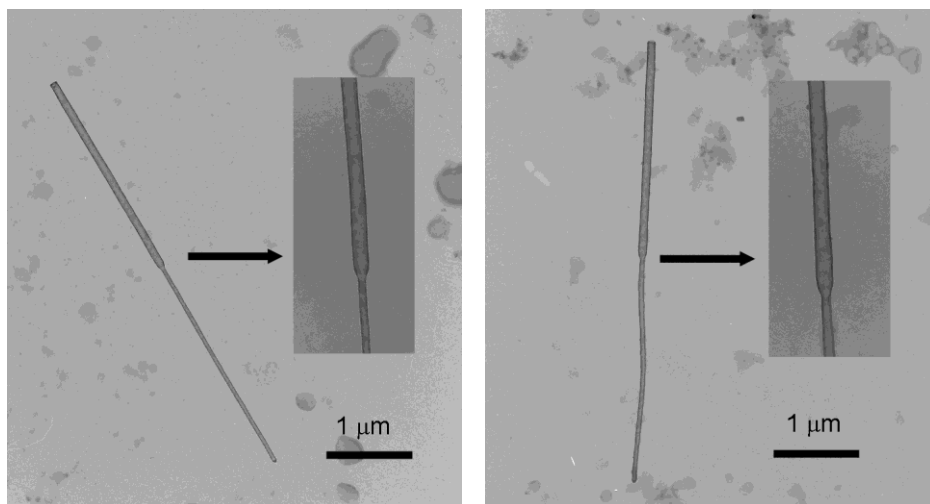


**Figure 3-5.** (left) TEM image of the SNTs with two segments (right) TEM image of the antibody-modified SNTs from the same sample in PBS buffer after two months. The inserted images are the nanotubes at higher magnification (50K).

The motion of SNTs with tubular structures in water is complex, influenced by gravity, viscous drag force (or buoyancy), Brownian motion, van der Waals force and electrostatic interaction between nanotubes. A simple model involving only gravity and viscous drag force was set up by converting one silica nanotube (length 4.6  $\mu\text{m}$ , o.d. 80 nm, i.d. 60 nm, density of silica 2.17  $\text{g cm}^{-3}$ , water in the inner space, thus the calculated nominal average density 1.5  $\text{g cm}^{-3}$ ) into a sphere whose diameter was 353 nm with the same nominal density.<sup>82</sup> From Stokes law, the calculated settling velocity was  $3.4 \times 10^{-6}$  cm/s (0.12 mm/hr). On the other hand, the kinetic random speed of the sphere (diameter 350 nm, density 1.5  $\text{g cm}^{-3}$ ) controlled only by Brownian motion was 1.5 cm/s.<sup>82</sup> These theoretical results suggest that Brownian motion would dominate the behavior of the SNTs, which would stably disperse in the solution and never settle down to the bottom of the vials.

However, the SNT dispersion in water is practically a more complex process that involves van der Waals force and electrostatic interaction between nanotubes. The average sedimentation rate of SNTs in DI water was 8% after 1 h and 15% after 48 h. Even after 144 hours, more than 50% of the SNTs were suspended in the solution (as shown in Figure 3-6).

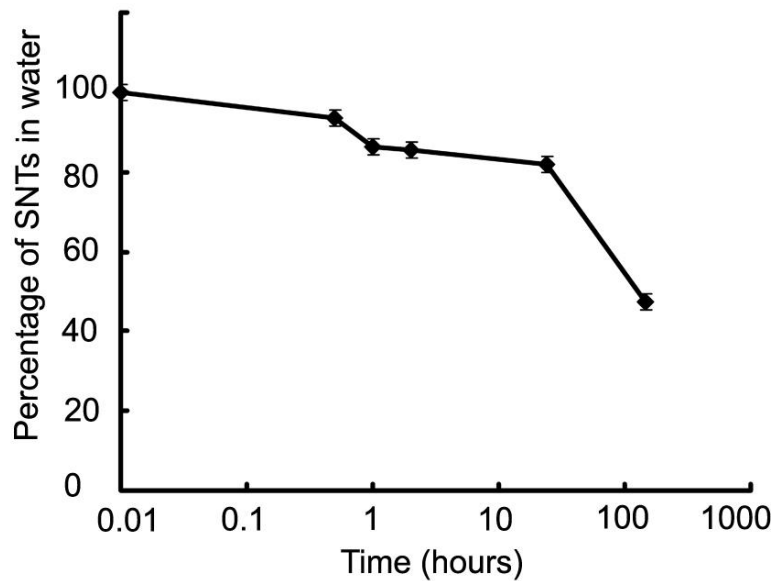


**Figure 3-6.** The sedimentation rate of SNTs in DI water. A volume of 0.5  $\mu\text{l}$  solution was taken ( $2 \times 10^5$  NTs/ml) from the SNTs solution after 0h, 0.5h, 1h, 2h, 24h and 144h, and dispersed on a glass slide. The number of SNTs (about 100) was counted under the optical microscope.

**Quantitative Sandwich Assays.** The sensitivity of the SNT suspension array is affected by the amount of the protein carriers (SNTs), the types of the antibodies (monoclonal or polyclonal), and the detectors (confocal microscope or normal fluorescence microscope). In this study, we exploited mainly the effect of SNT concentration on the sensitivity. Sandwich type immunoassay was performed to detect rabbit IgG in the concentration range of 6 pM to 0.6  $\mu\text{M}$  (Figure 3-7). The result clearly shows that the fluorescence signal intensity increased with the decrease of the number of the SNTs used in the assay. The detection limitation was improved from 600 pM to 6 pM by decreasing the number of SNTs used in the assay from  $3.8 \times 10^7$  NTs/mL to  $1.5 \times 10^6$  NTs/mL.

According to the ambient analyte assay theory, with decreasing the detection area occupied by probe molecules, the total amount of captured analyte IgG begins to decrease, but the signal density begins to increase.<sup>91</sup> This phenomenon is valid if the concentration of probing IgG is smaller than  $0.1/K$ , where  $K$  is the binding constant between analyte IgG and probing IgG. Hence, the maximum signal density can be obtained by reducing detection area, which results in the enhancement in sensitivity.

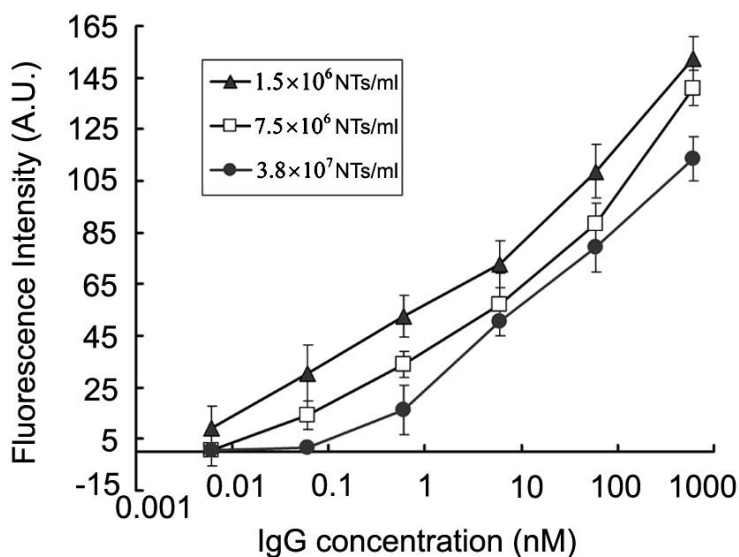


**Figure 3-7.** Diagram of the fluorescence intensity from SNTs vs. the concentration of the analyte (rabbit IgG) in the presence of  $1.5 \times 10^6$  NTs/mL (closed triangles),  $7.5 \times 10^6$  NTs/mL (open squares),  $3.8 \times 10^7$  NTs/mL (closed circles) SNTs.

**Multiplexed Sandwich Assays.** Multiplexed sandwich assays were performed with three different shape SNTs, SNT1, SNT2 and SNT3, modified with three different antibodies individually. Figure 3-8 shows the scheme of the process of the sandwich assay and the microscope images of the resulting mixture of SNT1,

SNT2, and SNT3. In the optical dark field image (Figure 3-8B), the shape of each nanotube can be clearly distinguished. In the designed experiment, there were only two analytes in the solution, rabbit IgG and mouse IgG. Because of the specific binding between IgG and its corresponding antibody, only antirabbit-IgG-bound SNT1 and antimouse-IgG-bound SNT2 would interact with corresponding rabbit IgG and mouse IgG, whereas antihuman-IgG-bound SNT3 would not. Therefore, we can expect that red fluorescence signals will be shown only on SNT1 and SNT2, not on SNT3 after incubation with all three types of red-dye-labeled secondary antibodies. As anticipated, the fluorescence microscope image (Figure 3-8C) revealed that the analytes (rabbit IgG and mouse IgG) bind selectively to the corresponding nanotubes (SNT1 and SNT2) by giving the strong red fluorescence signal only on SNT1 and SNT2. There is no detectable nonspecific interaction between SNT3 and rabbit/mouse IgG (Figure 3-9 for quantitative data). It is practical to design clinical suspension arrays with antibody-bound-SNTs of many different shapes to detect multiple analytes at a time.

As shown in the above multiplexed assay, there is another advantage in barcoded SNTs system: only one dye is necessary in SNTs microarrays because the shapes of the SNTs would identify the types of analytes binding on them. This avoids the fluorescence spectral overlap problem existing in most color encoded particles arrays.

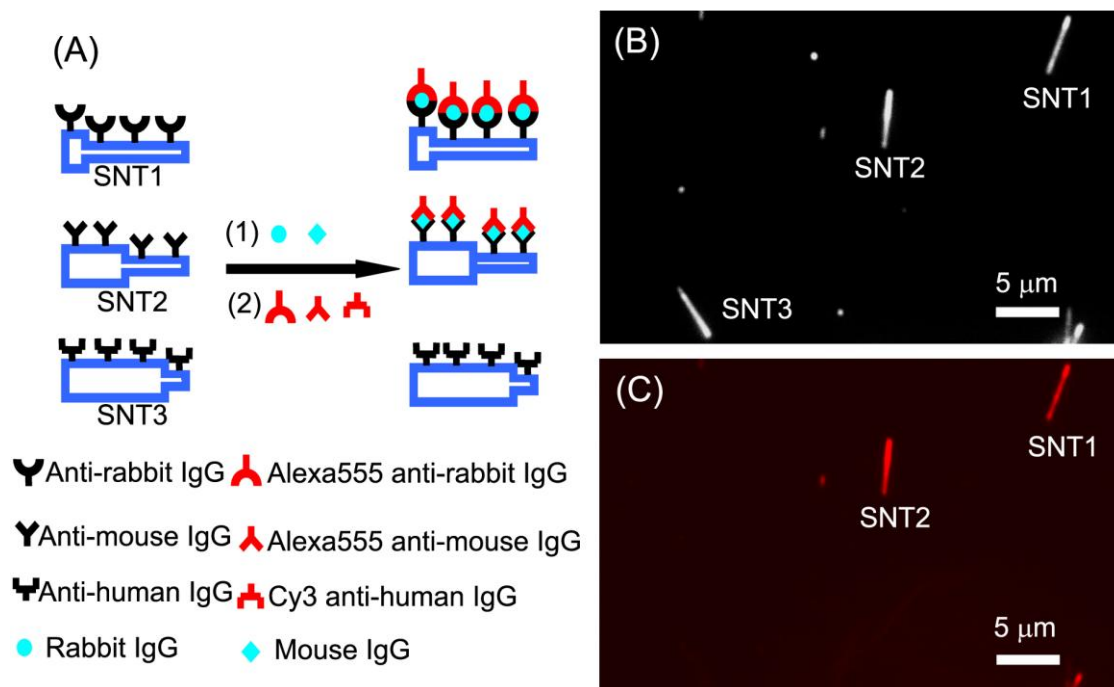


**Figure 3-8.** (A) Scheme of the multiplexed sandwich assay with the mixture of barcoded SNTs, SNT1, SNT2, and SNT3. (B) Optical (in the dark field) and (C) fluorescence microscope images of the mixed SNTs after incubation with the mixture of IgGs (rabbit IgG and mouse IgG) and the mixture of three corresponding red-dye-labeled antibodies.

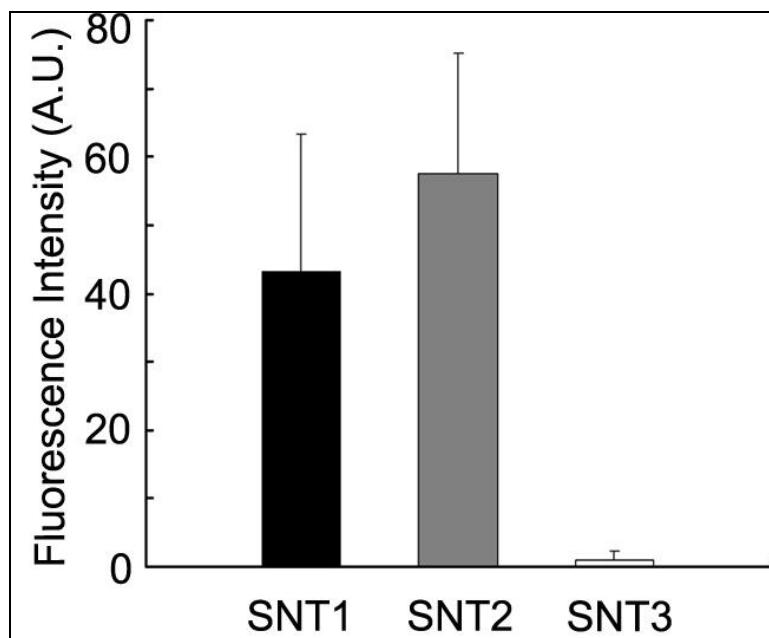


**Figure 3-9.** Average fluorescence intensity from SNT1, SNT2 and SNT3 in the multiplexed sandwich immunoassays.

The specificity experiment with two different fluorescent labels on two secondary antibodies was also performed (as shown in Figure 3-10). As expected, SNT2 nanotubes only showed blue and SNT3 nanotubes only showed red. This experiment proved the specificity of each secondary antibody to its corresponding IgG. In other words, there is no nonspecific between antimouse IgG (or anti-rabbit IgG) with rabbit IgG (or mouse IgG).

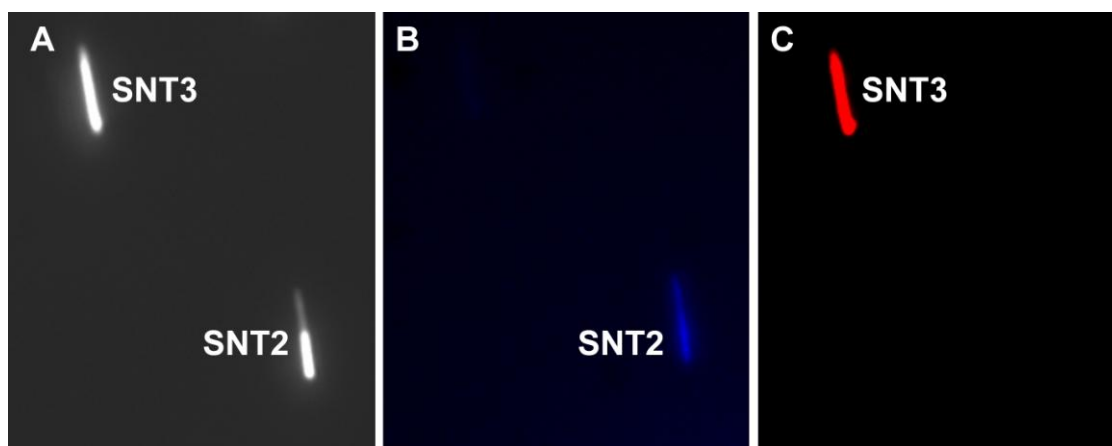
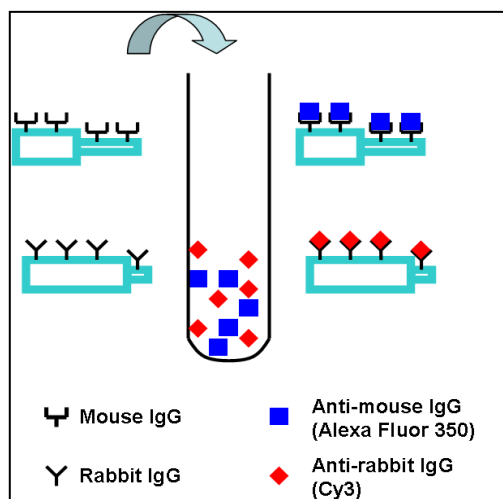


**Figure 3-10.** The specificity experiment with two different fluorescent labels on each secondary antibody. (Upper) Scheme of multiplexed immunoassay performed with the mixture of barcoded SNTs, SNT2 and SNT3 nanotubes. The SNT2 nanotubes and SNT3 nanotubes were modified with mouse IgG and rabbit IgG respectively. (Lower) (A) Optical (in the dark field), and (B & C) fluorescence microscope images of the mixed SNTs passed by blue filter set and red filter set respectively after incubation with the mixture of antibodies, Cy3 antirabbit IgG (red) and Alexa Fluor 350 antimouse (blue).

### 3.4 CONCLUSION

Barcoded SNTs in suspension arrays for multiplexed bioassays were fabricated by template synthesis method. The multistep anodization technique

successfully synthesized well-defined cylindrical pores with four different diameter segments on the aluminum foil. Each shape of the SNTs prepared from the template represented one biomolecular code because it could be easily distinguished by the reflectance and the length of each segment on this nanotube under a conventional optical microscope. The SNTs are highly suspension in aqueous solution because of their tubular structures, and have been stable in DI water without any visible degradation for 7 months. The multiplexed immunoassay experiments have demonstrated the high selectivity of the SNTs array for the detection of multi-analytes. Quantitative analysis has been optimized by decreasing the number of nanotubes involved in the assay. With decreasing the concentration of SNTs as low as  $1.5 \times 10^6$  SNTs/mL in assay, the sensitivity of the assay has been enhanced and analyte IgG was successfully detected at 6 pM concentration. However, the number of nanotubes used in assay has to be decreased and optimized further to get better sensitivity. The barcoded SNTs provide a solution for the problems that current suspension arrays have, such as spectral overlap, quenching of fluorescence signals and degradation of materials.

### **3.5 ACKNOWLEDGEMENT**

This work was supported by the National Institutes of Health, University of Maryland, College Park, and the Laboratory for Physics Science.

# **Chapter 4: Barcoded Silica Nanotubes Coupled with Magnetic Bead Separation for Bioassays**

## **4.1 INTRODUCTION**

In the previous chapters, we successfully fabricated barcoded SNTs by using multistep anodization template synthesis, and applied them in suspension arrays for detection and quantitative analysis of target proteins. Filtration and centrifugation are the main technologies to separate and wash the mixtures. Although they work well and obtain high sensitivity, it is difficult to combine them with microchip technology for rapid, integrated, and automatic detection and screening of biomolecules.

Magnetic field separation is one promising alternative to filtration or separation by centrifugation. It provides rapid, gentle, reliable and reproducible isolation of target analytes, and is easily adapted to automated platforms, such as microchips or microplates. Combining barcoded SNTs with microchips will make barcoded SNT technology not only a novel concept in the labs, but also a powerful tool for basic research and clinical practice. There are two strategies for employing magnetic field separation in barcoded SNT suspension arrays. One way is to couple barcoded particles with commercially available magnetic beads (MBs), the other way is to endow these barcoded SNTs themselves with superparamagnetic properties. This chapter will focus on the first technique and next chapter will introduce the second strategy, in which barcoded magnetic nanotubes (BMNTTs) are fabricated and applied in bioanalysis.

Reliable commercially available MBs are selected to be coupled with barcoded SNTs. The MBs are superparamagnetic polymer microbeads, which are embedded with iron oxide nanoparticles in their matrices. MBs provide a platform for rapid capturing, enrichment, and isolation of target analytes in the samples.<sup>67, 92-94</sup> Spherical MBs have a large surface area per volume, provide fast reaction kinetics in solutions in comparison with filtration and centrifugation. MBs have been applied for isolating bacteria,<sup>95, 96</sup> and for removing environmental toxins such as heavy metals and chemical waste.<sup>97, 98</sup>

MBs have also been employed in sandwich immunoassays for the detection and screening of biological species by using fluorophore-labeled reporter antibodies. However, a major problem in using MBs for these assays is that the beads' autofluorescence strongly interferes with the reporter molecules' fluorescence signal. In addition, the fluorescence signal of organic dyes may have other problems, like low intensity, broad emission spectra and poor photostability.

For the purpose of solving the above problems, we use antibody-modified barcoded SNTs as reporter signals to replace the fluorescence-labeled antibodies. The barcoded particles are very stable and easily dispersed evenly in a buffer solution. In our strategy, first, two (or three) types of antibody-modified barcoded SNTs are mixed with the biotinylated analytes. The target proteins in the analyte solution will be captured by the specific SNTs which are modified with their corresponding antibodies. Then, the mixture is incubated with the streptavidin-coated MBs. Because of streptavidin-biotin binding, the barcoded SNTs that are bound with target biotinylated proteins (named as target SNTs) will interact with MBs and be isolated

from the mixture by magnetic field separation. After that, the interaction between the target SNTs and MBs is broken in acid solution, and the SNTs are separated and collected. The barcodes on the target SNTs represent the species of analytes, and the numbers of the target SNTs quantify these analytes. The barcode information of these SNTs can be “read-out” directly with a conventional optical microscope, as well as the numbers of the SNTs. No complex instruments are required for both barcode identification and signal detection. Barcoded SNTs suspension arrays coupled with separation by MBs overcome the drawbacks in fluorescence signal arrays, and allow simple, gentle, and rapid separation and detection of target biological species.

## 4.2 EXPERIMENTAL SECTION

**Materials.** Silicon tetrachloride ( $\text{SiCl}_4$ , 99.8%, Acros Organics), oxalic acid (dehydrate, Acros), o-phosphoric acid (85%, Fisher), chromic acid (10%, W/C, LabChem, Inc), ethanol (Pharmco-AAPER), 3-glycidyloxypropyltrimethoxysilane (95%, TCI America), hexane (Fisher), methanol (Fisher), and perchloric acid (70%, Fisher) were used as supplied without further purification. Aluminum foils (99.99%) were purchased from Alfa Aesar. Deionized (DI) water was obtained by a Milli-Q A10 system. Phosphate-buffered saline (pH 7.4, PBS), bovine serum albumin (BSA), N-Hydroxysuccinimidobiotin (NHS-biotin), mouse IgG, bovine IgG, rabbit IgG, goat antimouse IgG, goat antirabbit IgG, mouse monoclonal antibovine IgG, and mouse monoclonal antirabbit IgG were obtained from Sigma-Aldrich. Alexa Fluor 555 goat antirabbit IgG (H+L) and streptavidin-coated MBs: Dynabeads MyOne Streptavidin

C1 (diameter 1  $\mu\text{m}$ ) and Dynabeads M-280 Streptavidin (diameter 2.8  $\mu\text{m}$ ), were purchased from Invitrogen, Inc., Carlsbad CA.

MBs (Dynabeads Myone Streptavidin C1 and Dynabeads M-280 Streptavidin) are uniform, superparamagnetic, polymer beads with a monolayer of streptavidin covalently attached to the bead surface. When MBs are used in combination with a biotinylated probe/ligand, any target molecule can be captured, isolated and further manipulated. The specific surface areas of these MBs are 4-8  $\text{m}^2/\text{g}$  and their density is 1.4  $\text{g}/\text{cm}^3$ . Streptavidin-coated Dynabeads is the gold standard for isolation and handling of biotinylated antibodies, nucleic acids or other biotinylated ligands and targets. The very high binding affinity of the streptavidin-biotin interaction is utilized in a vast number of molecular applications. The beads have a monolayer, not a multilayer, of recombinant streptavidin. This leaves the vast majority of the biotin binding sites sterically available for binding, not only of free biotin, but also for binding of biotinylated ligands/targets. The absence of excess physically adsorbed streptavidin ensures that only a negligible amount of streptavidin will be able to leak. Batch-to-batch variability is minimized, and the reproducibility is optimized.

**Measurement.** Barcoded SNTs and MBs were characterized by a transmission electron microscope (TEM, Zeiss EM10CA) and fluorescence microscope (Zeiss, Axioskop 2 MAT) with a CCD camera (AxioCam MRm). MBs were separated by BioMag multi-6 microcentrifuge tube separator (PolySciences, Inc.)

**Fabrication of Barcoded SNTs.** Barcoded SNTs were fabricated by template synthesis and the “surface sol-gel” (SSG) method, as described in Chapter 3. Briefly,

the alumina templates with multisegment cylindrical pores were fabricated by a multistep anodization technique. Then sub-nanometer-thick silica layers were deposited on the walls of these pores cycle-by-cycle by the SSG method. The length, diameter, and wall thickness of each SNT can be controlled in single nanometer scale. Three shapes of barcoded SNTs, name as SNT1, SNT2, and SNT3, were fabricated with the length ratio of larger diameter (75 nm) segments to smaller diameter (45 nm) segments as 1:5, 1:1, and 5:1, respectively. The total length of each SNT was 4.6  $\mu\text{m}$ .

**Barcoded SNTs Functionalized with Probe IgGs.** First, the 100  $\mu\text{l}$  of SNTs solution ( $3 \times 10^8$  NTs/mL) was treated with 500  $\mu\text{l}$  10% (v/v) glycidyloxypropyltrimethoxysilane (GPTMS) ethanol/water (v/v, 95%/5%) solution for 30 min. The epoxide groups of GPTMS formed covalent bonds with the amine groups of proteins.<sup>25</sup> After washing in a centrifuge at 9000 rpm for three sessions with 500  $\mu\text{l}$  of ethanol/water (95%/5%) solution and one time with 500  $\mu\text{l}$  of PBS buffer solution (pH 7.4), SNT2 and SNT3 nanotubes were then mixed with 100  $\mu\text{l}$  of antimouse IgG (1mg/mL) and antirabbit IgG (1mg/mL) at 4°C overnight, respectively. The unreacted epoxide groups of GPTMS on the SNTs' surfaces were then passivated by 1% bovine serum albumin (BSA) PBS buffer solution for 2 h. These antibody- modified SNTs were then used for detecting rabbit IgG.

**Analyte IgGs Functionalized with Biotins.** Biotinylated proteins were obtained by reacting N-Hydroxysuccinimidobiotin (NHS-biotin) with IgGs in a standard procedure<sup>99</sup> provided by Sigma-Aldrich with minor modification. First, IgG PBS buffer solution was washed 4 times with carbonate buffer (0.1 M sodium carbonate buffer pH 9.5) in a filtered microcentrifuge tube. After that, protein

concentration was adjusted to 10 mg/mL. NHS-biotin was dissolved in DMSO immediately prior to use with a concentration of 10 mg/mL. Then IgG solution and NHS-biotin solution were mixed together with the volume ratio as 10:1, and incubated at room temperature for four hours. Finally, the mixture was washed thoroughly with PBS buffer (pH 7.4), and the biotinylated antibody was stored at -20 °C.

**Barcoded SNTs Coupled with MBs for Protein Detection in Immunoassays.** As shown in Figure 4-1, two types of barcoded SNTs solutions, SNT2 and SNT3, which were modified with antimouse IgG and antirabbit IgG, were mixed together and the final volume was adjusted to 100  $\mu$ l. The mixed solution was then incubated with 10  $\mu$ l of target biotinylated proteins, such as biotinylated rabbit IgG (1mg/mL), in PBS buffer for 2 h. After centrifugation to remove the unreacted proteins, the mixture of SNTs was incubated with 25  $\mu$ l MBs with a final volume of 1 mL in a microcentrifuge tube at room temperature for 30 min with gentle shake. Then, the mixture of MBs binding with SNTs was isolated on the walls of the microcentrifuge tubes by BioMag multi-6 microcentrifuge tube separator, and the supernatant was discarded. The mixture was redispersed in 1mL buffer solution. By magnetic field separation, the mixture was washed 4 times with PBS buffers and 4 times with DI water. The unbound SNTs were removed by washing with PBS buffer for 4 times. All PBS buffer solutions contained 1% BSA to reduce nonspecific interactions. In the next elution step, the binding interaction between target SNTs and MBs was broken in 12.5% phosphoric acid solution overnight. Finally, MBs were separated by the magnet and the SNTs in the supernatant were collected. Images of

the final SNTs were taken by the optical microscope after thoroughly washing with DI water by filtration. The types and numbers (more than 100 in each experiment) of barcoded SNTs were identified and counted in the optical images.

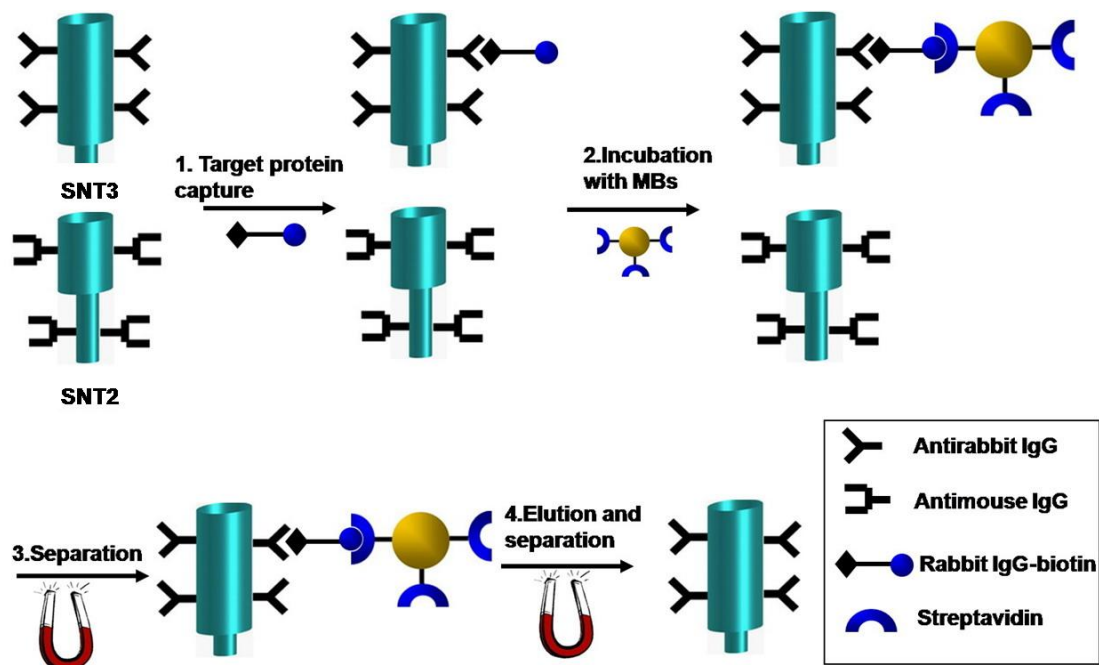


**Figure 4-1.** Scheme of the principle of barcoded SNTs coupled with MB separation for target protein detection.

**Quantitative Sandwich Assays.** For quantitative analysis, three types of barcoded SNTs: SNT1 ( $3 \times 10^5$  NTs/mL), SNT2 ( $3 \times 10^8$  NTs/mL) and SNT3 ( $3 \times 10^8$  NTs/mL), were modified with biotin, monoclonal antibovine IgG, and monoclonal antirabbit IgG, respectively. SNT1 nanotubes was first modified with 3-aminopropyltriethoxysilane (APTS),<sup>32</sup> and then with NHS-biotin. Three SNTs solutions, each with volume of 100  $\mu$ L, were mixed together to a final volume of 100

$\mu\text{l}$ . Then, the solution mixture was incubated with target proteins: biotinylated rabbit IgGs (from 0.6 nM to 60 nM) at room temperature for 2 h. The following separation and target SNTs collection procedures are same with the above experiments for protein detection.

#### **4.3 RESULTS AND DISCUSSION**

**Illustrations of Interaction between Barcoded SNTs and MBs.** The immunoassays were performed with only SNT3 nanotubes to detect the interaction between barcoded SNTs and MBs. First, antirabbit IgG modified SNT3 nanotubes were incubated with biotinylated rabbit IgG for 2h. After thoroughly washing, SNTs with biotin groups on the surface were incubation with MBs, which are covalently attached with a monolayer of streptavidin on their surface. The optical images of MBs in PBS buffer with a sealed cover slide were taken before and after their incubation with SNTs. As shown in Figure 4-2, before the incubation, MBs were dispersed randomly and separately in PBS buffer solution. However, after the incubation with the barcoded SNTs that were coated with biotinylated IgGs, these streptavidin-modified MBs were assembled in groups with the number of 2 to 10. These images proved that there was interaction between SNTs and MBs caused by streptavidin-biotin binding. Unfortunately, it was not easy to get SNTs images with clear shapes when they interacted with MBs in PBS buffer. There may be three reasons: first, MBs are much brighter than SNTs; second, the refractive index of SNTs and that of PBS buffer solution is very close; third, Brownian motion of SNTs in aqueous solution makes it difficult to take a still image, especially in dark field.

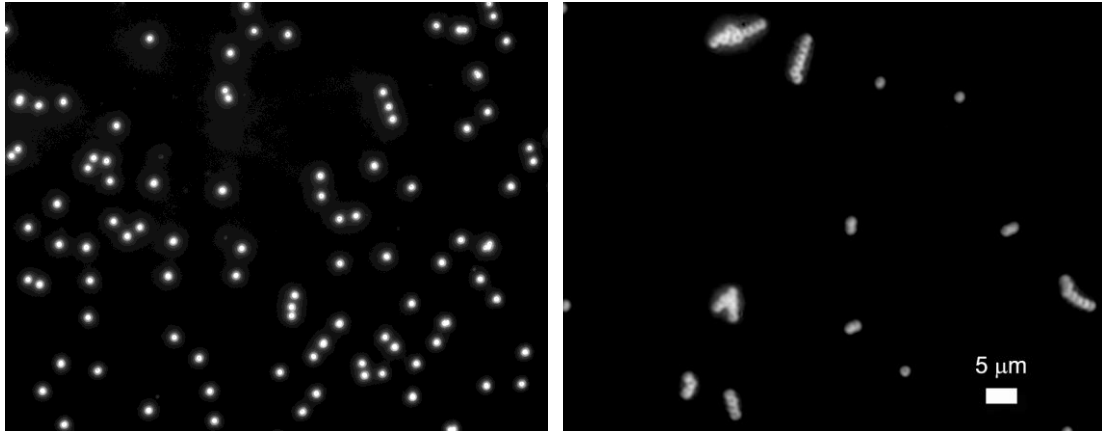


**Figure 4-2.** Optical microscope images of streptavidin-coated MBs interact with biotin bound SNTs in dark field. Only MBs in PBS buffer solution (left); after incubation with SNTs (right).

To further prove that there was interaction between MBs and SNTs, we modified SNTs with Alexa Fluor 555 (red) goat antirabbit IgG. The red dye antirabbit IgG modified SNTs were first incubated with biotinylated rabbit IgG, then with MBs. The optical and fluorescent images are shown in Figure 4-3 after incubation of MBs with SNTs. From fluorescent images, we can figure out that the assembling of MBs was caused by their interaction with SNTs because of streptavidin-biotin binding. Optical and TEM images (Figure 4-4) of MBs and SNTs in the same area further demonstrate this result. Therefore, target SNTs with analytes can separated and collected by their interaction with these superparamagnetic MBs.

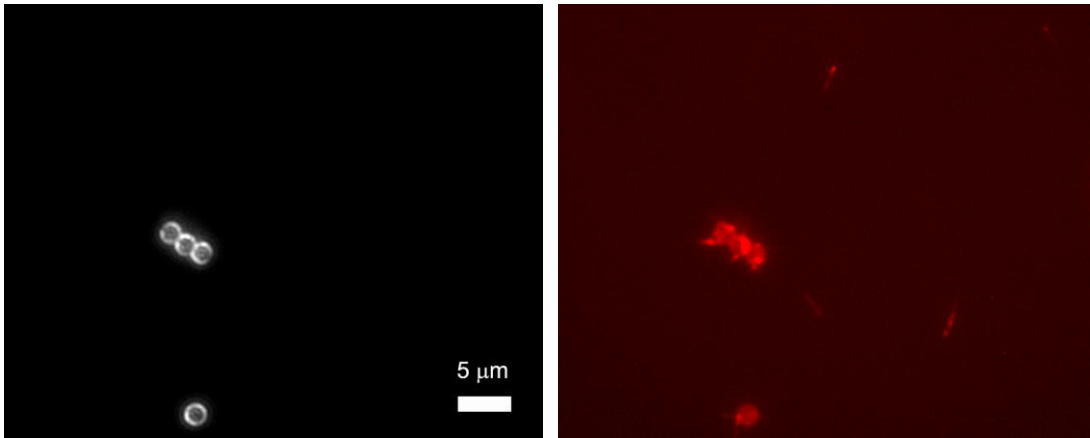


**Figure 4-3.** Images of barcoded SNTs interacting with MBs. (A) optical image in dark field (B) fluorescent image of SNTs and MBs in PBS buffer. The red dye antirabbit IgG modified SNTs were first incubated with biotinylated rabbit IgG, then with MBs.

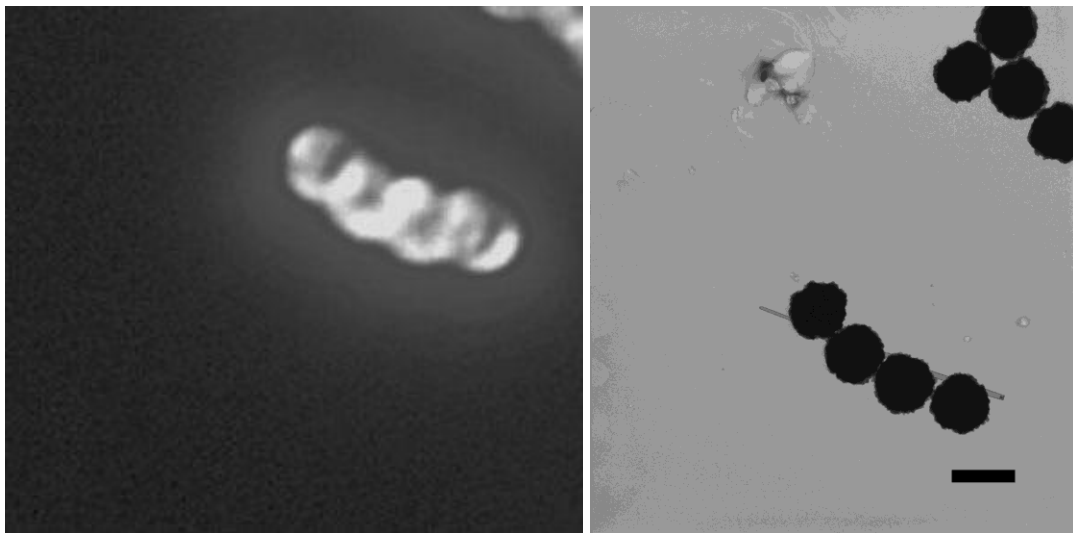


**Figure 4-4.** (A) Optical image in dark field (B) TEM image of SNTs interacting with MBs in the same area on an index grid where the position of each mesh is labeled with letters and numbers. The scale bar is 2 μm.

### **Selectivity Values of Barcoded SNTs Coupled with MBs Suspension**

**Arrays.** In this paper, the selectivity value of the barcoded SNTs coupled with MBs suspension array is defined as the ratio of the number of target barcoded SNTs that are modified with analyte specific antibody to that of nonspecific barcoded SNTs, which were modified with other type of antibodies. The types and numbers (more than 100 in each experiment) of barcoded SNTs were identified and counted in the optical images. We used two types of barcoded SNTs, SNT2 and SNT3 in the protein detection assays coupled with MBs. To optimize the conditions, we investigated the effects of surface modification on the nonspecific SNTs, types of antibodies on SNTs, and amount of MBs to the selectivity values of the assays.

To study the influence of surface modification, we modified SNT2 nanotubes with nothing, BSA, and antimouse IgG, respectively. Then they were mixed with the same amount of SNT3 nanotubes which were bound with antirabbit IgG in three groups. After incubation with biotinylated rabbit IgG and MBs (1  $\mu\text{m}$ ), the MBs bound SNTs were separated by magnetic field and collected after elution. The types and numbers (more than 100) of barcoded SNTs were counted by the optical images. The selectivity values of these three groups were calculated as the ratio of the number of SNT3 to that of SNT2. The result is shown in Table 4-1. The selectivity percentage means that the percentage of target SNTs (SNT3) among all the collected SNTs. The modification on nonspecific SNT2 nanotubes influenced the selectivity values. When the structure of proteins on the SNT2 nanotubes became close to that of the specific antibody, nonspecific binding between the analytes and these proteins will increase, and thus the selectivity of Group 3 was lower than that of Group 2, and much lower

than that of Group 1. Therefore, the selectivity value can be increased by increasing the structure difference between the surface modification on the target SNTs and that on the nonspecific SNTs.

**Table 4-1.** The effect of different surface modifications on selectivity values.

<b>Group</b>	<b>1</b>	<b>2</b>	<b>3</b>
Modification on SNT2	Bare	BSA	Antimouse IgG
Modification on SNT3	Antirabbit IgG	Antirabbit IgG	Antirabbit IgG
Analytes	Rabbit IgG	Rabbit IgG	Rabbit IgG
<b>Selectivity value</b>	<b>30.0</b>	<b>7.7</b>	<b>5.0</b>
Selectivity percentage	96.8%	88.5%	83.3%

Next, we investigated the effect of the types of antibodies on the selectivity value of the assays. We designed two assays in Group 4 and Group 5: one was performed with polyclonal antibodies on barcoded SNTs and the other with monoclonal antibodies. The result is shown in Table 4-2. The selectivity values can be increased by using monoclonal antibodies instead of polyclonal ones because the former can decrease the nonspecific binding between the analyte, rabbit IgG, with the SNT2 nanotubes. Therefore, we used monoclonal antibodies modified on SNTs in all the next assays.

**Table 4-2.** The effect of the types of antibodies on selectivity values.

<b>Group</b>	<b>4</b>	<b>5</b>
Modification on SNT2	Polyclonal antibovine IgG	Monoclonal antibovine IgG
Modification on SNT3	Polyclonal antirabbit IgG	Monoclonal antirabbit IgG
Analytes	Rabbit IgG	Rabbit IgG
<b>Selectivity value</b>	<b>5.1</b>	<b>8.4</b>
Selectivity percentage	83.6%	89.4%

The effect of the amount of MBs to the selectivity values of the assays was also researched. The selectivity value increased 1.6 times when the MBs volume increased from 25  $\mu\text{l}$  to 200  $\mu\text{l}$ . That may be because the more MBs are in the solution, the more target SNTs will bind with MBs. In summary, the selectivity value of barcoded SNTs coupled with MBs suspension array can be increased by increasing the structure difference of surface modification on the SNTs, using high specific antibodies, and adding more MBs.

**Table 4-3.** The effect of the volume of MBs on selectivity values.

<b>Group</b>	<b>8</b>	<b>9</b>	<b>10</b>
Volume of MBs	25 $\mu\text{l}$	100 $\mu\text{l}$	400 $\mu\text{l}$
<b>Selectivity value</b>	<b>8.1</b>	<b>8.6</b>	<b>12.8</b>
Selectivity percentage	89.1%	89.6%	92.7%

**Quantitative Analysis of Target Proteins.** The quantitative analysis experiments were performed by using the optimized conditions as shown above: monoclonal antibodies and large volumes of MBs. SNT2 and SNT3 nanotubes were modified with monoclonal antibody IgG and monoclonal antirabbit IgG,

respectively. For accurately monitoring biotin-streptavidin binding, SNT1 nanotubes which were modified with only biotin were added into the mixture of SNT2 and SNT3. The concentration of SNT1 nanotubes was only 1/1000 as that of SNT2 or SNT3 to minimize the effect of SNT1 bound biotin to the streptavidin-coated MBs. Immunoassays were performed to detect biotinylated rabbit IgG at the concentration of 0, 0.6, 6 and 60 nM (Figure 4-5). The results clearly showed that the number of target SNT3 increased with the increase of the concentration of the analyte. The number of target SNT3 was about ten times higher than that of non-target SNT2, in other words, the selectivity percentage or the accuracy of this detection strategy is about 92.9%. Thus, we can use the barcoded SNTs coupled with MBs for protein detection and quantitative analysis in immunoassays.

There was nonspecific interaction between SNT2 and MBs. It may be caused by the nonspecific binding between antibodies on SNTs and the analyte proteins, or by MBs separation process where the three dimensional MBs net trapped SNT2 nanotubes. Interestingly, from the data we found that the number of the nonspecific SNT2 was also increased with the increase of the concentration of biotinylated rabbit IgG, however, the number of biotin modified SNT1 was almost same in all the assays. Therefore, most of the interaction between SNT2 and MBs was caused by the nonspecific binding between monoclonal antibody and rabbit IgG.

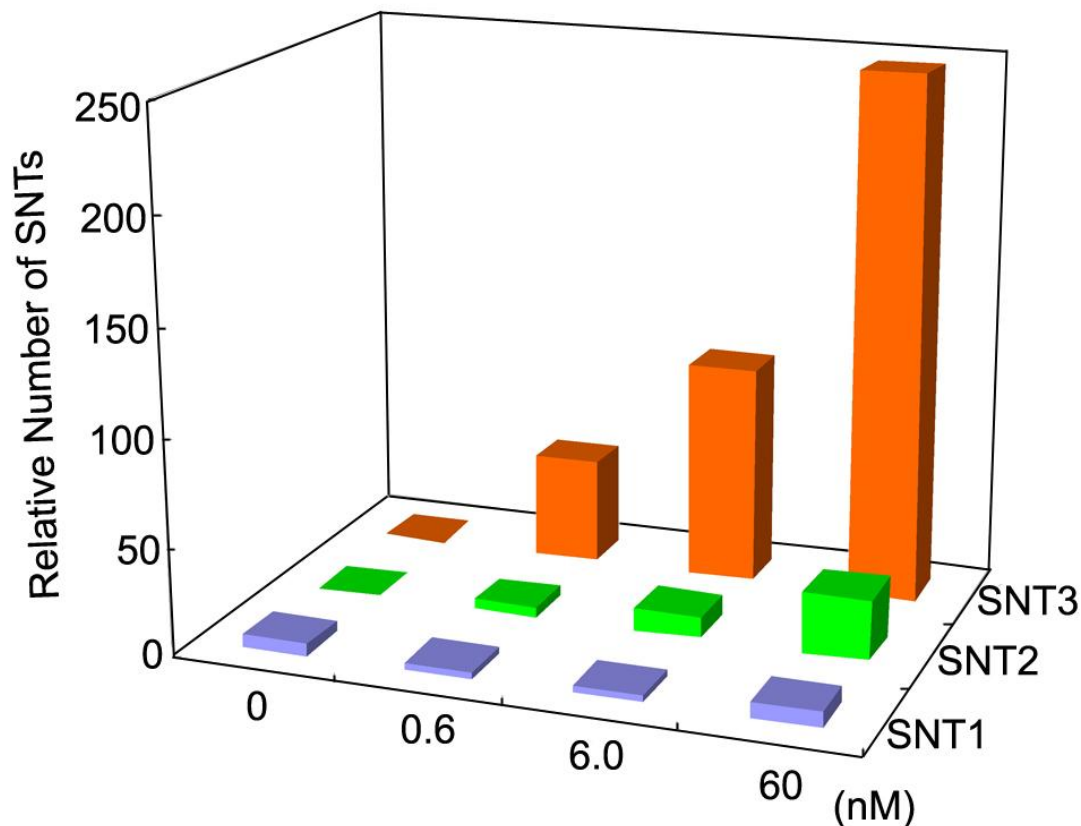


**Figure 4-5.** Diagram of the relative number of SNTs vs. the concentration of the analyte protein. SNT3, SNT2 and SNT1 nanotubes were modified with specific antibody, nonspecific antibody and only biotin, respectively. SNT1 was a control group with 1/1000 amount as that of SNT3.

**Images of SNTs Taken After Elution.** The interaction between the SNTs and MBs was broken in acid solution by destroying antibody-analyte binding. Final SNTs were collected in the supernatant after MBs separation in magnetic field. Filtration was one method to concentrate and wash SNTs in DI water. The images of the SNTs collected by filtration were shown in Figure 4-6. The barcoded shapes of SNTs can be clearly identified in the dark field after SNTs were dried on the slides in the air. Filtration method is reliable and reproducible. However, it is difficult to combine

filtration with microchip technology for integrated and automatic protein analysis by using barcode SNTs coupled with MBs.

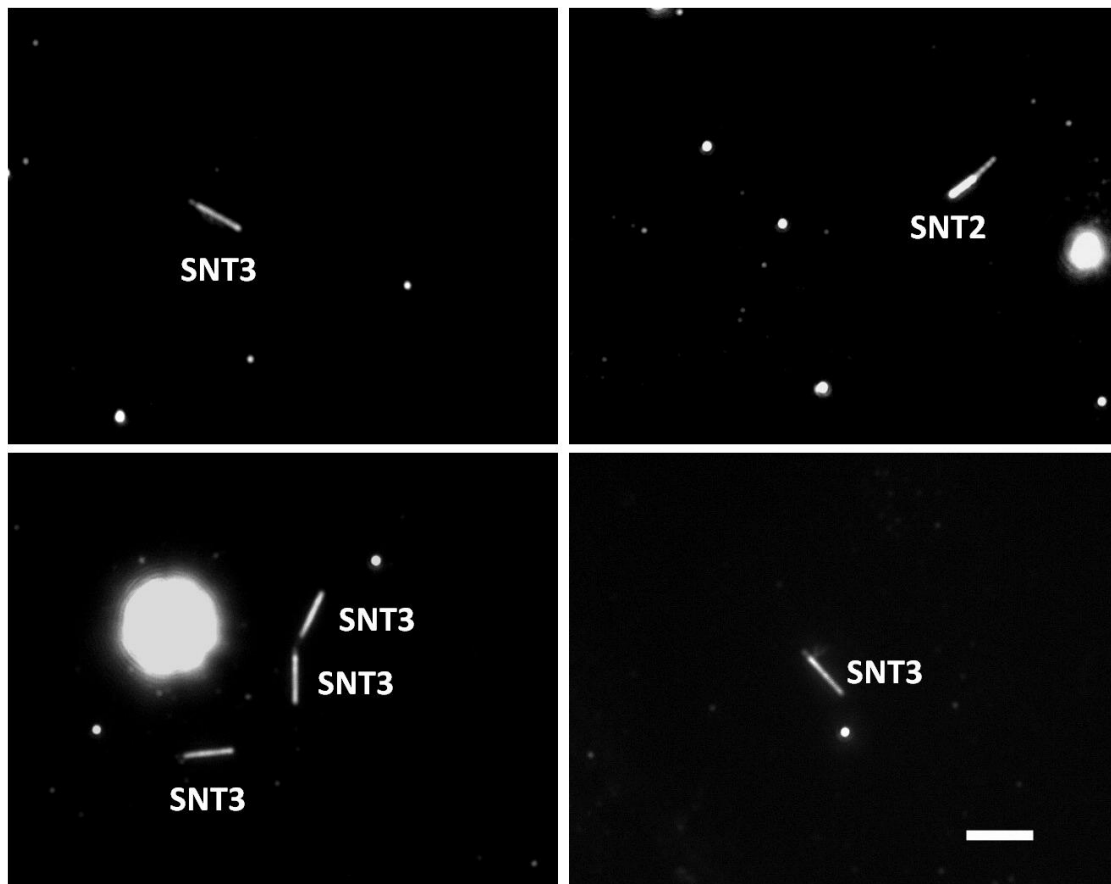


**Figure 4-6.** Optical images of final SNTs dried in the air after being collected and washed in DI water solution by filtration. The scale bar is 5  $\mu\text{m}$ .

Interestingly, we found that barcoded SNTs in the bubbles of PBS buffer solution showed distinct shapes without any influence of salts or bright MBs. The figures of SNTs in bubbles before incubation with MBs and after elution in acid solution were shown in Figure 4-7. This may be because the bubbles were filled with saturated vapor and SNTs can show clear shapes in the vapor instead of buffer

solutions. The ratio of numbers of SNT2 to that of SNT3 in the bubbles was the same with the ratio of these nanotubes dried in the air washed by DI water with filtration. To take images in bubbles may be an alternative to record images after filtration, and it provides an effective imaging method to be combined with microchip technology for rapid and automatic separation and detection.

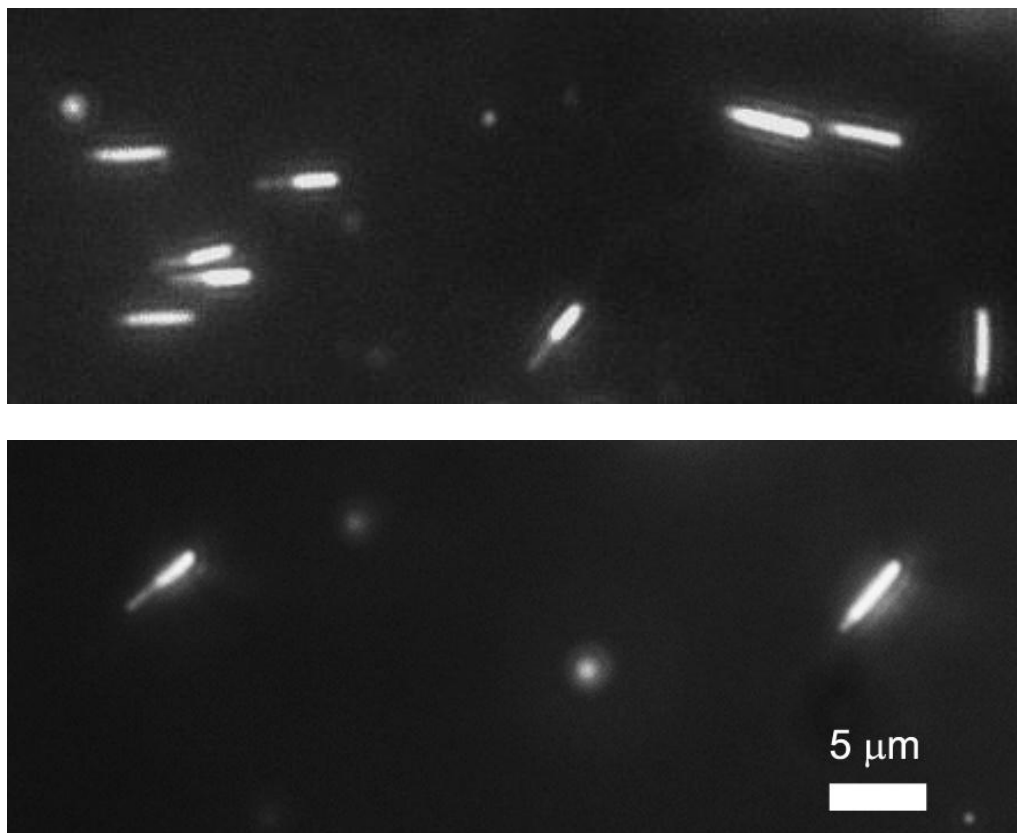


**Figure 4-7.** Images of the mixture of SNTs in the *bubbles* of PBS buffer before incubation with MBs (upper), and after elution of MBs in acid solution (lower).

#### **4.4 CONCLUSION**

Suspension arrays on the basis of combination of barcoded SNTs with MBs separation have been developed for fluorescence-free protein detection and analysis. The species and numbers of the final collected SNTs represent the types and amount of analyte proteins in the samples. Barcoded information can be easily “read-out” with a conventional optical microscope and no complex instruments are needed. By using barcoded SNTs as signals instead of fluorescence, these suspension arrays avoid fluorescence quenching and interference of MBs’ autofluorescence problems. In addition, magnetic field separation is mild, rapid, and effective. It is a great alternative of filtration or centrifugation separation. Selectivity values in the assays have been optimized by using proper surface modification, monoclonal antibodies and increasing the number of MBs. The quantitative analysis results demonstrated that the number of target SNTs quantified the concentration of analyte proteins. However, selectivity is still needed to be improved by using highly specific antibodies. Suspension arrays of barcoded SNTs coupled with MBs separation showed great potential to be combined with microchip technology for rapid, automatic, and integrated detection and analysis of multiplexed analytes biomolecules, such as proteins, DNA and cancer markers.

#### **4.5 ACKNOWLEDGEMENT**

This work was supported by the National Institutes of Health, University of Maryland, College Park, and the Laboratory for Physics Science.

# **Chapter 5: Barcoded Magnetic Nanotubes: Dual-Functional Microcarriers for Multiplexed Immunoassays and Cancer Marker Detection**

## **5.1 INTRODUCTION**

Magnetic particles have been extensively studied in the field of biomedical and biotechnological applications, including drug delivery, biosensors, chemical and biochemical separation and concentration of trace amounts of specific targets, such as bacteria or leukocytes, enzyme encapsulation, and contrast enhancement in magnetic resonance imaging (MRI).<sup>71, 100, 101</sup> In most applications, spherical nanoparticles have been used. However, spherical magnetic nanoparticles still need to be improved for controlling particle sizes, surface functionalizations, and their environmental compatibility due to the structural limitation of spherical particles when multifunctionality is required on their surfaces.

Since Martin and co-workers have demonstrated the differential functionalization of SNTs,<sup>72, 74</sup> tubular structure of nanoparticles has become highly attractive for the multifunctional nanoparticles due to their structural attributes, such as the distinctive inner and outer surfaces, over conventional spherical nanoparticles. Inner voids can be used for capturing, concentrating, and releasing species ranging in size from large proteins to small molecules because tube dimensions can be easily controlled by the template synthesis. Distinctive outer surfaces can be differentially functionalized with environment-friendly and/or probe molecules to a specific target. Therefore, by combining the attractive tubular structure with magnetic property, the

magnetic nanotube (MNT) can be an ideal candidate for the multifunctional nanomaterial toward biomedical applications, such as targeting drug delivery with MRI capability. In the Reference 32, we describe the synthesis of MNTs and their applications for magnetic-field-assisted chemical and biochemical separations, immunobinding, and drug delivery.

In this chapter, a novel type of MNTs, named as barcoded magnetic nanotubes (BMNTTs), have been successfully fabricated by embedding iron oxide nanocrystals into the inner voids of barcoded SNTs. BMNTTs combine the shape variety of barcoded SNTs (introduced in Chapter 2 and 3) and superparamagnetic properties of MNTs as dual-functional microcarriers for multiplexed immunoassays, and cancer biomarkers optical detection and magnetic separation. The commercially available single shape magnetic beads (MBs) can only detect or separate one analyte at one time, and the present barcoded particles do not have the ability to enrich and separate the analytes.<sup>38, 39,40</sup> In addition, the existing multi-functional particles, such as mesoporous silica beads embedded with semiconductor QDs and iron oxide nanocrystals, still suffer from the signal intensity attenuation induced by doping iron oxide in their matrices.<sup>102</sup>

BMNTs overcome the problems in the existing dual-functional particles. The iron oxide nanocrystals are evenly dispersed in the inner void of the tubular structures without interference with the optical barcoded patterns. BMNTs have a large surface area per volume, providing very rapid reaction kinetics compared to filters, plates and tubes. BMNTs have realized to detect, enrich and separate multiplexed analytes at the same time. In addition, BMNTs have the advantages of both barcoded SNTs and

MNTs: high stability and dispersibility, a large number of barcodes, and simple identification process. By using dual-functional BMNTs, the assay time will be shortened and procedures will be simplified. Magnetic field separation of BMNTs has several excellent advantages over tedious filtration or centrifugation separation. It provides rapid, convenient, gentle, reliable and reproducible isolation of target analytes, and is easily adapted to automated platforms, such as microchips or microplates.

## 5.2 EXPERIMENTAL SECTION

**Materials.** Silicon tetrachloride ( $\text{SiCl}_4$ , Aldrich), iron (II) chloride ( $\text{FeCl}_2 \cdot 4\text{H}_2\text{O}$ , Aldrich), iron (III) chloride ( $\text{FeCl}_3 \cdot 6\text{H}_2\text{O}$ , Alfa Aesar), oxalic acid (Fisher), perchloric acid (70%, Fisher) were used as supplied without further purification. Alexa Fluor 350 goat antimouse IgG (H + L) (heavy chains and light chains), Alexa Fluor 555 goat antimouse IgG (H + L), Alexa Fluor 555 goat antirabbit IgG (H+L), and Alexa Fluor 488 carboxylic acid, 2,3,5,6-tetrafluorophenyl ester (Alexa Fluor 488 5-TFP) were purchased from Invitrogen. Phosphate-buffered saline (pH 7.4, PBS), bovine serum albumin (BSA), mouse IgG, rabbit IgG, human IgG, goat antihuman IgG, goat antimouse IgG, goat antirabbit IgG, and Cy3 goat antihuman IgG were obtained from Sigma-Aldrich. Monoclonal antibody (MAb) to Alpha Fetoprotein (MAb AFP) with catalog number of H45301M and H45610M, MAb to Carcinoembryonic Antigen( MAb CEA) with catalog number of MAM02-008 and MAM02-009, Carcinoembryonic Antigen (CEA) were bought from Meridian Life Science. Alpha Fetoprotein (AFP) was purchased from United States Biological.

**Measurement.** BMNTs were characterized by transmission electron microscopy (TEM, Zeiss EM10CA) and fluorescence microscopy (Zeiss, Axioskop 2 MAT) with a CCD camera (AxioCam MRm). BMNTs were isolated in a microcentrifuge tube by BioMag multi-6 microcentrifuge tube separator (PolySciences, Inc.)

**Multisegment Alumina Templates Synthesis.** Alumina templates with multisegment pores were prepared according to Chapter 2 (Figure 2-1). Briefly, preannealed aluminum sheets (0.5mm thick) were degreased in acetone, then electropolished in a 1:5 volume mixture of  $\text{HClO}_4$  and ethanol at 5 °C and 15 V. Preanodization was conducted in a 0.3 M oxalic acid solution for 15~20 h at 10 °C and 40 V, then the resultant aluminum oxide layer was subsequently removed using a solution of phosphoric acid (6 wt%) and chromic acid (1.5 wt%) at 60 °C. After that, the first anodization was performed at 40 V for the desired time, followed by the first pore widening step with 0.1 M phosphoric acid solution at 38 °C for 20 min to expand the pore diameter. The first layer of cylindrical regular pores was formed on the surface of aluminum foil. Under the same conditions, the second anodization was performed, followed by a corresponding pore widening step (for 20 min), produced the second smaller pores consecutively below the bigger pores of the first layer. Anodization time determines the length of each segment within the pore. Two templates, named as T2 and T3 (Figure 2-2), were fabricated with anodization times of 30/30min, and 50/10 min, respectively.

**BMNTs Synthesis.** BMNTs (BMNT2 and BMNT3) were fabricated by using the homemade multisegment alumina templates, T2 and T3. The fabrication process

was as shown in Figure 5-1. A layer of silica was deposited on the walls of templates by the “surface sol-gel” method,<sup>32, 77</sup> which can control the wall thickness in single nanometer scale. Then, magnetic nanoparticles and nanocrystals were loaded by two different procedures.

The magnetic nanoparticles loading was following the process as described in the references.<sup>32, 103</sup> In brief, silica-coated templates were dipped in a 2:1 volume mixture of 1 M FeCl<sub>3</sub> and 2 M FeCl<sub>2</sub>, dried in an argon stream, immersed in 1M NH<sub>4</sub>OH for 5min, and washed thoroughly with deionized water. The reaction was shown in Figure 5-1. The magnetic nanocrystals were loaded following our group member Xia Bai’s MNTs fabrication process.<sup>104-106</sup> In brief, 0.027 g FeCl<sub>3</sub>, 0.025 g CH<sub>3</sub>COONa, and 1 mL H<sub>2</sub>O were mixed in 50 mL propanediol solution. The silica-coated templates were immersed in half volume of the mixture of for 1 h with sonication. Then, the templates were put into the other half of the mixture solution for 2 h with reflux at 230 °C. After loading of magnetic nanoparticles/nanocrystals, the surface coating materials were polished away. Finally, after dissolving the alumina templates in 0.1 M NaOH for 1h, free BMNTs were released.

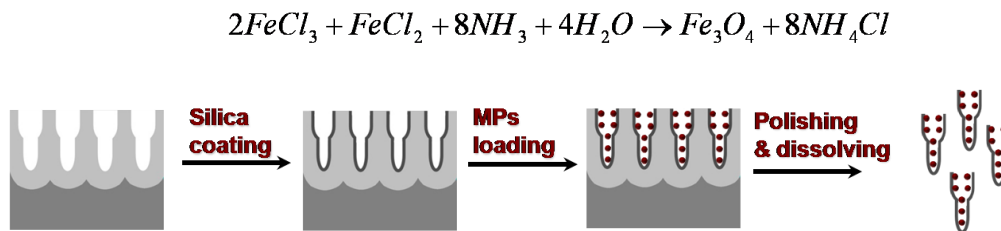


**Figure 5-1.** Schematic diagram for the fabrication of the BMNTs by using the homemade multisegment alumina templates.

**Monoclonal Antibodies Functionalized with Amine-Reactive Probes.** For cancer marker detection, MAb CEA and MAb AFP were modified with Alexa Fluor 488 5-TFP (Green) as probes proteins. The labeling protocol was following the procedure provided by the producer with minor change.<sup>107</sup> First, MAb PBS buffer solution was washed 4 times with carbonate buffer (0.1 M sodium carbonate buffer pH 9.0) in a filtered microcentrifuge tube. After that, protein concentration was adjusted to 5 mg/mL. Alexa Fluor 488 5-TFP was dissolved in DMSO immediately prior to use with a concentration of 5 mg/mL. Then, MAb solution and Alexa Fluor 488 5-TFP solution were mixed together with the volume ratio as 10:1, and incubated at room temperature for 1 hour with continuous stirring. Finally, the mixture was washed thoroughly with PBS buffer (pH 7.4), and the Alexa Fluor 488 conjugated MAbs were stored at -20° C.

**BMNTs Functionalized with Probe IgGs.** First, the 100  $\mu$ l of BMNTs solution ( $3 \times 10^8$  BMNTs/mL) was treated with 500  $\mu$ l 10% (v/v) glycidyloxypropyltrimethoxysilane (GPTMS) ethanol/water (v/v, 95%/5%) solution for 30 min. The epoxide groups of GPTMS formed covalent bonds with the amine groups of proteins.<sup>80</sup> After washing in a centrifuge at 9000 rpm for three sessions with 500  $\mu$ l of ethanol/water (95%/5%) solution and one time with 500  $\mu$ l of PBS buffer solution (pH 7.4), BMNTs were then mixed with 100  $\mu$ l of antibodies(1mg/mL) at 4 °C overnight. The unreacted epoxide groups of GPTMS on the SNTs' surfaces were then passivated by 1% bovine serum albumin (BSA) PBS buffer solution for 2 h. These antibodies-modified BMNTs were then used for IgG protein detection, multiplexed immunoassays, and cancer marker detection.

**Proteins Detection and Multiplexed Immunoassays.** A volume of 100  $\mu\text{L}$  ( $3.0 \times 10^8$  NTs/mL) BMNT2 and BMNT3 nanotubes were first modified with mouse IgG and rabbit IgG, respectively. Then they were mixed together and the final volume was adjusted to 1 ml in a microcentrifuge tube. The mixture solution was then incubated with analyte solution in PBS buffer for 2 h. For protein detection experiment, the analyte sample is 10  $\mu\text{l}$  Alexa Fluor 555 goat antirabbit IgG (1mg/mL). For multiplexed immunoassays, the analyte solution is 10  $\mu\text{l}$  of Alexa Fluor 555 goat antimouse IgG (1mg/mL) and 10  $\mu\text{l}$  Alexa Fluor 555 goat antirabbit IgG. All buffer solutions contained 1% BSA to reduce nonspecific interactions. Then, BMNTs were isolated on the walls of the microcentrifuge tubes by BioMag multi-6 microcentrifuge tube separator for 4 min, and the supernatant was discarded. BMNTs were resuspended in 1mL buffer solution. By magnetic field separation, the mixtures of BMNTs were washed 4 times with PBS buffers and 4 times with DI water. Finally, optical microscopy images in dark field (for identifying BMNTs) and fluorescence images (for detect proteins) were taken after drying 5  $\mu\text{l}$  BMNTs solution on a glass slide in the air.

**Cancer Marker Detection.** Sandwich assays were performed with BMNT2 and BMNT3 nanotubes for cancer markers AFP detection. The process of assays was following the procedure to detect IgGs as describe above with minor changes. First, a volume of 100  $\mu\text{L}$  ( $3.0 \times 10^8$  BMNTs/mL) BMNT2 and BMNT3 nanotubes were modified with MAb AFP and MAb CEA, respectively. Then, the mixture of BMNT2 and BMNT3 was incubated with 5  $\mu\text{l}$  AFP (1 mg/mL) solution with final volume as 1mL for 2 h. The BMNTs mixture was isolated by magnetic tube separators and

washed with PBS. Next, the BMNTs were incubated with 40  $\mu$ l Alexa Fluor 488 MAb AFP (1mg/mL) and Alexa Fluor 488 MAb CEA (1 mg/mL) solution for 1 h. Finally, optical and fluorescence microscope images of BMNTs were taken after washing them thoroughly with PBS buffers and DI water by magnetic separation.

**Identification Software.** The shapes of barcoded SNTs have been identified by naked eyes and their fluorescence intensity have been analyzed by Adobe Photoshop. The automated identification process of the acquired images was also performed by the custom image processing software: **NBSee**, which is developed by Nanoplex Technologies Inc. (now Oxonica Inc.),<sup>108</sup> with courtesy of Professor Keating in Pennsylvania State University.

### 5.3 RESULTS AND DISCUSSION

**BMNTs Fabrication and Characterization.** Multisegment alumina templates were fabricated by multistep anodization technique.<sup>69, 82</sup> Silica layers were deposited on the walls of templates by “surface sol-gel” method,<sup>32, 77</sup> which can control the wall thickness in a single nanometer scale. BMNTs have been fabricated by loading magnetic nanoparticles or nanocrystals into the inner voids of the templates. After the surface coating materials were polished away and selectively dissolving the alumina templates, free BMNTs were released in DI water.

TEM images of BMNTs (Figure 5-2B and C) show clearly that the magnetic nanoparticles and nanocrystals are coated on the inner surface of the nanotubes, whereas bare SNTs have only smooth tubular wall surfaces (Figure 5-2A). Because the saturation magnetizations of BMNTs loaded with magnetic nanocrystals are

higher than those of BMNTs with magnetic nanoparticles (Xia's data), we applied the former in all the assays. Both of these two BMNTs are superparamagnetic.<sup>32</sup>

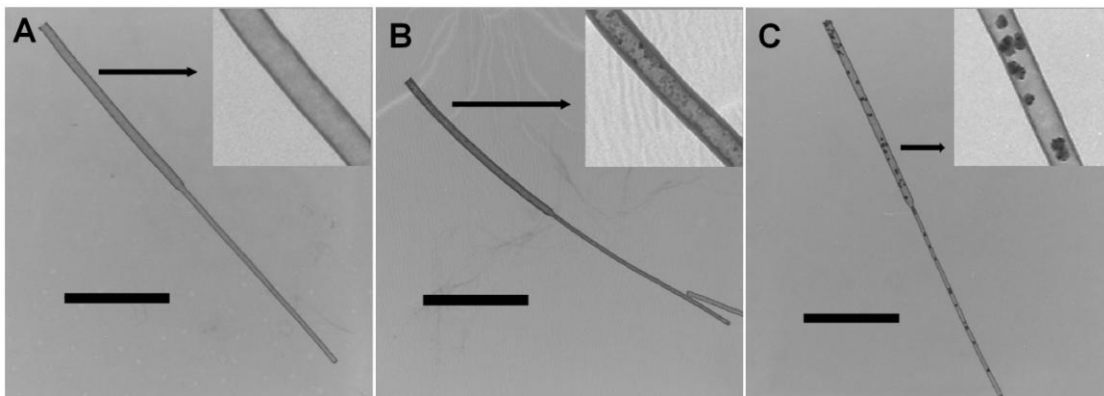


**Figure 5-2.** TEM images of (A) bare SNT2 and (B, C) BMNT2 nanotubes. There is nothing inside the SNT2 nanotubes. Magnetic nanoparticles (B) and nanocrystals (C) are loaded in the inner voids of BMNTs. The scale bar is 1  $\mu\text{m}$ .

For multi-functional particles, it is very important that the loaded magnetic nanocrystals will not influence the barcoded patterns. BMNTs have realized to dope iron oxide nanocrystals inside without interfere with the optical barcoded patterns. As shown in Figure 5-2C, the magnetic nanocrystals are evenly dispersed in the inner voids of the tubular structures. The optical microscope images of SNTs and BMNTs (Figure 5-3) further demonstrate that BMNTs can show clearly distinguishable patterns without any signal intensity attenuation.

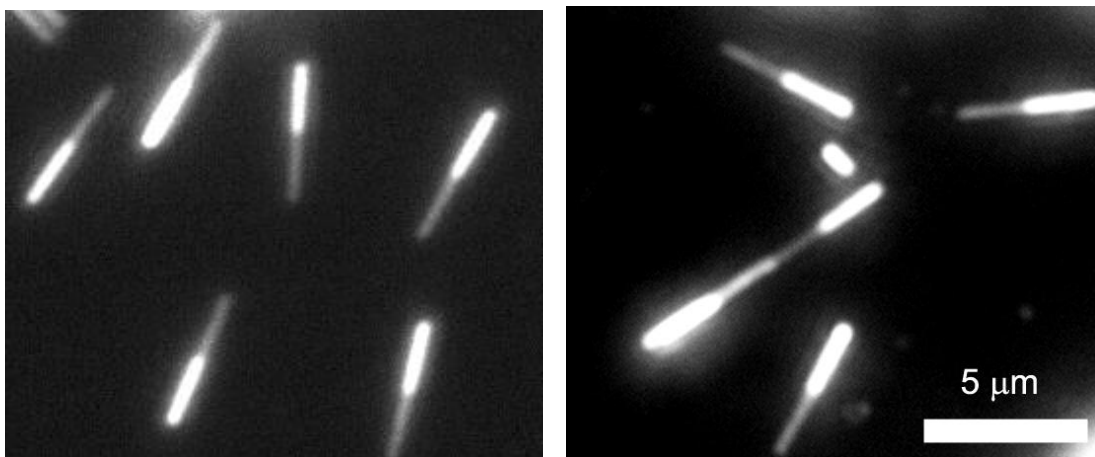


**Figure 5-3.** The comparison of optical microscope images of SNT2 (left), and BMNT2 nanotubes (right).

**Magnetic Field Separation.** Because BMNTs exhibit superparamagnetic properties, we use magnetic separation instead of filtration or centrifugation separation. As shown in Figure 5-4 B and C, most of BMNTs have been isolated on the walls of the microcentrifuge tubes by BioMag multi-6 microcentrifuge tube separator after only 2-3 minutes. The mixture in Tube 1 is for protein detection assays and the mixture in Tube2 is for multiplexed assays. Then the supernatant is discarded and BMNTs are redispersed in buffer solution.

Magnetic separation is more rapid than filtration or centrifugation. As described in Chapter 3, it takes 20 min to settle most of SNTs down to the bottom of microcentrifuge tubes by centrifuge washing. In addition, magnetic separation is a gentle process of isolating particles from supernatant without any strong force which may destroy barcoded particles, like large pressures existing in filtration or centrifugation. Therefore, the assay time will be shortened and procedures will be simplified by using magnetic field to separate the dual-functional BMNTs. Magnetic

field separation of BMNTs provides rapid, convenient, gentle, reliable and reproducible isolation of target analytes, and is easily adapted to integrated automated platforms, like microchips or microplates.



**Figure 5-4.** Photos of magnetic field separation of BMNTs. (A) before and (B and C) after magnetic field separation with BioMag multi-6 microcentrifuge tube separator. The mixture solution in Tube 1 is for protein detection assays and the mixture in Tube 2 is for multiplexed assays.

**Proteins Detection and Multiplexed Immunoassays.** Proteins detection and multiplexed assays have been carried out with BMNT2 and BMNT3 nanotubes which are modified with mouse IgG and rabbit IgG, respectively. Figure 5-5 shows the scheme of the assay for Alexa Fluor 555 (red) antirabbit IgG detection and the microscope images of the resulting mixture of BMNT2 and BMNT3. All the BMNTs isolation and washing steps are accomplished by magnetic field separation. In the optical dark field image (Figure 5-5B), the barcode of each nanotube can be clearly distinguished. Because of the specific binding between IgG and its corresponding antibody, only rabbit-IgG-bound BMNT3 would interact with corresponding red-dye-antirabbit IgG, whereas mouse-IgG-bound BMNT2 would not. Therefore, we can expect that red fluorescence signals will be shown only on BMNT3, not on BMNT2.

As anticipated, the fluorescence microscope image (Figure 5-5C) reveals that the analytes (Alexa Fluor 555 antirabbit IgG) bind selectively to the corresponding nanotubes by giving the red fluorescence signal only on BMNT3. There is no detectable nonspecific interaction between BMNT2 and red-dye-antirabbit IgG (Figure 5-7 for quantitative data).

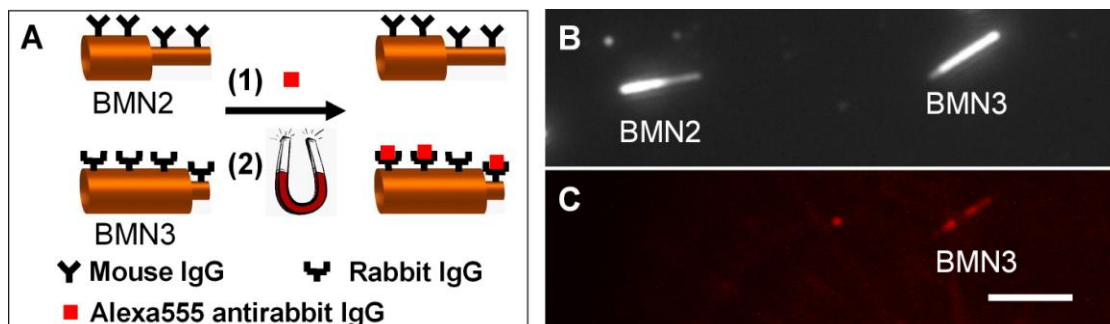


**Figure 5-5.** (A) Scheme of the protein detection assay with BMNT2 and BMNT3 nanotubes which were modified with mouse IgG and rabbit IgG, respectively. (B) Optical (in the dark field) and (C) fluorescence microscope images of the mixed BMNTs after incubation with the analyte: red-dye-labeled antirabbit IgG. The scale bar is 5  $\mu\text{m}$ .

We also performed multiplexed assays with two analytes: Alexa Fluor 555 antirabbit IgG and Alexa Fluor 555 antimouse IgG. Figure 5-6 shows the scheme of the multiplex assay for the two analytes and the microscope images of the resulting mixture of BMNT2 and BMNT3. All the BMNTs isolation and washing steps in this assay are accomplished by magnetic field separation. After incubation with red-dye-antirabbit IgG and red-dye-antimouse IgG, both of BMNT2 and BMNT3 show red fluorescence signals. Figure 5-7 shows quantitative data for both protein detection and multiplexed immunoassay. Each fluorescence intensity value is averaged on the

measurement of at least 10 nanotubes. It is practical to design clinical suspension arrays with antibody-bound-BMNTs of many different barcodes to detect multiple analytes simultaneously.

As shown in the above multiplexed assay, there is another advantage in barcoded BMNTs system: only one dye is necessary in BMNTs microarrays because the barcodes (or shapes) of the BMNTs would identify the types of analytes binding on them. This avoids the fluorescence spectral overlap problem existing in most color encoded particles arrays.

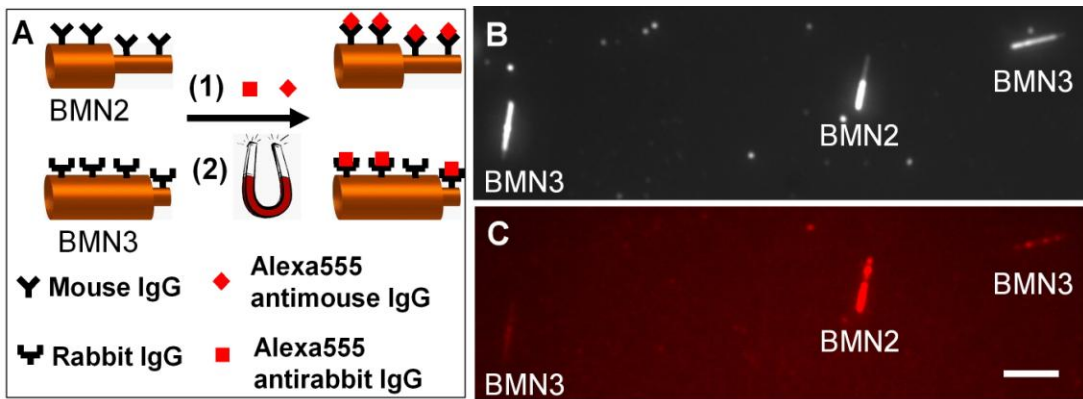


**Figure 5-6.** (A) Scheme of the multiplexed assay with the mixture of BMNT2 and BMNT3 nanotubes which were modified with mouse IgG and rabbit IgG, respectively. (B) Optical (in the dark field) and (C) fluorescence microscope images of the mixed BMNTs after incubation with the analyte: red-dye-labeled antirabbit IgG and red-dye-labeled antimouse IgG. The scale bar is 5  $\mu\text{m}$ .

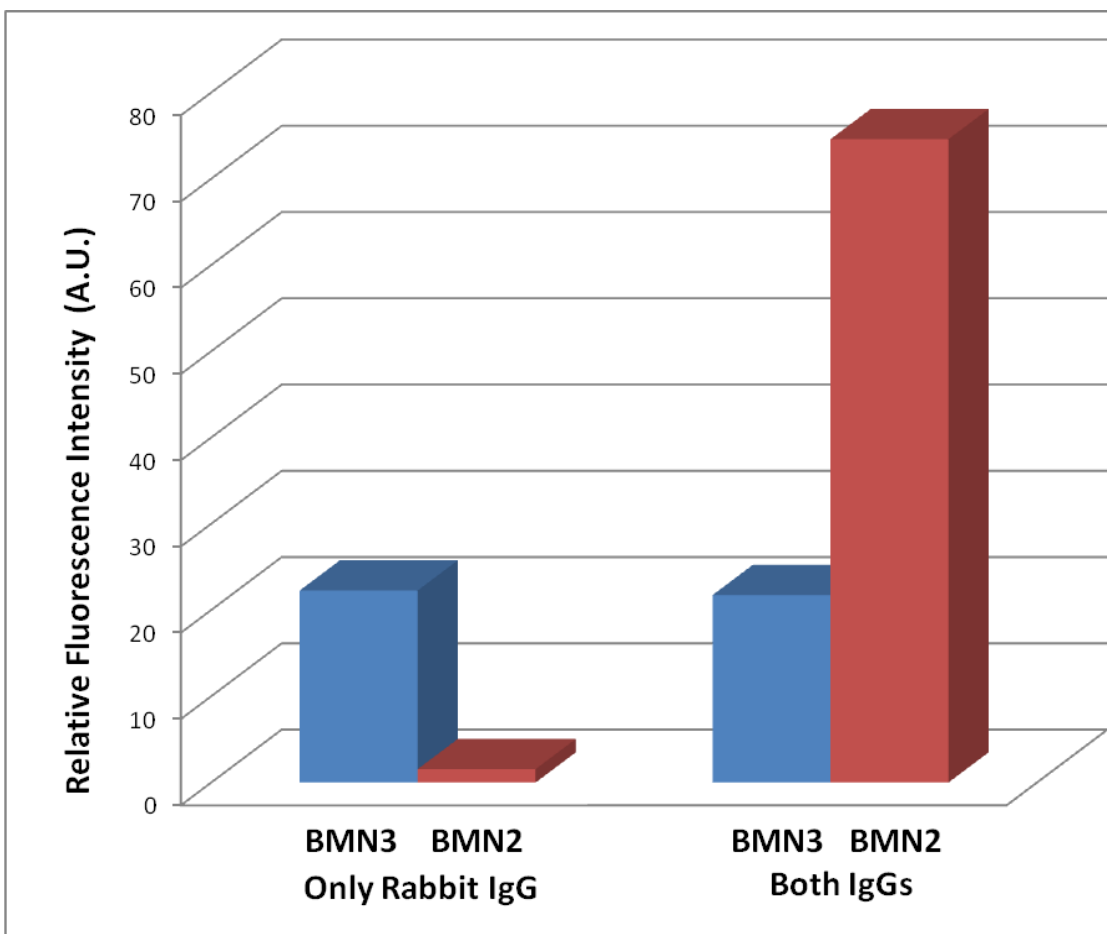


**Figure 5-7.** Average fluorescence intensity from BMNT3 and BMNT2 for single IgG detection and multiplexed immunoassays.

**BMNTs for Cancer Marker Detection with Magnetic Field Separation.**

Biomarker detection is very important for diseases diagnosis. Suspension arrays with BMNTs provide a new opportunity for rapid, automated and accurate detect single or multiple cancer markers. We have applied BMNTs in a proof-of-concept cancer marker detection experiment. A sandwich immunoassay (Figure 5-8A) was designed and performed to detect target cancer marker AFP with the mixture of BMNT2 and BMNT3 nanotubes.

First, BMNT2 and BMNT3 were modified with MAb AFP and MAb CEA, respectively. Then, a 1:1 mixture solution of BMNT2 and BMNT3 was prepared and incubated with AFP (60 nM). After being isolated with magnetic field and washed with PBS, the mixture of BMNTs was incubated with Alexa488 MAb AFP (Green) and Alexa488 MAb CEA (Green). Optical and fluorescence microscope images of BMNTs were taken after thoroughly washing them with PBS buffers and DI water by magnetic separation. The barcode (shape) of each BMNT can be clearly distinguished in the optical dark field image (Figure 5-8B). BMNT2 has MAb AFP on its surface and is supposed to recognize AFP, followed by binding with Alexa488 MAb AFP resulting in a green fluorescent signal, whereas MAb CEA modified SNT3 does not. The fluorescence microscope image (Figure 5-8C) demonstrates the above expectation that the analyte (AFP) binds selectively to the corresponding nanotubes (BMNT2) by giving the strong green fluorescence signal only on BMNT2. There is no detectable nonspecific interaction between BMNT3 and AFP.

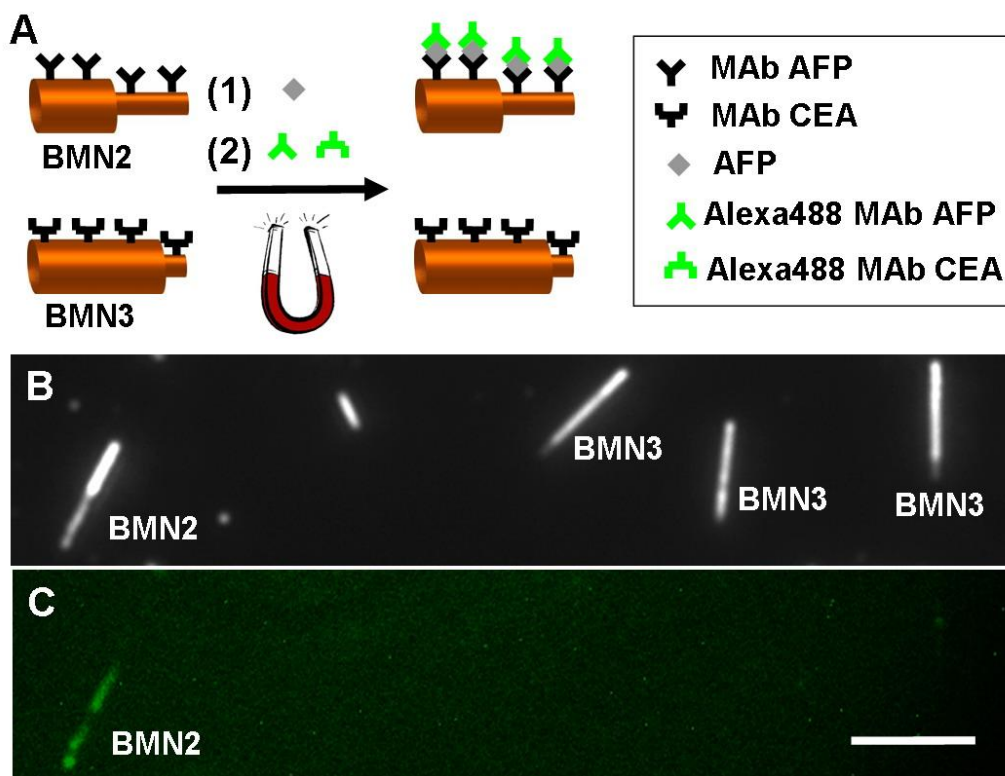
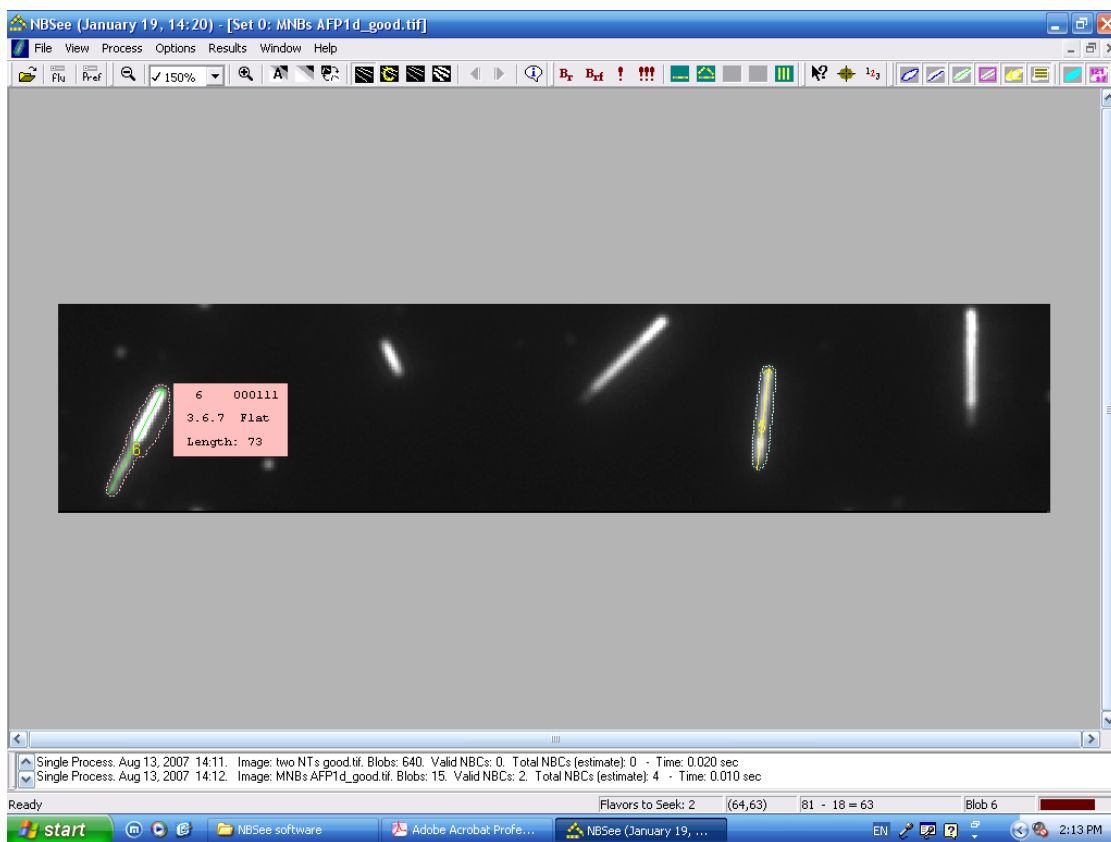


**Figure 5-8.** (A) Scheme of the sandwich assay with the mixture of BMNT2 and BMNT3 nanotubes for cancer marker detection. (B) Optical (in dark field), and (C) fluorescence microscope images of BMNTs after incubation with AFP, and the mixture of Alexa488 MAb AFP (Green) and Alexa488 MAb CEA (Green). The scale bar is 5  $\mu\text{m}$ .

**Identification of BMNTs.** The shapes of barcoded SNTs have been identified by naked eyes and their reflectance values/fluorescence intensity have been analyzed by Adobe Photoshop. A powerful tool for rapid and automated identification and fluorescence intensity is necessary for large amount of data analysis. Before we develop our own software for this purpose, we have tried NBSee program, which have been developed by Nanoplex Technologies Inc. (now Oxonica Inc.)<sup>108</sup> for automated identification of striped metallic nanowires (Please see Chapter 1 for more information). These metallic nanowires show barcoded patterns with a series of dark

and bright lines under a certain wavelength light because of different reflectivity values of metals.<sup>47-49</sup> Similarly, BMNTs developed by our group also use reflectance patterns as barcodes. We have tried BMNT2 and BMNT3 in NBSee program with the codes of 000111 and 011111, respectively. Interestingly, as shown in Figure 5-9, NBSee can identify these BMNTs very well and summary data correctly except some special cases, for example, BMNTs too close to the edge.



NBSee (January 19, 14:20) - [Set 0: MNBs AFP1d\_good.tif]

File View Process Options Results Window Help

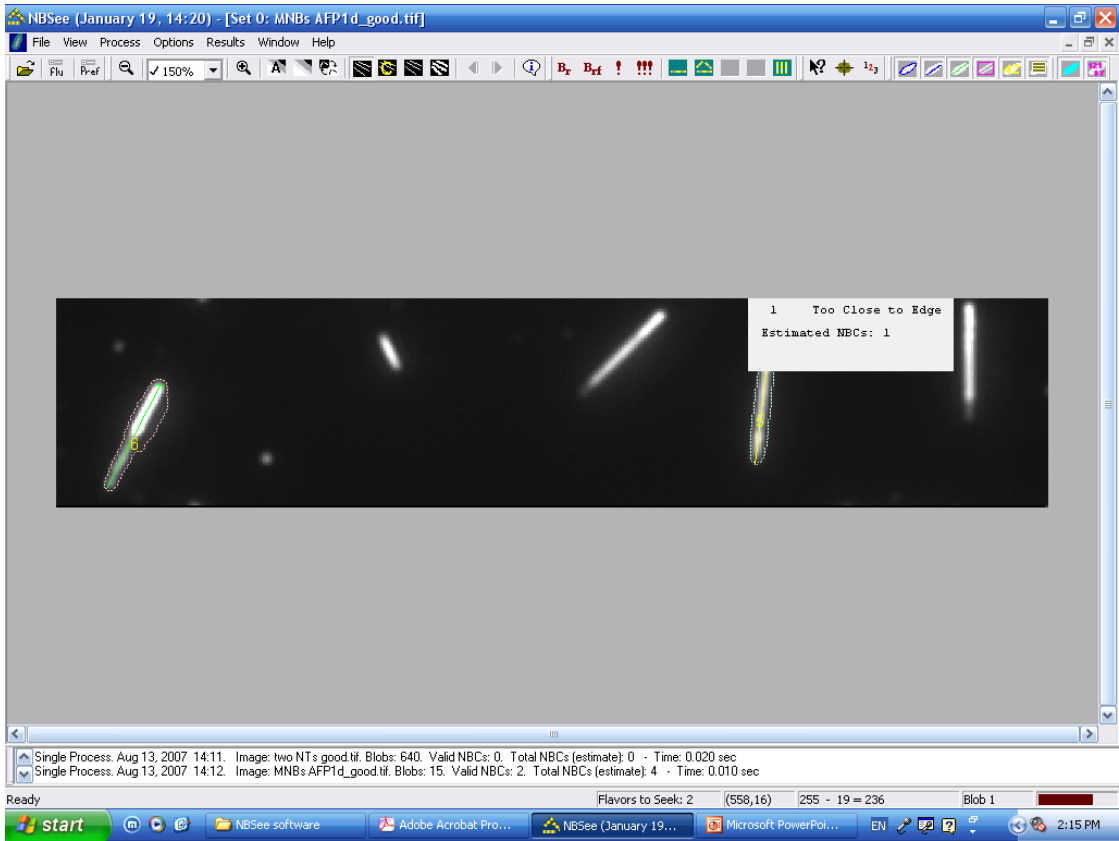
Flu Pref 150% B<sub>x</sub> B<sub>ref</sub> ! !!!

5	011111
3.6.31	Flat
Length: 63	

Single Process: Aug 13, 2007 14:11. Image: two NTs good.tif. Blobs: 640. Valid NBCs: 0. Total NBCs (estimate): 0. Time: 0.020 sec  
 Single Process: Aug 13, 2007 14:12. Image: MNBs AFP1d\_good.tif. Blobs: 15. Valid NBCs: 2. Total NBCs (estimate): 4. Time: 0.010 sec

Ready Flavors to Seek: 2 (438,57) 61 - 18 = 43 Blob 5

start NBSee software Adobe Acrobat Pro... NBSee (January 19... Microsoft PowerPol... EN 2:14 PM



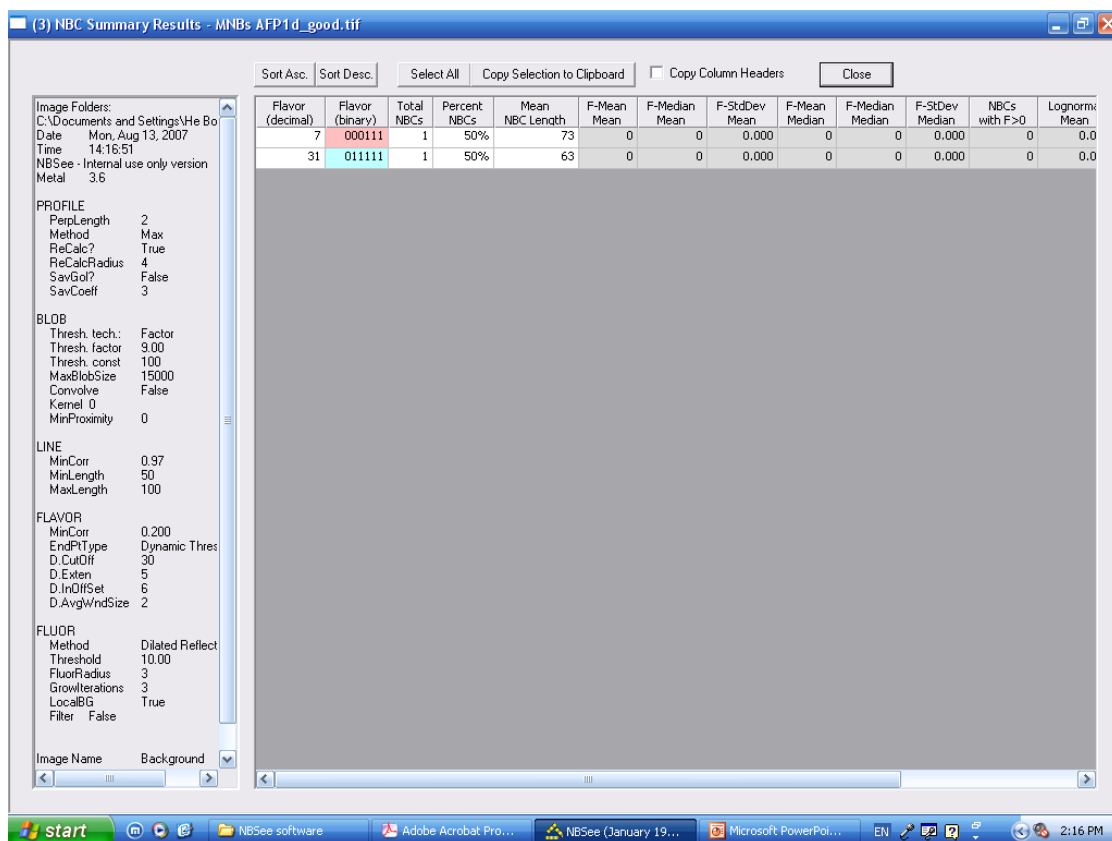


**Figure 5-9.** Automated identification of BMNTs by software: NBSee program (Courtesy of Professor Keating and Nanoplex Technologies Inc., now Oxonica Inc.). The codes for BMNT2 and BMNT3 are designed as 000111 and 011111.

## 5.4 CONCLUSION

In this chapter, we successfully fabricated BMNTs as dual-functional microcarriers for multiplexed immunoassays and cancer biomarker detection with magnetic separation. BMNTs combine the shape variety of barcoded SNTs and superparamagnetic properties of magnetic nanocrystals. BMNTs overcome the problems in the existing dual-functional particles. The iron oxide nanocrystals are evenly dispersed in the inner void of the tubular structures without interference with the optical barcoded patterns. BMNTs have been applied in multiplexed assays and

cancer biomarker detection and obtained high selectivity. By using dual-functional BMNTs with magnetic field separation, the assay time will be shortened and procedures will be simplified. Magnetic field separation of BMNTs has dominating advantages over tedious filtration or centrifugation separation. It provides rapid, gentle, reliable and reproducible isolation of target analytes. The identification of BMNTs with software shows promising results for a large amount of data analysis. BMNTs show great potential to be adapted to integrated and automated platforms, such as microchips.

## **5.5 ACKNOWLEDGEMENT**

This work was supported by the Laboratory for Physical Sciences and University of Maryland. We thank Xia Bai for her help with magnetic nanocrystals loading. We specially thank Professor Keating and Nanoplex Technologies Inc. for their help with NBSee software.

## Chapter 6: Conclusions

We have invented and developed a new species of graphical encoding particles: barcoded SNTs which could give us an opportunity to solve the problems existing in the present barcoded particles suspension arrays, such as spectral overlap, quenching of fluorescence signals and degradation of materials. Barcoded SNTs have been fabricated by template synthesis method and applied in suspension arrays for multiplexed bioassays and cancer marker detection. The multistep anodization technique successfully synthesizes well-defined cylindrical pores with four different diameter segments on the aluminum foil. Each shape of the SNTs prepared from the templates represents one biomolecular code because it can be easily distinguished by the reflectance and the length of each segment on this nanotube under a conventional optical microscope. The barcoded SNTs are evenly dispersed in aqueous solution because of their tubular structures, and have been stable in DI water without any visible degradation for 7 months. The multiplexed immunoassay experiments have demonstrated high selectivity of the SNTs arrays for detection of multianalytes. Quantitative analysis has been optimized by decreasing the number of nanotubes involved in the assay. With decreasing the concentration of SNTs as low as  $1.5 \times 10^6$  SNTs/mL in assay, the sensitivity of the assay has been enhanced and analyte IgG have been successfully detected at 6 pM concentration. The number of nanotubes used in assay can be further decreased and optimized to get better sensitivity.

It is attractive to combine barcode SNTs with microchip technology for rapid, integrated, and automatic detection and screening of biomolecules, which will make barcoded SNTs technology not only a novel concept in the labs, but also a powerful

tool for basic research and clinical practice. Magnetic field separation is one promising technique to realize this goal. It provides rapid, gentle, reliable and reproducible isolation of target analytes, and is easily adapted to automated platforms, such as microchips or microplates.

We have coupled barcoded SNTs with MBs separation for protein detection and analysis. The species and numbers of final collected SNTs represent the types and concentrations of analyte proteins in the samples. By using barcoded SNTs as signals instead of fluorescence, these suspension arrays avoid fluorescence quenching and interference of MBs' autofluorescence problems. Barcoded SNTs have been fabricated by template synthesis method with multistep anodization. Barcoded information can be easily "read-out" with a conventional optical microscope. Magnetic field separation is mild, rapid, and effective and it is a great alternative of filtration or centrifugation separation. Selectivity values have been optimized by using proper surface modifications, monoclonal antibodies and increasing the number of MBs involved in the assays. The quantitative analysis results have demonstrated that the number of target SNTs can quantify the concentration of analyte proteins. Suspension arrays of barcoded SNTs coupled with MBs have shown great potential to be combined with microchip technology for rapid, automatic, and integrated detection and analysis of multiplexed analytes biomolecules, such as proteins and cancer markers.

We have also successfully fabricated BMNTs as dual-functional microcarriers for multiplexed immunoassays and cancer biomarker detection with magnetic separation. BMNTs combine the shape variety of barcoded SNTs and

superparamagnetic properties of magnetic nanocrystals. BMNTs overcome the problems in the existing dual-functional particles. The iron oxide nanocrystals are evenly dispersed in the inner void of the tubular structures without interference with the optical barcoded patterns. BMNTs have been applied in multiplexed assays and cancer biomarker detection and obtained high selectivity. By using dual-functional BMNTs with magnetic field separation, the assay time will be shortened and procedures will be simplified. Magnetic field separation of BMNTs has several excellent advantages over tedious filtration or centrifugation separation. It provides rapid, gentle, reliable and reproducible isolation of target analytes. The automated identification of BMNTs with software shows promising results for a large amount of data analysis. BMNTs provide a promising way to integrate barcoded nanoparticles inside a microchip for ultrafast, efficient, and automated detection of target chemical/biochemical molecules for diseases diagnosis and drug screening.

## REFERENCES

1. Patolsky, F.; Zheng, G.; Lieber, C. M., Nanowire sensors for medicine and the life sciences. *Nanomedicine (London, United Kingdom)* **2006**, 1, (1), 51-65.
2. Tyagi, S.; Kramer, F. R., Molecular beacons: probes that fluoresce upon hybridization. *Nature Biotechnology* **1996**, 14, (3), 303-308.
3. Taton, T. A.; Lu, G.; Mirkin, C. A., Two-Color Labeling of Oligonucleotide Arrays via Size-Selective Scattering of Nanoparticle Probes. *Journal of the American Chemical Society* **2001**, 123, (21), 5164-5165.
4. Watson, A.; Wu, X.; Bruchez, M., Lighting up cells with quantum dots. *BioTechniques* **2003**, 34, (2), 296-298,300,303.
5. Chan, W. C. W.; Maxwell, D. J.; Gao, X.; Bailey, R. E.; Han, M.; Nie, S., Luminescent quantum dots for multiplexed biological detection and imaging. *Current Opinion in Biotechnology* **2002**, 13, (1), 40-46.
6. Jaiswal, J. K.; Mattoussi, H.; Mauro, J. M.; Simon, S. M., Long-term multiple color imaging of live cells using quantum dot bioconjugates. *Nature Biotechnology* **2003**, 21, (1), 47-51.
7. Alivisatos, P., The use of nanocrystals in biological detection. *Nature Biotechnology* **2004**, 22, (1), 47-52.
8. Gao, X.; Cui, Y.; Levenson, R. M.; Chung, L. W. K.; Nie, S., In vivo cancer targeting and imaging with semiconductor quantum dots. *Nature Biotechnology* **2004**, 22, (8), 969-976.
9. Wu, X.; Liu, H.; Liu, J.; Haley, K. N.; Treadway, J. A.; Larson, J. P.; Ge, N.; Peale, F.; Bruchez, M. P., Immunofluorescent labeling of cancer marker Her2 and other cellular targets with semiconductor quantum dots. *Nature Biotechnology* **2003**, 21, (1), 41-46.
10. Morales, A. M.; Lieber, C. M., A laser ablation method for the synthesis of crystalline semiconductor nanowires. *Science (Washington, D. C.)* **1998**, 279, (5348), 208-211.
11. Lieber, C. M., Nanoscale science and technology: building a big future from small things. *MRS Bulletin* **2003**, 28, (7), 486-491.
12. Cui, Y.; Lieber, C. M., Functional nanoscale electronic devices assembled using silicon nanowire building blocks. *Science (Washington, DC, United States)* **2001**, 291, (5505), 851-853.
13. Jin, S.; Whang, D.; McAlpine, M. C.; Friedman, R. S.; Wu, Y.; Lieber, C. M., Scalable Interconnection and Integration of Nanowire Devices without Registration. *Nano Letters* **2004**, 4, (5), 915-919.
14. Zheng, G.; Lu, W.; Jin, S.; Lieber, C. M., Synthesis and fabrication of high-performance n-type silicon nanowire transistors. *Advanced Materials (Weinheim, Germany)* **2004**, 16, (21), 1890-1893.
15. Chen, R. J.; Bangsaruntip, S.; Drouvalakis, K. A.; Kam, N. W. S.; Shim, M.; Li, Y.; Kim, W.; Utz, P. J.; Dai, H., Noncovalent functionalization of carbon nanotubes for highly specific electronic biosensors. *Proceedings of the National Academy of Sciences of the United States of America* **2003**, 100, (9), 4984-4989.

- 16.Chen, R. J.; Choi, H. C.; Bangsaruntip, S.; Yenilmez, E.; Tang, X.; Wang, Q.; Chang, Y.-L.; Dai, H., An investigation of the mechanisms of electronic sensing of protein adsorption on carbon nanotube devices. *Journal of the American Chemical Society* **2004**, 126, (5), 1563-1568.
- 17.Penn, S. G.; He, L.; Natan, M. J., Nanoparticles for bioanalysis. *Mirai Zairyo* **2005**, 5, (9), 8-16.
- 18.Harisinghani Mukesh, G.; Barentsz, J.; Hahn Peter, F.; Deserno Willem, M.; Tabatabaei, S.; van de Kaa Christine, H.; de la Rosette, J.; Weissleder, R., Noninvasive detection of clinically occult lymph-node metastases in prostate cancer. *N Engl J Med FIELD Full Journal Title:The New England journal of medicine* **2003**, 348, (25), 2491-2499.
- 19.Akerman, M. E.; Chan, W. C. W.; Laakkonen, P.; Bhatia, S. N.; Ruoslahti, E., Nanocrystal targeting in vivo. *Proceedings of the National Academy of Sciences of the United States of America* **2002**, 99, (20), 12617-12621.
- 20.Dubertret, B.; Skourides, P.; Norris, D. J.; Noireaux, V.; Brivanlou, A. H.; Libchaber, A., In vivo imaging of quantum dots encapsulated in phospholipid micelles. *Science (Washington, DC, United States)* **2002**, 298, (5599), 1759-1762.
- 21.Csaki, A.; Moller, R.; Straube, W.; Kohler, J. M.; Fritzsche, W., DNA monolayer on gold substrates characterized by nanoparticle labeling and scanning force microscopy. *Nucleic Acids Res FIELD Full Journal Title:Nucleic acids research* **2001**, 29, (16), E81.
- 22.Cao, Y. C.; Jin, R.; Mirkin, C. A., Nanoparticles with Raman spectroscopic fingerprints for DNA and RNA detection. *Science (Washington, DC, United States)* **2002**, 297, (5586), 1536-1540.
- 23.Mulvaney, S. P.; Musick, M. D.; Keating, C. D.; Natan, M. J., Glass-Coated, Analyte-Tagged Nanoparticles: A New Tagging System Based on Detection with Surface-Enhanced Raman Scattering. *Langmuir* **2003**, 19, (11), 4784-4790.
- 24.Authier, L.; Grossiord, C.; Brossier, P., Gold nanoparticle-based quantitative electrochemical detection of amplified human cytomegalovirus DNA using disposable microband electrodes. *Anal Chem FIELD Full Journal Title:Analytical chemistry* **2001**, 73, (18), 4450-4456.
- 25.Ozsoz, M.; Erdem, A.; Kerman, K.; Ozkan, D.; Tugrul, B.; Topcuoglu, N.; Ekren, H.; Taylan, M., Electrochemical genosensor based on colloidal gold nanoparticles for the detection of factor V Leiden mutation using disposable pencil graphite electrodes. *Analytical Chemistry* **2003**, 75, (9), 2181-2187.
- 26.Zhang, C.; Zhang, Z.; Yu, B.; Shi, J.; Zhang, X., Application of the biological conjugate between antibody and colloid Au nanoparticles as analyte to inductively coupled plasma mass spectrometry. *Analytical Chemistry* **2002**, 74, (1), 96-99.
- 27.Schultz, D. A., Plasmon resonant particles for biological detection. *Current Opinion in Biotechnology* **2003**, 14, (1), 13-22.
- 28.Bao, P.; Frutos, A. G.; Greef, C.; Lahiri, J.; Muller, U.; Peterson, T. C.; Warden, L.; Xie, X., High-sensitivity detection of DNA hybridization on microarrays using resonance light scattering. *Analytical Chemistry* **2002**, 74, (8), 1792-1797.
- 29.Dardzinski, B. J.; Schmithorst, V. J.; Holland, S. K.; Boivin, G. P.; Imagawa, T.; Watanabe, S.; Lewis, J. M.; Hirsch, R., MR imaging of murine arthritis using

- ultrasmall superparamagnetic iron oxide particles. *Magnetic Resonance Imaging* **2001**, 19, (9), 1209-1216.
- 30.Saleh, A.; Schroeter, M.; Jonkmanns, C.; Hartung, H.-P.; Modder, U.; Jander, S., In vivo MRI of brain inflammation in human ischaemic stroke. *Brain FIELD Full Journal Title:Brain : a journal of neurology* **2004**, 127, (Pt 7), 1670-1677.
- 31.Kooi, M. E.; Cappendijk, V. C.; Cleutjens, K. B. J. M.; Kessels, A. G. H.; Kitslaar, P. J. E. H. M.; Borgers, M.; Frederik, P. M.; Daemen, M. J. A. P.; van Engelshoven, J. M. A., Accumulation of Ultrasmall Superparamagnetic Particles of Iron Oxide in Human Atherosclerotic Plaques Can Be Detected by In Vivo Magnetic Resonance Imaging. *Circulation* **2003**, 107, (19), 2453-2458.
- 32.Son, S. J.; Reichel, J.; He, B.; Schuchman, M.; Lee, S. B., Magnetic nanotubes for magnetic-field-assisted bioseparation, biointeraction, and drug delivery. *Journal of the American Chemical Society* **2005**, 127, (20), 7316-7317.
- 33.Son, S. J.; Bai, X.; Nan, A.; Ghandehari, H.; Lee, S. B., Template synthesis of multifunctional nanotubes for controlled release. *Journal of Controlled Release* **2006**, 114, (2), 143-152.
- 34.Cui, Y.; Wei, Q.; Park, H.; Lieber, C. M., Nanowire nanosensors for highly sensitive and selective detection of biological and chemical species. *Science FIELD Full Journal Title:Science (New York, N.Y.)* **2001**, 293, (5533), 1289-1292.
- 35.Hahm, J.-i.; Lieber, C. M., Direct ultrasensitive electrical detection of DNA and DNA sequence variations using nanowire nanosensors. *Nano Letters* **2004**, 4, (1), 51-54.
- 36.Zheng, G.; Patolsky, F.; Cui, Y.; Wang, W. U.; Lieber, C. M., Multiplexed electrical detection of cancer markers with nanowire sensor arrays. *Nature Biotechnology* **2005**, 23, (10), 1294-1301.
- 37.Patolsky, F.; Zheng, G.; Hayden, O.; Lakadamyali, M.; Zhuang, X.; Lieber, C. M., Electrical detection of single viruses. *Proceedings of the National Academy of Sciences of the United States of America* **2004**, 101, (39), 14017-14022.
- 38.Braeckmans, K.; De Smedt, S. C.; Leblans, M.; Pauwels, R.; Demeester, J., Encoding microcarriers: present and future technologies. *Nature Reviews Drug Discovery* **2002**, 1, (6), 447-456.
- 39.Wilson, R.; Cossins, A. R.; Spiller, D. G., Encoded microcarriers for high-throughput multiplexed detection. *Angewandte Chemie, International Edition* **2006**, 45, (37), 6104-6117.
- 40.Finkel, N. H.; Lou, X.; Wang, C.; He, L., Barcoding the microworld. *Analytical Chemistry* **2004**, 76, (19), 352A-359A.
- 41.Prabhakar, U.; Eirikis, E.; Davis, H. M., Simultaneous quantification of proinflammatory cytokines in human plasma using the LabMAP assay. *Journal of Immunological Methods* **2002**, 260, (1-2), 207-218.
- 42.Yang, L.; Tran, D. K.; Wang, X., BADGE, beadsArray for the detection of gene expression, a high-throughput diagnostic bioassay. *Genome Research* **2001**, 11, (11), 1888-1898.
- 43.Dunbar, S. A.; Jacobson, J. W., Application of the Luminex LabMAP in rapid screening for mutations in the cystic fibrosis transmembrane conductance regulator gene: a pilot study. *Clinical Chemistry (Washington, D. C.)* **2000**, 46, (9), 1498-1500.

44. Smith, P. L.; Walker-Peach, C. R.; Fulton, R. J.; DuBois, D. B., A rapid, sensitive, multiplexed assay for detection of viral nucleic acids using the FlowMetrix system. *Clinical Chemistry (Washington, D. C.)* **1998**, 44, (9), 2054-2056.
45. Oliver, K. G.; Kettman, J. R.; Fulton, R. J., Multiplexed analysis of human cytokines by use of the FlowMetrix system. *Clinical Chemistry (Washington, D. C.)* **1998**, 44, (9), 2057-2060.
46. Zhou, H.; Roy, S.; Schulman, H.; Natan, M. J., Solution and chip arrays in protein profiling. *Trends Biotechnol FIELD Full Journal Title: Trends in biotechnology* **2001**, 19, (10 Suppl), S34-39.
47. Nicewarner-Pena, S. R.; Griffith Freeman, R.; Reiss, B. D.; He, L.; Pena, D. J.; Walton, I. D.; Cromer, R.; Keating, C. D.; Natan, M. J., Submicrometer metallic barcodes. *Science (Washington, DC, United States)* **2001**, 294, (5540), 137-141.
48. Nicewarner-Pena, S. R.; Carado, A. J.; Shale, K. E.; Keating, C. D., Barcoded metal nanowires: optical reflectivity and patterned fluorescence. *Journal of Physical Chemistry B* **2003**, 107, (30), 7360-7367.
49. Keating, C. D.; Natan, M. J., Striped metal nanowires as building blocks and optical tags. *Advanced Materials (Weinheim, Germany)* **2003**, 15, (5), 451-454.
50. Stoermer, R. L.; Sioss, J. A.; Keating, C. D., Stabilization of Silver Metal in Citrate Buffer: Barcoded Nanowires and Their Bioconjugates. *Chemistry of Materials* **2005**, 17, (17), 4356-4361.
51. Stoermer, R. L.; Keating, C. D., Distance-Dependent Emission from Dye-Labeled Oligonucleotides on Striped Au/Ag Nanowires: Effect of Secondary Structure and Hybridization Efficiency. *Journal of the American Chemical Society* **2006**, 128, (40), 13243-13254.
52. Dames, A.; England, J.; Colby, E. Bio-assay technique. 99-GB3109 2000016893, 19990917., 2000.
53. Evans, M.; Sewter, C.; Hill, E., An encoded particle array tool for multiplex bioassays. *Assay and Drug Development Technologies* **2003**, 1, (1-2), 199-207.
54. Pregibon, D. C.; Toner, M.; Doyle, P. S., Multifunctional Encoded Particles for High-Throughput Biomolecule Analysis. *Science (Washington, DC, United States)* **2007**, 315, (5817), 1393-1396.
55. Dendukuri, D.; Pregibon, D. C.; Collins, J.; Hatton, T. A.; Doyle, P. S., Continuous-flow lithography for high-throughput microparticle synthesis. *Nature Materials* **2006**, 5, (5), 365-369.
56. Braeckmans, K.; De Smedt, S. C.; Roelant, C.; Leblans, M.; Pauwels, R.; Demeester, J., Encoding microcarriers by spatial selective photobleaching. *Nature Materials* **2003**, 2, (3), 169-173.
57. Matthias, S.; Schilling, J.; Nielsch, K.; Muller, F.; Wehrspohn, R. B.; Gosele, U., Monodisperse diameter-modulated gold microwires. *Advanced Materials (Weinheim, Germany)* **2002**, 14, (22), 1618-1621.
58. Brummel, C. L.; Lee, I. N. W.; Zhou, Y.; Benkovic, S. J.; Winograd, N., A mass spectrometric solution to the address problem of combinatorial libraries. *Science (Washington, DC, United States)* **1994**, 264, (5157), 399-402.
59. Hochlowski, J. E.; Whittern, D. N.; Sowin, T. J., Encoding of Combinatorial Chemistry Libraries by Fluorine-19 NMR. *Journal of Combinatorial Chemistry* **1999**, 1, (4), 291-293.

60. Neilly, J. P.; Hochlowski, J. E., Elemental analysis of individual combinatorial chemistry library members by energy-dispersive x-ray spectroscopy. *Applied Spectroscopy* **1999**, 53, (1), 74-81.
61. Rahman, S. S.; Busby, D. J.; Lee, D. C., Infrared and Raman Spectra of a Single Resin Bead for Analysis of Solid-Phase Reactions and Use in Encoding Combinatorial Libraries. *Journal of Organic Chemistry* **1998**, 63, (18), 6196-6199.
62. Lam, K. S.; Lebl, M.; Krchnak, V., The "One-Bead-One-Compound" Combinatorial Library Method. *Chemical Reviews (Washington, D. C.)* **1997**, 97, (2), 411-448.
63. Czarnik, A. W., Encoding methods for combinatorial chemistry. *Current Opinion in Chemical Biology* **1997**, 1, (1), 60-66.
64. Han, M.; Gao, X.; Su, J. Z.; Nie, S., Quantum-dot-tagged microbeads for multiplexed optical coding of biomolecules. *Nature Biotechnology* **2001**, 19, (7), 631-635.
65. Gao, X.; Chan, W. C. W.; Nie, S., Quantum-dot nanocrystals for ultrasensitive biological labeling and multicolor optical encoding. *Journal of Biomedical Optics* **2002**, 7, (4), 532-537.
66. Gao, X.; Nie, S., Quantum Dot-Encoded Mesoporous Beads with High Brightness and Uniformity: Rapid Readout Using Flow Cytometry. *Analytical Chemistry* **2004**, 76, (8), 2406-2410.
67. Xu, H.; Sha, M. Y.; Wong, E. Y.; Uphoff, J.; Xu, Y.; Treadway, J. A.; Truong, A.; O'Brien, E.; Asquith, S.; Stubbins, M.; Spurr, N. K.; Lai, E. H.; Mahoney, W., Multiplexed SNP genotyping using the Qbead system: a quantum dot-encoded microsphere-based assay. *Nucleic Acids Research* **2003**, 31, (8), e43/41-e43/10.
68. Nolan, J. P.; Sklar, L. A., Suspension array technology: evolution of the flat-array paradigm. *Trends in Biotechnology* **2002**, 20, (1), 9-12.
69. He, B.; Son, S. J.; Lee, S. B., Shape-Coded Silica Nanotubes for Biosensing. *Langmuir* **2006**, 22, (20), 8263-8265.
70. Lee, S. B.; Mitchell, D. T.; Trofin, L.; Nevanen, T. K.; Soederlund, H.; Martin, C. R., Antibody-based bio-nanotube membranes for enantiomeric drug separations. *Science (Washington, DC, United States)* **2002**, 296, (5576), 2198-2200.
71. Martin, C. R.; Kohli, P., The emerging field of nanotube biotechnology. *Nature Reviews Drug Discovery* **2003**, 2, (1), 29-37.
72. Okamoto, K.; Shook, C. J.; Bivona, L.; Lee, S. B.; English, D. S., Direct Observation of Wetting and Diffusion in the Hydrophobic Interior of Silica Nanotubes. *Nano Letters* **2004**, 4, (2), 233-239.
73. Son, S. J.; Lee, S. B., Controlled Gold Nanoparticle Diffusion in Nanotubes: Platform of Partial Functionalization and Gold Capping. *Journal of the American Chemical Society* **2006**, 128, (50), 15974-15975.
74. Mitchell, D. T.; Lee, S. B.; Trofin, L.; Li, N.; Nevanen, T. K.; Soederlund, H.; Martin, C. R., Smart nanotubes for bioseparations and biocatalysis. *Journal of the American Chemical Society* **2002**, 124, (40), 11864-11865.
75. Zhao, X.; Tapecc-Dytioco, R.; Tan, W., Ultrasensitive DNA detection using highly fluorescent bioconjugated nanoparticles. *Journal of the American Chemical Society* **2003**, 125, (38), 11474-11475.

76. Penn, S. G.; He, L.; Natan, M. J., Nanoparticles for bioanalysis. *Current Opinion in Chemical Biology* **2003**, 7, (5), 609-615.
77. Kovtyukhova, N. I.; Mallouk, T. E.; Mayer, T. S., Templated surface sol-gel synthesis of SiO<sub>2</sub> nanotubes and SiO<sub>2</sub>-insulated metal nanowires. *Advanced Materials (Weinheim, Germany)* **2003**, 15, (10), 780-785.
78. Lee, J. S.; Gu, G. H.; Kim, H.; Jeong, K. S.; Bae, J.; Suh, J. S., Growth of carbon nanotubes on anodic aluminum oxide templates: Fabrication of a tube-in-tube and linearly joined tube. *Chemistry of Materials* **2001**, 13, (7), 2387-2391.
79. Xu, T. T.; Fisher, F. T.; Brinson, L. C.; Ruoff, R. S., Bone-Shaped Nanomaterials for Nanocomposite Applications. *Nano Letters* **2003**, 3, (8), 1135-1139.
80. Lamture, J. B.; Beattie, K. L.; Burke, B. E.; Eggers, M. D.; Ehrlich, D. J.; Fowler, R.; Hollis, M. A.; Kosicki, B. B.; Reich, R. K.; Smith, S. R., Direct detection of nucleic acid hybridization on the surface of a charge coupled device. *Nucleic Acids Res FIELD Full Journal Title: Nucleic acids research* **1994**, 22, (11), 2121-2125.
81. Won, J.; Kim, M.; Yi, Y.-W.; Kim, Y. H.; Jung, N.; Kim, T. K., A Magnetic Nanoprobe Technology for Detecting Molecular Interactions in Live Cells. *Science (Washington, DC, United States)* **2005**, 309, (5731), 121-125.
82. He, B.; Son, S. J.; Lee, S. B., Suspension Array with Shape-Coded Silica Nanotubes for Multiplexed Immunoassays. *Analytical Chemistry (Washington, DC, United States)* **2007**, 79, (14), 5257-5263.
83. Walt, D. R., Techview: molecular biology. Bead-based fiber-optic arrays. *Science FIELD Full Journal Title: Science (New York, N.Y.)* **2000**, 287, (5452), 451-452.
84. Vignali, D. A. A., Multiplexed particle-based flow cytometric assays. *Journal of Immunological Methods* **2000**, 243, (1-2), 243-255.
85. Herr, J. K.; Smith, J. E.; Medley, C. D.; Shangguan, D.; Tan, W., Aptamer-Conjugated Nanoparticles for Selective Collection and Detection of Cancer Cells. *Analytical Chemistry* **2006**, 78, (9), 2918-2924.
86. Nam, J.-M.; Thaxton, C. S.; Mirkin, C. A., Nanoparticle-based bio-bar codes for the ultrasensitive detection of proteins. *Science (Washington, DC, United States)* **2003**, 301, (5641), 1884-1886.
87. Wang, L.; Yang, C.; Tan, W., Dual-luminophore-doped silica nanoparticles for multiplexed signaling. *Nano Letters* **2005**, 5, (1), 37-43.
88. Eastman, P. S.; Ruan, W.; Doctolero, M.; Nuttall, R.; de Feo, G.; Park, J. S.; Chu, J. S. F.; Cooke, P.; Gray, J. W.; Li, S.; Chen, F. F., Qdot Nanobarcodes for Multiplexed Gene Expression Analysis. *Nano Letters* **2006**, 6, (5), 1059-1064.
89. Piehler, J.; Brecht, A.; Valiokas, R.; Liedberg, B.; Gauglitz, G., A high-density poly(ethylene glycol) polymer brush for immobilization on glass-type surfaces. *Biosensors & Bioelectronics* **2000**, 15, (9-10), 473-481.
90. Lee, W.; Ji, R.; Goesele, U.; Nielsch, K., Fast fabrication of long-range ordered porous alumina membranes by hard anodization. *Nature Materials* **2006**, 5, (9), 741-747.
91. Templin, M. F.; Stoll, D.; Schrenk, M.; Traub, P. C.; Vohringer, C. F.; Joos, T. O., Protein microarray technology. *Trends in Biotechnology* **2002**, 20, (4), 160-166.
92. Agrawal, A.; Sathe, T.; Nie, S., Single-Bead Immunoassays Using Magnetic Microparticles and Spectral-Shifting Quantum Dots. *Journal of Agricultural and Food Chemistry* **2007**, 55, (10), 3778-3782.

93. Ahmed, A. R. H.; Olivier, G. W. J.; Adams, G.; Erskine, M. E.; Kinsman, R. G.; Branch, S. K.; Moss, S. H.; Notarianni, L. J.; Pouton, C. W., Isolation and partial purification of a melanocyte-stimulating hormone receptor from B16 murine melanoma cells. A novel approach using a cleavable biotinylated photoactivated ligand and streptavidin-coated magnetic beads. *Biochemical Journal* **1992**, 286, (2), 377-382.
94. Ossendorp, F. A.; Bruning, P. F.; Van den Brink, J. A.; De Boer, M., Efficient selection of high-affinity B cell hybridomas using antigen-coated magnetic beads. *J Immunol Methods FIELD Full Journal Title: Journal of immunological methods* **1989**, 120, (2), 191-200.
95. Yitzhaki, S.; Zahavy, E.; Oron, C.; Fisher, M.; Keysary, A., Concentration of Bacillus Spores by Using Silica Magnetic Particles. *Analytical Chemistry* **2006**, 78, (18), 6670-6673.
96. Yang, L.; Li, Y., Simultaneous detection of Escherichia coli O157:H7 and Salmonella Typhimurium using quantum dots as fluorescence labels. *Analyst (Cambridge, United Kingdom)* **2006**, 131, (3), 394-401.
97. Ngomsik, A.-F.; Bee, A.; Siaugue, J.-M.; Cabuil, V.; Cote, G., Nickel adsorption by magnetic alginate microcapsules containing an extractant. *Water Research* **2006**, 40, (9), 1848-1856.
98. Rorrer, G. L.; Hsien, T. Y.; Way, J. D., Synthesis of porous-magnetic chitosan beads for removal of cadmium ions from wastewater. *Industrial & Engineering Chemistry Research* **1993**, 32, (9), 2170-2178.
99. Guesdon, J. L.; Ternynck, T.; Avrameas, S., The use of avidin-biotin interaction in immunoenzymatic techniques. *J Histochem Cytochem FIELD Full Journal Title: The journal of histochemistry and cytochemistry : official journal of the Histochemistry Society* **1979**, 27, (8), 1131-1139.
100. Huang, Y.; Nan, A.; Rosen, G. M.; Winalski, C. S.; Schneider, E.; Pei, T.; Ghandehari, H., N-(2-hydroxypropyl)methacrylamide (HPMA) copolymer-linked nitroxides: Potential magnetic resonance contrast agents. *Macromolecular Bioscience* **2003**, 3, (11), 647-652.
101. Bucak, S.; Jones, D. A.; Laibinis, P. E.; Hatton, T. A., Protein Separations Using Colloidal Magnetic Nanoparticles. *Biotechnology Progress* **2003**, 19, (2), 477-484.
102. Sathe, T. R.; Agrawal, A.; Nie, S., Mesoporous Silica Beads Embedded with Semiconductor Quantum Dots and Iron Oxide Nanocrystals: Dual-Function Microcarriers for Optical Encoding and Magnetic Separation. *Analytical Chemistry* **2006**, 78, (16), 5627-5632.
103. Berger, P.; Adelman, N. B.; Beckman, K. J.; Campbell, D. J.; Ellis, A. B.; Lisensky, G. C., Preparation and properties of an aqueous ferrofluid. *Journal of Chemical Education* **1999**, 76, (7), 943-948.
104. Feldmann, C.; Jungk, H.-O., Polyol-mediated preparation of nanoscale oxide particles. *Angewandte Chemie, International Edition* **2001**, 40, (2), 359-362.
105. Ammar, S.; Helfen, A.; Jouini, N.; Fievet, F.; Rosenman, I.; Villain, F.; Molinie, P.; Danot, M., Magnetic properties of ultrafine cobalt ferrite particles synthesized by hydrolysis in a polyol medium. *Journal of Materials Chemistry* **2001**, 11, (1), 186-192.

106. Deng, H.; Li, X.; Peng, Q.; Wang, X.; Chen, J.; Li, Y., Monodisperse magnetic single-crystal ferrite microspheres. *Angewandte Chemie, International Edition* **2005**, 44, (18), 2782-2785.
107. Brinkley, M., A brief survey of methods for preparing protein conjugates with dyes, haptens and crosslinking reagents. *Bioconjugate Chemistry* **1992**, 3, (1), 2-13.
108. Sha, M. Y.; Walton, I. D.; Norton, S. M.; Taylor, M.; Yamanaka, M.; Natan, M. J.; Xu, C.; Drmanac, S.; Huang, S.; Borchering, A.; Drmanac, R.; Penn, S. G., Multiplexed SNP genotyping using nanobarcode particle technology. *Analytical and Bioanalytical Chemistry* **2006**, 384, (3), 658-666.